Aalto University
School of Engineering

Aishwarya Dharamsi

An Experimental Investigation of a Hydrogen, Methane and Helium Gas Jet Behavior using Single Hole and Hollow Cone Piezoelectric Injector

Master's Thesis
Espoo 23.05.2021
Supervisor: Professor Martti Larmi
Advisor: PhD Qiang Cheng

Author Aishwarya Bhavesh Dharamsi

Title of thesis An Experimental Investigation of a Hydrogen, Methane and Helium Gas Jet Behavior using Single Hole and Hollow Cone Piezoelectric Injector

Master programme Mechanical Engineering **Code** ENG25

Thesis supervisor Professor Martti Larmi

Thesis advisor(s) Ph.D. Qiang Cheng

Date 23.05.2021 **Number of pages** 56+6 **Language** English

Abstract

There is now an increasing need for using alternative fuels especially in the transportation sector, which are more environmentally friendly fuels due to a decrease in fossil fuels and also more importantly a rapid increase in global warming. Use of Hydrogen in Hydrogen internal combustion engine either as a dual fuel option along with diesel or even better, as a sole fuel, is much better for the environment considering the emissions and their impact on the environment. But to shift from present infrastructure to a completely clean and green hydrogen economy might take many years, resources, and finance. The use of Hydrogen as a dual fuel option would provide a bridge towards the hydrogen economy. Also, the use of methane is seen as one of the potential options to get closer to the full hydrogen economy. Direct injection (DI) is a well-established technology and the combustion of hydrogen has a possibility of further being studied in a similar way as that of diesel. Further research on optimizing DI engines using Hydrogen has the potential of achieving higher efficiency and reduced nitrogen oxides (NOx) emissions.

Jets of Helium, Hydrogen, and Methane are studied in the experimental part of this thesis. These gas jets were injected into quiescent nitrogen with variable injection and chamber pressures and pressure ratios. Helium and Hydrogen have similar jet characteristics but their variations are confirmed through experimental analysis if any. Data between methane and hydrogen jets are compared in this thesis. To study these invisible, high-speed gas jets, a high-speed schlieren imaging technique was used to analyze the geometrical properties of the jets. The images obtained were post-processed to acquire geometrical attributes of jets such as penetration, width and area. Also, two different types of injectors i.e., single hole injector and hollow cone injector were used for all these jets and their results were compared and analyzed. A hollow cone injector like the one used in this thesis is already being used for gasoline engines. These injectors are capable of injecting gases up to 100 bar. The jet characteristics were also studied for different voltages for the hollow cone injector.

The results showed that the jet penetration was more for the single hole injector as compared to the hollow cone injector for the same conditions. Also, it was found that with increasing pressure ratio, penetration was more for both the injectors but the area for single hole injector got reduced over time faster compared to the hollow cone injector due to quicker dispersion of gas for single hole injector. Also, it was found that increased needle lift has a higher penetration length due to higher injection pressure.

Keywords Helium, Hydrogen, Methane, Gas jet, Schlieren imaging, Direct injection, Single hole injector, Hollow cone piezoelectric injector

Foreword

Jet behaviour studies especially Hydrogen jet studies have gained momentum in research conducted in the ICE laboratory of Aalto University. I have been really lucky to be a part of this thesis and get an opportunity to work under the guidance of Professor Martti Larmi. I would like to thank my supervisor Professor Larmi to allow me to contribute to the field of Hydrogen technology and for providing me this wonderful opportunity to work on this thesis. I would always be grateful to him for this. I would like to thank my advisor Jonny who helped me with everything in the execution and completion of this thesis work. I would also like to thank Olli and Otto for helping me with the construction and setup of the apparatus used for this thesis.

I am also grateful to my parents, grandparents, sister, and my friends who have always been there for me in my thick and thins. I would like to thank all these people who stood by me in my tough times and given me the strength to move forward in life.

Espoo 23.05.2020

Aishwarya Dharamsi

`

Table of Contents

Symbols

λ	[-]	Stoichiometric combustion air ratio
p_k	[Bar]	fuel-supply pressure
p_o	[Bar]	back-pressure
A_n	[m^2]	Nozzle exit area
d	[mm]	Diameter of the nozzle
h_n	[µm]	needle lift
n	[-]	refractive index
c_o	[m/s]	the speed of light in vacuum
c	[m/s]	the speed of light in a specific medium
k	[m^3/kg]	Gladstone-Dale coefficient
ρ	[kg/m^3]	density
n_o	[-]	refractive index of ambient medium
L	[mm]	length along the optical axis
$\frac{\partial n}{\partial x}, \frac{\partial n}{\partial y}$	[1/mm]	gradients of refractive index
$\varepsilon x, \varepsilon y$	[-]	the angular ray deflection
T_0	[K]	the stagnation temperature
T_n	[K]	Temperature at the nozzle
γ	[-]	The ratio of specific heats
ρ_o	[Bar]	Stagnation Pressure
ρ_n	[Bar]	Pressure at the nozzle exit
$\dot{M}$	[kgm/s^2]	Momentum flux (of jet)
Z_t	[m]	Jet penetration length
Γ	[-]	Jet penetration constant
t	[s]	time
ρ_r	[-]	Ratio of nozzle exit plane density and chamber gas density

Abbreviations

E.G.R.	Emissions Gap Report
CO_2	Carbon dioxide
PEI	Piezoelectric injector
IP	Injection Pressure
CP	Chamber Pressure
ICEs	Internal combustion engines
FC	Fuel cell
NOx	Nitrogen oxides
H_2	Hydrogen
CH_4	Methane
O_2	Oxygen
H_2O	Water
He	Helium
HHV	Higher heating value
LHV	Lower heating value
IC	Internal Combustion
SI	Spark ignition
DF	Dual fuel
CI	Compression ignition
DEE	Diethyl ether
DI	Direct injection
LED	Light emitting diode
M_a	Mach number
PFI	Port fuel injection
EGR	Exhaust gas recirculation
SH	Single hole
HC	Hollow cone
SOI	Start of injection
PR	Pressure ratio
ASOI	After start of injection
SULEV	Super Ultra Low Emission Vehicle
GDI	Gasoline direct injection
EU	European union
$PM_{2.5}$	Particulate matter (with a diameter of 2.5 μm or less)

1. Introduction

We are lagging way behind in the race of time for fighting against global warming. Every 1.5°C rise in temperature has a possibility of us losing around 70% of the coral reefs! Even worse, rise in 2°C and we might end up losing 99% of the reefs. Similarly, insects that are vital for pollination could lose half their habitat at the 1.5°C rise mark. But the number of losses in habitat becomes thrice if it reaches the 2°C mark. And of course, there are many such worse effects for all the species on this planet if the climate crisis is not taken seriously and dealt with in a state of emergency. So what should be done? It is estimated that to prevent a temperature rise of 1.5°C mark, emissions should be reduced every year by at least 7.6% from this year until 2030 (E.G.R. 2019) [1]. The more it gets delayed to fail to reach this target, the cost and difficulty level to tackle this problem goes up. So which are the biggest offenders of global warming? [2]

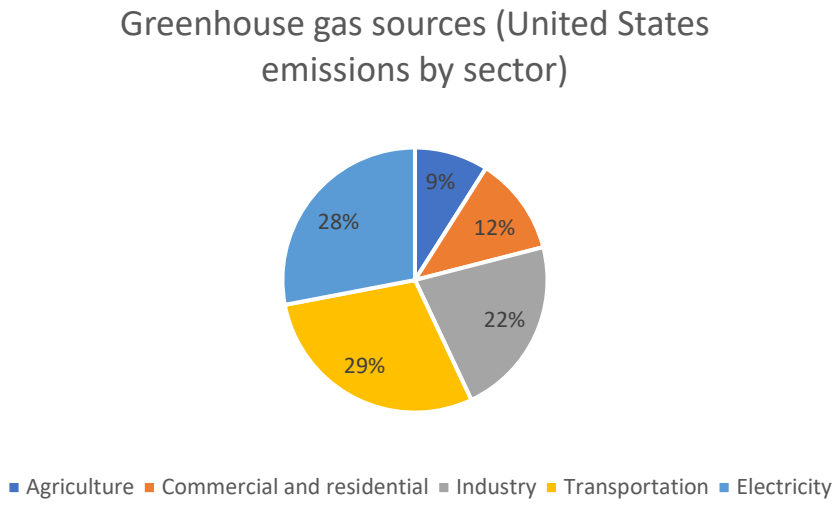

Figure 1.1. Total greenhouse gases emissions in 2018 from different sectors equivalent to 6,677 Million Metric Tons of CO2 (independent rounding off of percentages). *[3]*

Human activities have accounted for greenhouse gas emissions amongst which CO2 accounts for 64% of man-made global warming gas. It is currently 40% higher in concentration compared to the pre-industrialization era. Other greenhouse gases are currently in much smaller quantities (Methane 17% and nitrous oxide 6% amongst others) and they trap heat more effectively than CO2 (sometimes a thousand times stronger). [4]

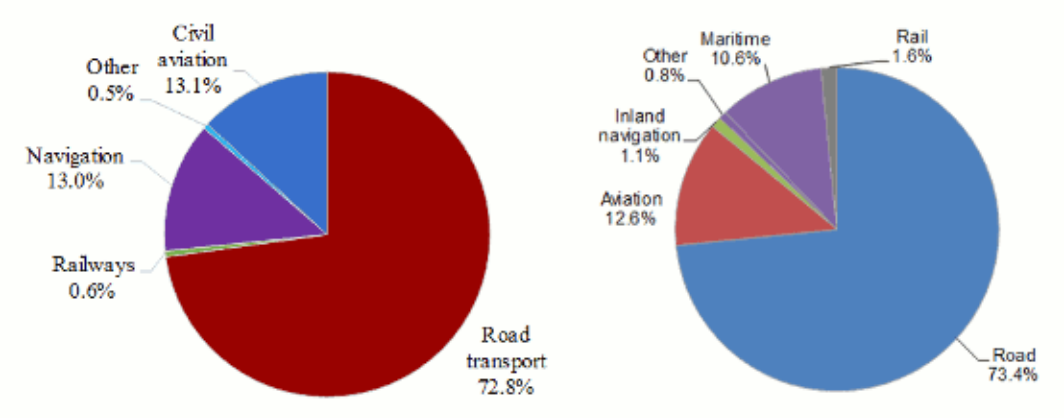

Figure 1.2. Emissions of greenhouse gases in Europe in 2014 by different modes of the transportation sector. [4]

As we can see in the Figure 1.2. above, transportation is the biggest contributor in global warming in two major contribution lands of global warming offenders i.e., US and Europe.

In the EU itself, road transportation accounted for around 72% of the emission in 2016, and amongst that, cars were the biggest contributor followed by heavy-duty trucks and then light-duty trucks. Emissions from automobiles are currently a dominant source of air pollution representing 70% of carbon monoxide, 41% of oxides of nitrogen, 38% of hydrocarbon emissions globally. In addition, 25% of the man-made CO_2 emissions globally add to the greenhouse effect, which results in global warming. 23% of the EU's total CO_2 emissions and more than 30% of NOx in the EU come from road transportation along with roughly 12% of $PM_{2.5}$ emissions. [5]

Currently, the majority of these vehicles use conventional fuels such as petrol and diesel. Transportation still being one of the major emitters of greenhouse gases, there have been many studies, especially in the last few years for alternative fuels used in CI engines. Petroleum-based fuels not only cause air pollution but also they might get extinct shortly. Good alternative fuel to this conventional fuel would be cost-efficient, easily available, and environmentally friendly. Hydrogen is one of the potential fuels since it does not have carbon; hence, the formation of hydrocarbon, carbon monoxide, carbon dioxide during combustion can be completely avoided; however, traces of these compounds may be formed due to the partial burning of lubricating oil in the combustion chamber [6] [7].

As seen in Figure 1.3., nations like the US still emit around 22% of emissions from industry and 27% in electricity. But hydrogen has the potential to replace natural gas which is used for household heating. To transition from existing infrastructure to a hydrogen economy involves a lot of money and it would take time to make such a big change. Although the use of hydrogen in ICE is possible even with comparatively minor modifications in the existing technology relating to the manufacturing of ICEs up to even distribution of hydrogen [6]. It might also be possible to first use methane and then transition to hydrogen economy [8]. Hydrogen use is found to have a better performance compared to electric vehicles or even vehicles using conventional fossil hydrocarbons. Moreover, it is found that hydrogen use is safer compared to conventional fuels [9].

Hydrogen is a very good alternative fuel to reduce the burden of greenhouse emissions. Hydrogen use in commercial vehicles so far can be potentially achieved either by internal combustion engines (ICEs) or by fuel cell (FC) vehicles. Emissions created by the use of hydrogen are found out to be much better for the environment than the emissions obtained by conventional fuels because CO_2 emissions can be dramatically reduced but the issue of emissions of nitrogen oxides (NOx) do exist for ICE vehicles. Although this problem can be solved by optimizing the combustion process. Hydrogen is nowadays seen to be used in industries such as steel-producing industries, but the full potential of the use of hydrogen is not being met.

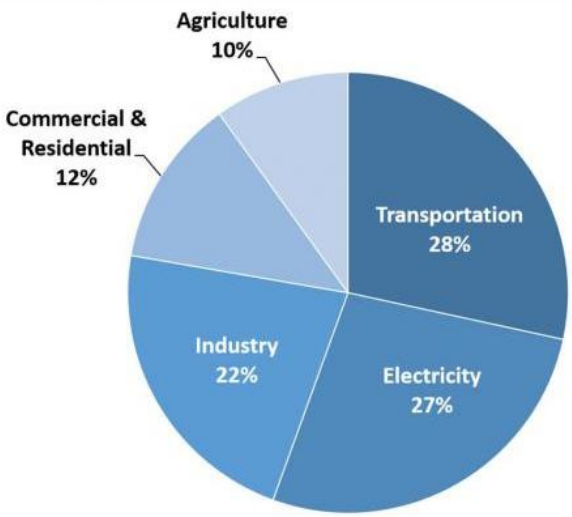

Figure 1.3. Total greenhouse gases emissions in the U.S. in 2018 from different sectors equivalent to 6,677 Million Metric Tons of CO_2 [10]

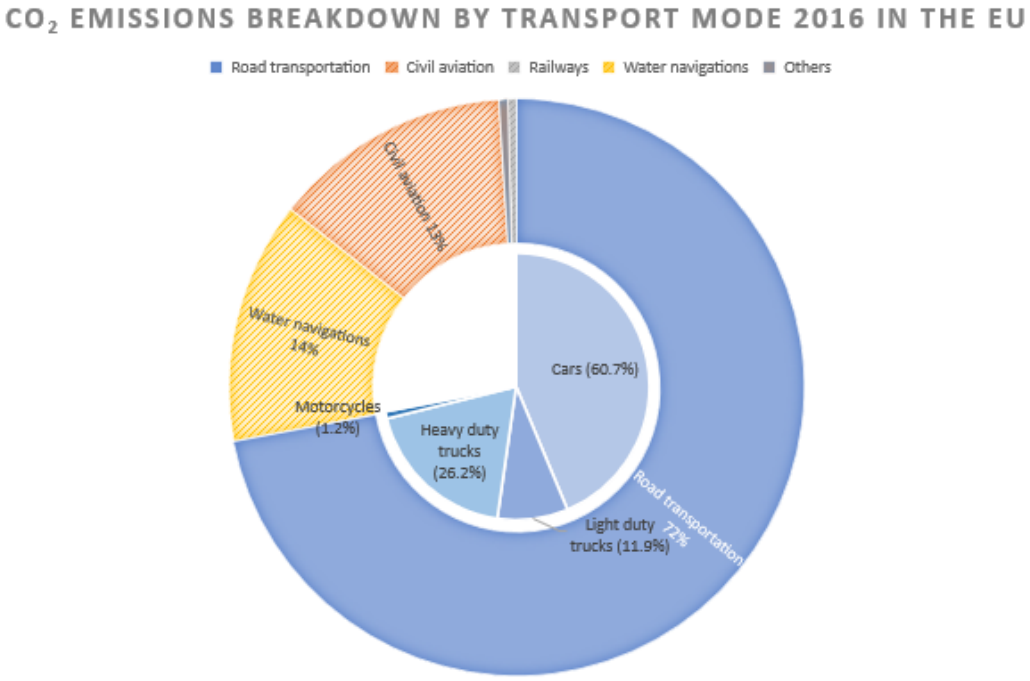

Figure 1.4. Cars account for 60% of transport CO_2 emissions [11]

1.1. Properties of hydrogen

Hydrogen is a non-toxic, environmentally neutral gas for Earth which means that it does not cause harmful effects on the Ecosystem of the earth.

H symbol for hydrogen comes from the Latin name hydrogenium, but it was first termed by a French chemist Antoine Laurent de Lavoisier using Greek words “hydor” (water) and “genes” (producing) in 1787. It is the first element of the periodic table with the lowest atomic weight of 1.008 grams per mol (g/mol) and is simplest in composition. It has a positively charged proton in its nucleus and one negatively charged electron in its orbit. There are three most stable types of isotopes of Hydrogen. Amongst those, the most common (99.985% of all available Hydrogen) is ordinary or light hydrogen called 1H (protium). The other two with additional neutrons are heavy hydrogen (2H) or deuterium (D) which is twice as heavy as protium and super-heavy hydrogen (3H) or tritium (T) which is thrice as heavy as protium. Atomic hydrogen does not occur at standard temperature and an atmospheric pressure of 1.013 bar or in other words, it occurs only in molecular forms. Molecular hydrogen (H2) weights 2.016 g/mol. According to the Los Alamos National Laboratory, hydrogen is the most abundantly found element in the universe (90%). Hydrogen is nowadays considered to have the potential to be a green and clean fuel source on Earth.

1.1.1. Physical Properties

Hydrogen having low molecular weight and high molecular velocity can penetrate through even very small spaces and occupies the given volume rapidly. Although one of its drawback is hydrogen is very prone to leakages, if ventilation is good, or if it is used in open spaces, it flushes out quicky without any damage. Similarly, Hydrogen has less interference with the background compared to other gases like Helium which stick to surfaces more easily than Hydrogen. This is a desired property of Hydrogen especially for testing as there are lesser gross leaks or residual gas in tested objects. Viscosity of air is higher than Helium and viscosity of Helium is higher than Hydrogen. Hydrogen/nitrogen mixtures have higher viscosity than hydrogen, but still lower than that of air. Also, Hydrogen, Helium and Methane are gases lighter than air.

Table 1.1 : Properties of Hydrogen and Methane (8)

	Hydrogen	**Methane**
Molecular formula	H_2	CH_4
Molecular weight	2.016	16.043
Density of Gas at NTP, kg/m^3	0.08376	0.65119
Temperature to Achieve NTP Neutral Buoyancy in Air (1.204 kg/m^3),K	22.07	164.3
Phase at room temperature	Gas	Gas
Melting point	–259.34 °C	-182 °C
Boiling Point	–252.76°C (20.3 K)	111 K
Stoichiometric volume fraction in air,(vol %)	29.53	9.48
Limits of flammability in air, (vol %)	4-75	5.3-15
Auto ignition temp. K	858	813
Flame temp in air K	2318	2148
Minimum energy for ignition in air, J	0.02	0.29
Burning velocity in NTP air, m/s	2.6-3.2	0.37-0.45
Diffusivity in air, cm^2/s	0.63	0.2
Percentage of thermal energy radiated	17-25	23-33*
Normalized flame emissivity	1.00	1.7*
Equivalence ratio	0.1-7.1	0.7-4*
Calorific value (kJ/kg)	150000	50000
Flashpoint	< –423 ºF (< –253 ºC; 20 K)	–306 ºF (–188 ºC; 85 K)
Autoignition Temperature	1085 ºF (585 ºC)	1003 ºF (540 ºC)
Octane Number	130+ (lean burn)	125
Vapor Density (at 68 ºF; 20 ºC, 1 atm)	0.005229 lb/ft^3 (0.08376 kg/m^3)	0.0406 lb/ft^3 (0.65 kg/m^3)
Liquid Density (at normal boiling point, 1 atm)	4.432 lb/ft^3 (70.8 kg/m^3)	26.4 lb/ft^3 (422.8 kg/m^3)
Specific Volume (at 68 ºF (20 ºC) and 1 atm)	For gas: 191.3 ft^3/lb (11.9 m^3/kg)	
Specific Volume (at –423 ºF (–253 ºC) and 1 atm.)	For liquid: 0.226 ft^3/lb (0.014 m3/kg)	
Maximum flame velocity	346cm/s	43cm/s
Lower heating value (mass)	120.0 MJ/kg	45.9 MJ/kg
Lower heating value (volume)	10.1 (g) MJ/m^3	35.2 (g) MJ/m^3

1.1.2. Fuel properties of hydrogen

Calorific value

Complete combustion of fuel leads to release of energy which is the calorific value. Fuel's higher heating value (HHV) and lower heating value (LHV) can be experimentally calculated by energy released when fuel reacts with oxygen. Energy needed to convert liquid fuel into gaseous fuel is "Heat of vaporization" which is the difference between HHV and LHV.

Flash point

A fuel's ability or ease to be converted into gas vapor is the flashpoint. Combustion occurs only in a gaseous state, i.e., liquid fuels like gasoline or diesel need to be converted to a gaseous state to use them as fuels. Although methane and hydrogen are already gases at standard room temperature. Flashpoint is the minimum temperature required for fuel to produce enough vapours so that the mixture can ignite. Although it is not the temperature at which fuel bursts into flames that is the autoignition temperature. The boiling point is always higher than the flashpoint. For gaseous fuels like methane and hydrogen, the flashpoint is irrelevant because it is far below standard atmospheric temperature. But for liquid fuels, flashpoint can be treated as a lower flammability limit.

Flammability

The flame of hydrogen burnt at normal temperature is barely visible in daylight due to its low heat radiation and a high ultraviolet component. Hydrogen is combustible in a very broad spectrum compared to other fuels with its ignition range ranging from concentration of 4 vol% up to 77 vol%. Lean air/hydrogen gas mixtures is possible due to wide ignition limits with hydrogen as a fuel for combustion in internal combustion engines. It is achievable with hydrogen powered engine for stoichiometric combustion air ratio(λ) to attain up to 10, while the modern diesel engines and petrol engines can retain up to $\lambda=2$ and $\lambda=1$ respectively [12]. Although stoichiometric combustion is not as efficient for fuel consumption as lean consumption. With a high autoignition temperature (585°C)and minimum ignition energy (0.02 MJ) which is much lower than other fuels, it makes it a highly flammable gas. Hydrogen has a strong molecular bond and therefore high temperature is needed to separate hydrogen molecule to form new bonds. Atomic hydrogen exists only above 6000 K. Not just high temperature, but catalysts might also be used to form new hydrogen containing molecular bonds. Although at standard temperature, molecular hydrogen is relatively inert. Although a chain reaction resulting in an exponential rise in temperature can be triggered by periodic heating at approximately 600°C of 2:1 hydrogen / oxygen mixture (oxyhydrogen gas). This high heat results in greater volume occupied by water vapour which leads to oxyhydrogen or Knallgas reaction. Because of this reaction, while working with hydrogen, an oxyhydrogen gas sample has to be continuously taken or the addition of oxygen should only be done at the time of ignition. Gas mixtures containing chlorine or fluorine along with hydrogen result in explosive exothermic reactions. Therefore, although hydrogen has excellent combustion and automotive fuel properties, the handling of hydrogen requires extra care and has to comply with all the safety regulations. [12]

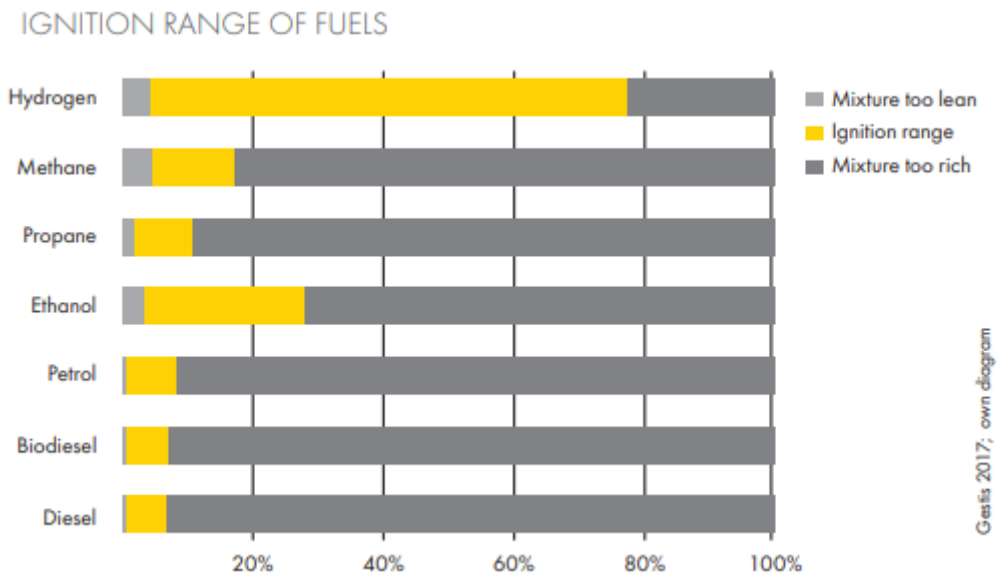

Figure 1.5. Ignition range of fuels

Auto-ignition temperature

The minimum temperature for a fuel too burst into flames to result in a combustion in absence of an ignition source is called as auto-ignition temperature. This temperature is quite high for Hydrogen / air mixture (585°C) which is quite difficult for self-ignition hence it requires an additional source for ignition.

Electro-conductivity

Hydrogen carrying equipment must be properly grounded because hydrogen has low electroconductivity which can result in sparks.

Octane number

The ability of a fuel to resist knocking in an internal combustion engine is described by its octane number. Knock occurs when the local temperature exceeds the autoignition temperature. It is a secondary detonation that occurs due to heat build-up in any part of the combustion chamber after fuel ignition. Due to a very high octane number of Hydrogen, even in very lean conditions, it is very resistant to knocking.

Ignition energy

The amount of energy supposed to be applied to a fuel to ignite it is called as ignition energy. This energy should be higher than the autoignition temperature and be of sufficient duration for fuel to vaporise and ignite. Flames and sparks are common ignition sources. Hydrogen has a higher autoignition temperature than methane, propane or gasoline along with a low ignition energy required for the fuel to ignite (0.02 mJ). In dry conditions, its enough for hydrogen to get ignition from an invisible spark or even from static electricity created by human body.

Quenching gap

The ability of flames in internal combustion engines to get extinguished is called as the quenching gap. It is the distance between the cylinder wall and the flame when it gets extinguished due to heat losses. The quenching gas of hydrogen is much lesser than that of other fuels such as gasoline which makes hydrogen difficult to quench or extinguish compared to gasoline flames. It also increases the chances of backfire.

1.1.3. Safety

Asphyxiation

Minimum level of oxygen required by humans to breathe is 19.5% [13]. Oxygen deficiency in low levels can cause breathing difficulties, disruption in mental functioning leading to diminished alertness or faulty judgement, fatigue etc. More harmful effects can include vomiting, unconsciousness, coma and even death amongst many other effects. In a small, poorly ventilated area, hydrogen leaks possesses a greater threat of asphyxiation due to leaks. Although very small leaks, if ventilated properly do not have any impact as rate of diffusivity for hydrogen is very high. Dangers of hydrogen in open areas is almost negligible due to its high buoyancy and diffusivity. Inhaling hydrogen is extremely dangerous not only because of its asphyxiation, but also considering it's flammable nature in closed space.

Leakage

Hydrogen is one of the smallest molecular size element (Helium being the smallest), it can easily seep through even smallest spaces which other gases might not be able to. This is also a reason why it is so difficult to store hydrogen. Liquid hydrogen is also difficult to store due to its low boiling point and hence it can easily evaporate. Hydrogen leaks possess a fire threat. However, due to high buoyancy and diffusivity, fire hazard is localised and gets dispersed pretty quickly especially in well ventilated areas. This actually makes it much safer to use as a fuel in vehicles because traditional fuels like gasoline or diesel, if they catch fire, they spread laterally and they evaporate very slowly which results in a prolonged fire. Propane gas has higher density than air and hence it can accumulate in lower areas and it diffuses slowly which can also result in an explosion in worst scenarios. Although methane is lighter than air but still it isn't as light as hydrogen so its dispersion rate is in between that of hydrogen and the conventional fuels.

Small leaks caused by Hydrogen often times have negligible effect due to presence of air currents from the atmospheric wind, slow motion of the vehicle or also because of radiator fan movement. Hence the effect of small leakage of Hydrogen and it's buoyancy, and diffusion effects in atmospheric air is often diminished. This property of Hydrogen actually reduces the risk of hire hazard. Although to use Hydrogen as a fuel for vehicles, special care should be taken in designing the fuel system so that it is capable of dispersing the leaked Hydrogen without any hindrance to functioning of the vehicle along with providing dedicated leak detection system for maximum safety.

If hydrogen seeps through leaks, it can possess a danger of catching a fire

- A mixture of H_2 and O_2 when heated creates water vapour(H_2O). While this process takes place, somewhere along the line, due to the generation of even more heat, the surrounding gases may get ignited if they are in high concentration. And if this process propagates, it may lead to an explosion.
- If hydrogen is less than 4 % in air, then it doesn't have the potential to create enough heat to ignite surrounding gases.
- Now, if the hydrogen concentration in air is in between the range of 4 % -12 %, and if there is a system to prevent heat loss from dissipation, then combustion can take place. Note that the condition for hydrogen explosion is only if the combustion propagates spontaneously. Just because concentration of hydrogen exceeds more than 4% is not a sufficient criterion for explosion. But if concentration is more than 18%, then propagation of combustion in air is very quick. And if this speed exceeds the speed of sound, then it results in a bang or detonation. For concentration more than 75%, there won't be any ignition due to lack of sufficient Oxygen.
- Up to 5.7% H_2 and around 95% N_2 mixture in air is non-flammable as either there is very less hydrogen or very little oxygen. But 10% H_2 and 90% N_2 mixture is classified as flammable according to ISO10156 and hence used in industries in controlled conditions. [14]

Hydrogen embrittlement

If metals when exposed to Hydrogen show "embrittlement" then this phenomenon is termed hydrogen embrittlement. It can cause leaks, cracks, and ultimately failure in metallic and even non-metallic components. The exact cause of hydrogen embrittlement is unknown but it's known to be possible due to the concentration of hydrogen present, susceptibility of the material to hydrogen embrittlement, and stresses involved. Factors such as pressure, temperature, the grain size of metal, moisture content, microstructure, and heat treatment are also thought of having an impact on this phenomenon. [15]

1.2. Goal and scope of thesis

This master's thesis gives information on the use of hydrogen as an energy carrier and its use in IC engines or spark ignition (SI) engine with direct injection (DI), but also it gives data about methane and it intends to give an insight on how to bridge the present infrastructure to the hydrogen economy. In this thesis, hydrogen and methane jets are studied using an optical technique of schlieren imaging. Furthermore, these jets are analyzed using image post-processing to get comparative data.

2. Theory and background

2.1. Hydrogen use in I.C. engines

It is now possible to use hydrogen as a single fuel in an SI engine. The problem of using hydrogen as a fuel in SI engines is, if the compression ratio is low, brake power is decreased whereas an increase in brake power causes knocking. Hence, use H_2 in a CI engine along with an ignition source is a much better strategy. Bi-fuel or dual fuel hydrogen engines at part load or no-load running at lean mixtures offer increased thermal efficiency along with reduced NOx emissions. [16]

Using H_2 in DF mode along with diesel in internal combustion (IC) compression-ignition (CI) engine have numerous advantages like improvement in H/C ratio of charge. Infact, uniform mixture and good combustion can be obtained by using hydrogen along with air-fuel mixture using diesel, Szwaja et al. (2009) [17] [18]. Additional benefit obtained during combustion using this is lesser emissions of unburnt hydrocarbon, carbon monoxide and carbon dioxide.

Hydrogen has a high self-ignition temperature which makes it difficult to be used as a sole fuel. To use H_2 in ICE engine, spark plug or glow plug is needed. Alternatively, H_2 can be used in a DF mode along with diesel which acts as an ignition source to initiate combustion. Such engines have higher thermal efficiency, decreased fuel consumption and reduced NOx emissions as they can function at leaner equivalence ratios at part loads. NOx emissions is a major known concern for H_2 operated DF engines which can be reduced using EGR (exhausted gas recirculation) , Saravanan et al. (2009), [17] [18]. Exhaust gases are reused in EGR which reduces oxygen concentration which reduces NOx emissions. Water can also be injected in combustion chamber to prevent knocking and pre-ignition. Water decreases the combustion rate by cooling and diluting the charge. Unfortunately, both these methods have disadvantages of reduced volumetric efficiency, Korakianitis et al. (2010), [17] [19]. By converting a conventional diesel engine into H_2 DF mode can potentially operate at 38% of full-load energy substitution without having adverse effects on power or efficiency [17] [20] [21].

2.1.1. Direct injection of hydrogen in cylinder

To use H_2 in ICE, at the end of compression source, pressurized H_2 can be directly injected into the combustion chamber. As, H_2 has high diffusivity, it instantaneously catches flames. In a DF mode, diesel or spark plugs can act as ignition source. H_2 induction / injection into manifold has a negative impact of power drop. This can be completely eliminated by In-cylinder direct injection of Hydrogen. Idling or part load conditions can slightly reduce the efficiency of engine. This is considered as the most efficient way of injecting H_2 in cylinder. 20% higher power output is observed in DI H_2 engine compared to gasoline engine and 42% power increase is observed using a carburettor [22]. Double power output can be achieved using DI strategy for H_2 in CI engine compared to same engine using a pre-mixture strategy

for fuel injection. This is because H_2 has higher stoichiometric heat of combustion per standard kilogram of air (approximately 3.37 MJ for hydrogen compared with 2.83 MJ for gasoline) (Antunes 2009) [23]. Since H_2 is not injected using manifold in this method, there is no question of pre-ignition in intake manifold, but there is still a possibility of occurrence of pre-ignition in the combustion chamber. But, since there is reduced timing for mixing of air-fuel mixture, it can be non-homogenous, Masood et al. (2007). [17] [24]

2.1.2. Why dual fuel?

Dual fuel engines are comparatively cost-effective along with considering the fact that they are better for the environment. Conventional diesel engines are compression ignition engines that do not operate on spark plugs, i.e., either the fuel itself is used for ignition or a pilot fuel can also be used for ignition in the combustion chamber. Due to this fact, alternative fuels can be used in these types of dual fuel engines which do not involve much of any infrastructure change. They run on the same principles as any diesel engine but, it enables us to use a much cheaper and/or cleaner fuel.

2.1.3. Combustion anomalies

Abnormal combustion

Combustion anomalies such as surface ignition and backfiring as well as auto ignition can occur due to wide flammability limits, low required ignition energy, and high flame speeds which can result in undesired combustion, Verhelst et al. (2009). [17] [25] [26]

Pre-ignition

Low ignition energy and wide flammability limits of hydrogen can often cause pre-ignition. Pre-ignition can cause a mixture to burn in compression stroke. This results in a rise in temperature in the combustion chamber which can result in a hot spot causing another pre-ignition in the next cycle, Verhelst et al. (2005). The process continues until pre-ignition occurs in intake stroke and causes backfire. As minimum ignition energy is dependent on equivalence ratio, when hydrogen-air mixture approaches stoichiometric levels, pre-ignition gets more dominant. Increased engine speed and engine load lead to higher gas and component temperatures making pre-ignition more likely. [25] [26]

Backfire

A more dangerous effect of pre-ignition is a backfire. If pre-ignition occurs when the inlet valve is open, the inflamed charge can travel into the inlet manifold putting it at risk of occurrence of a backfire. This phenomenon puts pre-mixed fuel inducted engines at a particularly higher risk as the ignitable fuel-air mix is present in the inlet manifold, Overend et al. (1999). Backfire and pre-ignition are differentiated based on the timing at which they occur, compression stroke, and the position of intake value being closed or open. Backfire results in combustion and pressure rise in the intake manifold which is quite audible and damaging for the intake system. They have a higher chance of occurrence where the mixture approaches stoichiometric conditions and has lower ignition energy. Although there is limited information available on combustion anomalies, it seems that pre-ignition is the cause of backfire and if pre-ignition can be avoided in the first place, there would be a much reduced risk of backfire. Optimizing of

fuel injection strategies in combustion with variable valve timing are research topics in hydrogen engines that can probably deal with some of the anomalies in combustion. [25] [26]

Auto-ignition

Engine knock (a common problem in hydrogen fuelled engines) occurs due to high amplitude pressure waves caused by auto-ignition which is a result of end gas conditions (pressure, temperature, time), this induces mechanical and thermal stresses resulting in damage to the engine. The engine design and properties of the fuel-air mixture also determine the engine's ability to knock. It is a distinct audible sound and can also be detected by oscillations in pressure during combustion. A most common type of knock (detonation knock) occurs due to self-ignition and explosion of the end gas – the unburnt gas ahead of the flame. [25] [26]

2.2. Applications of hydrogen engine

2.2.1. Bi-fuel engines

BMW's recent Hydrogen based 7 bi-fuel is the 7th edition sedan of hydrogen-powered IC engine line up that comes with 6 L V12 engine. It was built at BMW's Dingolfing plant in Germany along with BMW's 5th,6th, and 7 series except for the drive unit like a twelve-cylinder engine that was made in Munich, Germany. BMW's Hydrogen 7th edition comes with two distinct fuel systems to inject gasoline and hydrogen in each of the fuel systems to allow the vehicle to drive on both fuel systems.

One of the fuels gasoline will be injected directly into the internal combustion (IC) chambers whereas hydrogen will be injected into the intake manifold of the suction engine [27]. There are two kinds of tanks provided with the vehicle namely the regular gasoline tank and the latest cryogenic hydrogen tank is placed in the trunk of the vehicle. Out of the mileage range of the two tanks, the cryogenic hydrogen tank has the capacity of 8kg to fill with liquid hydrogen that provides a mileage of 200km whereas gasoline provides of extra 480km mileage [28]. To increase the range of engine speed, a model of hydrogen fuel-based coupled with turbocharger assisted with an electric motor is installed in Renesis engine to increase the performance through forced induction.

Recently, there is another generation hydrogen-based engine that comes with two compressed hydrogen tanks in which each can compress up to the pressure of 350 bar that can drive up to 100 km on hydrogen along with extra gasoline-powered mileage of 550km which comes from the 23% increased fuel efficiency due to the combustion of a mixture of lean and stoichiometric hydrogen contrast to the gasoline action. [25] [26]

2.2.2. Dedicated hydrogen vehicles

BMW has designed and built a customized hydrogen vehicle with a Hydrogen 7 mono fuel system based on BMW's Hydrogen 7 bi-fuel system to demonstrate the potential of emission reduction in a custom-built one on hydrogen. There are some significant variances that have taken place in the BMW customized Hydrogen 7 mono fuel from the BMW Hydrogen 7 bi-fuel namely the expulsion of the gasoline fuel system that includes fuel lines, fuel injectors, fuel pumps, fuel rail, and charcoal filters but the gasoline fuel tank has remained still for the stability of vehicle structure. To avoid parasitic losses vehicle's two pump systems are removed

and equipped with much better catalysts. Finally, the test results achieved emission levels to the fraction of standards of SULEV (Super Ultra-Low Emission Vehicle) for CO and NOx emissions whereas for non-methane hydrocarbon (NHMC) emissions decreased to atmospheric concentration. SULEV is one of the labeling standards to describe the emission level meeting standard prescribed by CARB (California Air Resources Board). SULEV standard vehicles emit 90% lower emissions than the current fossil fuel-run vehicles. Japan has a similar kind of designation with stars and 4-stars fall under the category of SULEV standard. During the FTP-75 test procedure(Federal Test Procedure) of Hydrogen 7, mono fuel system revealed fuel economy was 3.7 kg per 100 km which was equivalent to the 13.8 L of gasoline consumption per 100 km on an energy basis but by highway cycle, it was determined to be 2.1kg per 100 km that was equivalent to 7.8 L of gasoline per 100 km [29].

Since the late 1990s, Ford Motor Company had been assessing the Hydrogen based vehicle design with IC engines and released a hydrogen engine equipped production model named P2000 in the year 2001. Ford Motor's P2000 was a five-member sedan that was equipped with a 2L hydrogen IC engine, improved hydrogen port injection, H_2 gas fuel supply with pressure up to 250 bar, compression ratio of 14.5:1, and triple fuel safety system for sensing the H_2 gas, passive and active elements. This model had met SULEV standards for carbon emissions and increased fuel efficiency to 17.9% compared to gasoline [30]. Ford Motor company also demonstrated a commercially viable fleet of 30E-450 named shuttle buses that were equipped with a 6.8 L Triton engine running on hydrogen. Ford motor's hydrogen-powered shuttle bus aimed for 2010 Phase II heavy-duty standards, comes with a capacity of 8-12 passengers, 4.5-meter wheelbase, and bus weighs around 6373kg that can hold 29.6kg of H2 of pressure up to 350bar onboard providing the mileage of 240km-320km. [31] [32] [33] [34]

2.3. Hydrogen jets

2.3.1. Un-ignited jets

Irrespective of mixture formation strategies or system used, the use of Hydrogen as fuel involves the injection of Hydrogen into the air which consists of several steps. It can involve inducing Hydrogen into the nozzle, flow of Hydrogen from injector tip to intake manifold or combustion chamber, gas jet interaction with surrounding media, and resulting generation of heat and turbulence, mixing, and final combustion of the fuel. It is comparatively easy to inject gaseous fuel into a gaseous medium compared to liquid fuel, but the gas jet flow is completely different and can present challenges in computational modelling of the injection event. Considering choked flow of Hydrogen gas being a nearly perfect gas due to its flow being isentropic through the nozzle, the pressure ratio between upstream fuel-supply pressure, p_k, and back-pressure, p_o, is defined as:

$$\frac{p_k}{p_o} = \left(\frac{2}{\gamma + 1}\right)^{\frac{\gamma}{\gamma - 1}} \quad (1)$$

The critical pressure ratio for Hydrogen is around 0.53 considering its polytropic coefficient, γ approximately equal to 1.4 which requires the fuel-supply pressure to be roughly twice the back-pressure to obtain critical conditions. Usually, injections are sonic with short durations

and high mass flow rates. For the engine control strategy, critical injection conditions are beneficial as injected fuel amount is not dependent on back-pressure at critical conditions. [6]

The principal regions surrounding an under-expanded jet are documented in a simplified model in Figure 2.1. The flow at the exit plane of the nozzle is assumed to be choked, i.e., $M_a = 1$. The gas expands immediately after exiting the nozzle due to the high ratio of exit pressure compared to ambient pressure. The flow consecutively accelerates causing expansion waves and these waves after hitting the boundary reflect as compression waves that combine to form a barrel shape which is an oblique shock structure. This structure encloses a region "zone of silence" having supersonic flow where no entrainment takes place and mass flux is conserved at the nozzle exit. For a pressure ratio i.e., ratio of exit pressure to ambient pressure above approximately 2, the barrel shock then develops into disk-shaped normal shock known as a "Mach disk" and a reflected shock, but at appropriately high-pressure ratios, this process may repeat itself several times in consecutive barrel and shock structures. The shock reflected from the adjacent flow of the Mach disk is supersonic but the flow downstream of the last Mach disk is subsonic. Pressure is thought to be equivalent to that of the surrounding for subsonic flow after the abrupt changes in density after the Mach disk. It is estimated that the ratio of largest length scale and the jet penetration to the smallest length scale and variations of flow inside the orifice is 4000 [35], which results in preventing to analyse the entire process in a single computational mesh which could solve all length scales due to impractical computations.

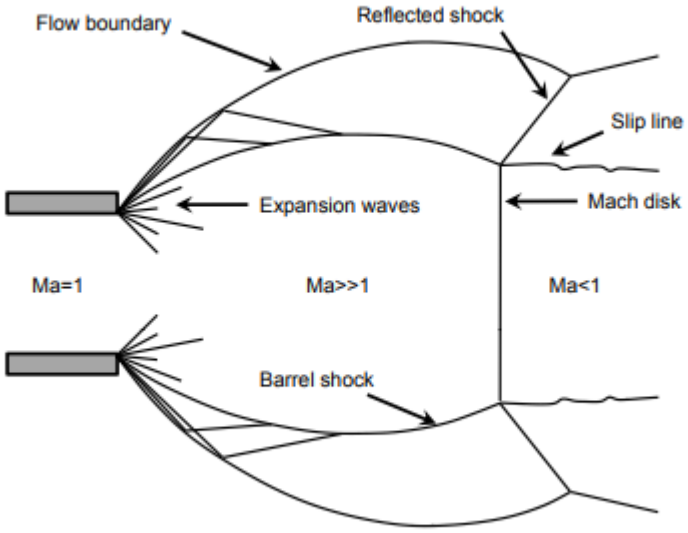

Figure 2.0.1. Principal regions around nozzle exit for an under expanded jet [36]

Different approaches are proposed to solve the above stated problems include dividing the motion problems into sections and scaling theories derived from equations of energy conservation and union of scaling and free jet theories [35] [37] [38]. The goal of the mentioned approaches is to predict injection properties such as blending, expansion, and depth of penetration of the jet. Research until now focuses on predicting general jet characteristics and has involved comparison results from injection test rigs or pressure chambers [3].

Other factors that can have an effect on mixture formation inside an engine include effects between adjoining injections, supply changes, in-cylinder charge motion, injection back pressure, injection jet surface interaction, etc. Experimental studies have done to study the effects of the motion of a charge and especially swirl on the growth of hydrogen jets of shorter duration [39]. Studies have shown that adjacent injection jets collapsed into a single jet injected from the multi-hole nozzle. Also, jets inside a cylinder get attracted to the surface when they are closer to the surface. Both events are a feature of the so-called Coanda effect [40]. Application of optical techniques to study hydrogen jets in hydrogen engine as well as growth and use of simulation tools have resulted in significant progress and helped in better understanding of important processes for blending of un-ignited hydrogen jets [41]

2.3.2. Port fuel injection

The port fuel injection (PFI) strategy for mixture formation for gasoline SI engines either uses intake manifold or the carburetor with use of mechanically or electronically operated injectors. Hydrogen can be injected at the beginning of the intake stroke so as to cool the hot spots or to dilute the left-over gasses [17]. The severity of pre-ignition is reduced due to presence of lesser gases. PFI has higher inlet supply pressure than carbureted or central injection system, although DI injections one has the highest. [36]

DI of Hydrogen is possible by directly injecting the fuel inside the cylinder. But Hydrogen PFI is a well worthy option to research on as the technology is already widely being used and the infrastructure exists for gasoline engine. This existing technology can be easily converted into Hydrogen engine which could prove to be cost effective. The injected volume of air every cycle is kept constant in PFI, and by controlling the amount of injected fuel into the air stream, power output can be controlled, and lean operating can be obtained. Metering of the injected fuel can either be done by varying the injection pressure or by controlling the signal pulse of the injector to change the duration of injection. [36]

It is difficult to ignite combustion in CI engines when using Hydrogen as a fuel in dual fuel mode. External support for ignition can be needed due to this. Di-ethyl ether can be used as an ignition source in such a scenario. Oxygenated based ignition improvers can be used to initiate ignition in these engines. Various options are available such as Dimethoxymethane (DMM), Dimethyl ether, Diethyl ether, and Di-tertiary butyl peroxide, etc. These ethyl ethers prove to be good ignition options to be used for Hydrogen engines. [17]

The maximum theoretical power density for different engines using different fuel injection strategies can be calculated by combining LHV of H_2, stoichiometric air requirement, and the density. Table 2.1. depict the comparison of theoretical power densities for H_2 and CH_4 fuelled engines with iso-octane powered engine as a reference for PFI and DI strategies. There is a dramatic increase in power density obtained for H_2 theoretically while using DI compared to PFI. PFI also tends to encounter problems such as knocking, backfire, and pre-ignition which makes DI a potential strategy. [25]

Table 2.1. Theoretical power densities of hydrogen-, methane- and iso-octane-fuelled engines. [25]

	Hydrogen	Methane	Iso-octane
PFI	86%	92%	100%
DI	119%	100%	100%

3. Experimental setup and methods

3.1. Gas injection system

For the experimental purpose of this thesis, hydrogen is directly injected into the spray chamber using the DI strategy. This strategy is thought to be the most optimum strategy for utilizing H_2 as fuel and hence jet studies are made using this strategy in this thesis. Furthermore, 2 injectors are used to study and compare jet properties in this thesis.

3.1.1. Injectors

In this thesis, two injectors are used i.e., piezoelectric hollow cone injector and single hole injector. The hollow cone injector has been used previously in the same laboratory by two other Master's thesis by Zaira Künsch [16] and by Tapio Laitinen [42].

3.1.1.1 Piezoelectric injector

When pressure is applied on certain piezo electric materials like ceramics, piezo electricity is generated. Reverse process is used to create a precise movement when electricity is applied and this phenomenon is extremely useful in piezoelectric injectors (PEIs) , i.e., in PEIs these materials lengthen when electricity is externally applied to these materials. Also, in absence of electricity, the material comes back to its original shape pretty much instantaneously. This makes these injectors useful for highly precise and super-fast operations of automated fuel injectors for opening and closing purpose. Expansion of one crystal is extremely tiny and hence not visible to the naked eye. An expansion of barely 0.00002 inch occurs when 140 volts electricity is induced on a slice of piezo material which is two-hundredths of an inch thick and this amount of expansion is insufficient to move the pintle of an injector, a part of an injector to seal the nozzle and when opened, used for injection of fuel. Commercially available injectors of these types have hundreds of little piezo slices stacked on each other so as to achieve a desirable expansion. Solenoid operated injectors can also be used but piezo injectors are quieter and more precise than solenoid units but a drawback is that they are more expensive.

For the experimental purposes of this thesis, hollow cone injector used is manufactured by Siemens VDO Automotive (Model no: 1353 7585261-09). It has a rail pressure capacity of 200 bar and is designed for applications based on GDI.

3.1.1.2 Single hole injector

The single hole injector used in this thesis is also manufactured by Siemens VDO Automotive (Model no: 1353 7585261-12) and has a rail pressure capacity of 200 bar. The hole diameter is 0.5 mm Single hole injectors are comparatively easier to model as there is lesser probability of unknown jet-to-jet interaction. Along with other multi-hole types of injectors, even hollow cone injectors can be affected due to such interactions. A schematic representation can be found in Figure 3.1.

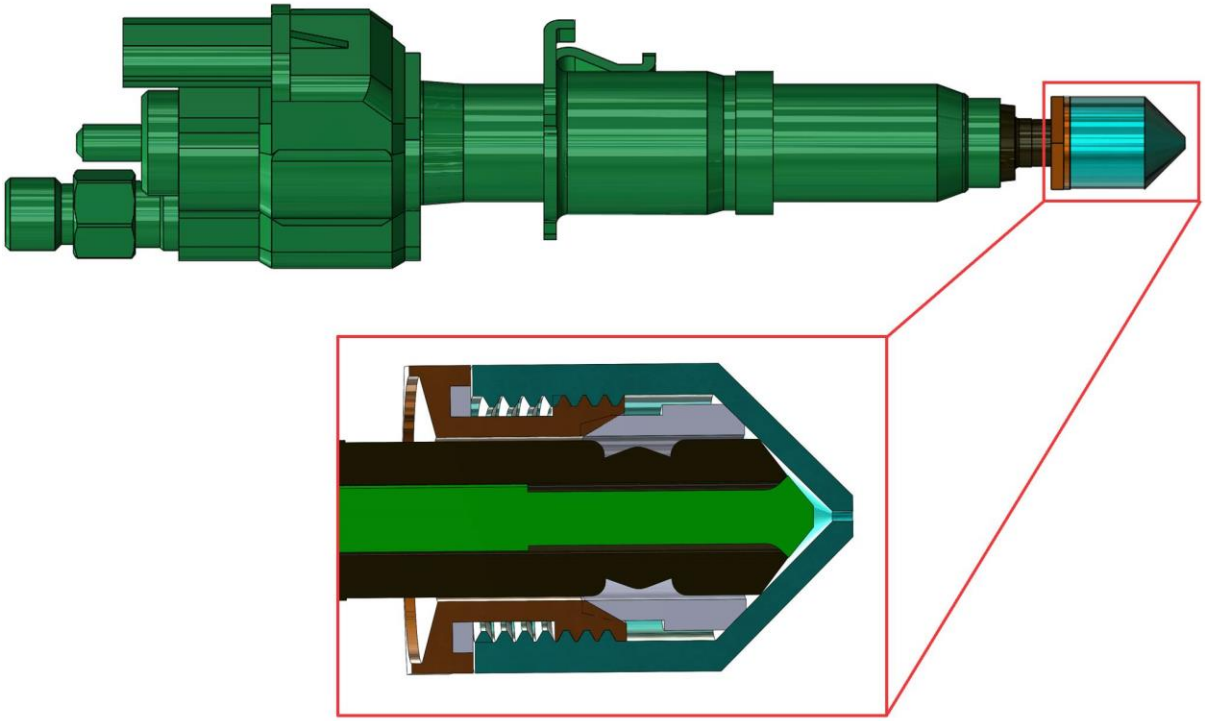

Figure 3.1. Schematic representation of a single hole injector

The actual injectors used for the experimental purposes are shown in Figure 3.2. below.

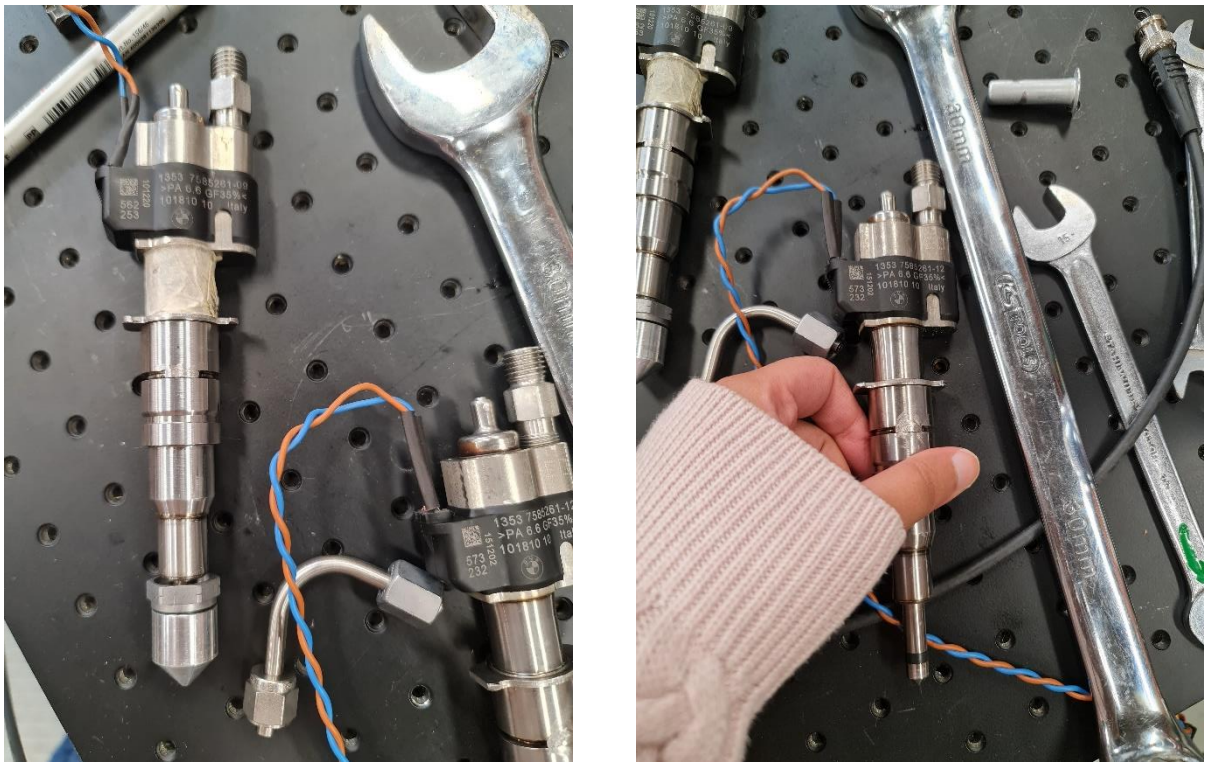

Figure 3.2. Hollow cone piezoelectric injector on the left and single hole injector on the right.

The nozzle exit area can be calculated by the formula

$$A_n = \pi d h_n \quad (2)$$

Now, as we know that the d for the HC injector is 3.44 mm and d for the single hole injector is 0.5 mm, also, needle lift can be determined while experimenting and this can vary according to the applied voltage.

To give a trigger signal to the injectors being used, the Driven Compact RIO DI Driver Module was used. LabVIEW software was used to operate the driver channels using LabView FPGA (Field Programmable Gate Array) card and RT (Real-Time) controller. The injection duration was 5 ms for all the experiments performed in this thesis. There was a simultaneous trigger given to the injector as well as the camera to acquire images at correct timings. For 100 V signal, needle lift was determined to be 24 μm.

3.1.2. Spray Chamber and gas system

The constant volume chamber used for this thesis is shown in Figure 3.3. It has a maximum pressure capacity of 35 bars. It should be note that the position of this spray chamber has been rotated in this thesis wherein vertical spray injections are being experimentally analyze compared to those used in the Master's thesis by Tapio Laitinen, [42] wherein, the spray chamber was positioned in such a way which could hold the injector in a horizontal position. More information about the apparatus used is discussed in the further section.

3.2. Gas visualization system

As the experiments performed in this thesis are non-reactive, the gas used to control chamber pressure is nitrogen which is supplied from nitrogen tanks. A pressure regulator is used to control the pressure of the nitrogen gas. A pressure relief valve is also provided beneath the gas chamber so as to relieve the excess chamber pressure out of the system whenever needed. More details about the gas system is provided in the thesis by Tapio Laitinen [42] as this thesis primarily uses the same experimental setup used during the mentioned thesis with some minor modifications done for acquiring better quality images in Schlieren imagining

Figure 3.3. shows a constant volume chamber with a capacity to withstand maximum pressure of 35 bars. This chamber has a place for injector to be mounted on top of the chamber (note: the chamber was rotated compared to what Tapio Laitinen [42] had used in his Master's thesis.) so as to study vertical jet characteristics. Along with this, there were two optical accesses provided for the chamber covered by 55 mm thick quartz windows. Nitrogen gas was used to control ambient or chamber pressure and Methane, Hydrogen or Helium gases were used to control injection pressure and study their jet characteristics. Furthermore, pressure and temperature sensors were attached to the setup to monitor the experimental conditions and provide data on to the computer.

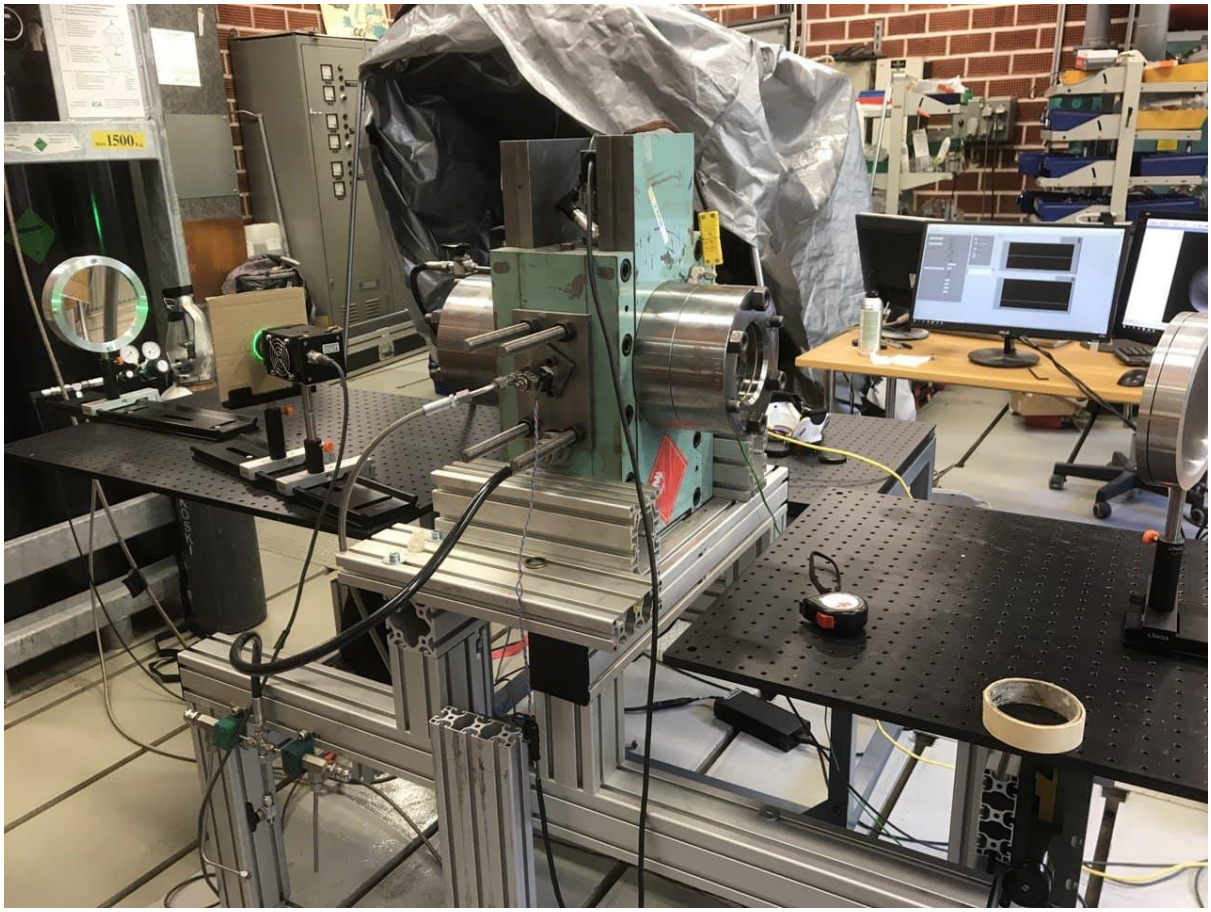

Figure 3.3. Constant volume chamber with optical setup

Schlieren imaging

Schlieren imaging or Schlieren photography is a technique used to visualize the flow of fluids of varying densities.

What it Shows?

Even a single mirror optical setup using schlieren can be used to visualize inhomogeneity in the air due to refraction. These refractions are a result of changes in pressure, density, or temperature of air currents. Using a high-speed camera and a monitor, even changes in air currents can be observed from a candle flame, mixing of cold air into the ambient air from a glass full of ice water, or even to visualize high speed jet injections of gases into the cylinder. This is a technique useful to observe the movement of gas jet inside a cylinder that would otherwise be invisible to the naked eye. Hence using this technique jet characteristics can be studied. Also, one advantage of this technique compared to some other optical techniques is that this method is non-intrusive and does not involve the utilization of a tracer gas which has the potential to distort results.

How It Works?

Quantitative data analysis of jets involving studying of jet properties like depth of penetration, width and area can be effectively studied using this technique provided there is sufficient density gradient between the gases used. Speed of light in different medium is different due to density variations which is similar to optical lenses but with a weaker effect. The formula for refractive index is given below where (c_o) is the speed of light in vacuum and (c) is the speed of light in a specific medium. [43]

$$n = \frac{c_o}{c} \tag{3}$$

In equation below, (n) represents refractive index of a particular medium and (ρ) is the density, k is the Gladstone-Dale coefficient of the particular gas.

$$n - 1 = k\rho \tag{4}$$

Practically, the value of n is almost similar for common gases and variance occurs in third or fourth decimal, but, these variations are sufficient to produce Schlieren effect. In two dimensional Schlieren the angular ray deflection (εx, εy) is [43]:

$$\varepsilon_x = \frac{L}{n_o}\frac{\partial n}{\partial x}, \varepsilon_y = \frac{L}{n_o}\frac{\partial n}{\partial y} \tag{5}$$

Here,

n_o = refractive index of ambient medium
L = length along the optical axis
$\frac{\partial n}{\partial x}, \frac{\partial n}{\partial y}$ = gradients of refractive index

These gradients are perpendicular to the orientation of the knife-edge and the optical axis. Now, if the knife-edge is vertical, horizontal gradients are visible in the imaging plane and vice versa is also true. The gradient in the z-direction is not included here as it is parallel to the optical axis. [43]

Optical Setup

For this thesis, z-type Schlieren is used which includes two parabolic mirrors, a point light source, spray chamber with quartz window, a pin-hole and a high speed camera. Supplementary electronics are provided to so as to trigger the high speed camera and the injector concurrently. A computer is attached to the setup for recording the videos of the jets which would further be used for post-processing the data. The function of the first mirror is to collimate the light beam and the other mirror is used to reflect and focus the light beam. The point light source which is a high power monochromatic (green) H_2 spotlight (using maximum 70 W electricity power) has a round aperture which can be adjusted according to requirement to achieve good Schlieren effects. This light source is focused on a parabolic mirror which collimates the light beam which further passes through the constant volume chamber where jets are sprayed and further analysed. This chamber has a quartz window. Now, once the beam of light passes this camber, it is further focused on another parabolic concave mirror. This light is further reflected to the pin-hole placed in front of the camera where light beam gets cut and then it finally enters the high-speed camera Phantom v2012. This arrangement was selected as it is comparatively easy to implement and can be adjusted to attain required degree of Schlieren effect by adjusting the focal length, mirror positions etc by trial and error method. Use of mirror is better than lenses as light can interact with only one surface resulting in fewer distortions.

The exposure time of the ultra-high-speed camera Phantom v2012 was 10 μs and the frame rate was 34000 with a resolution of 768x768, the injection time was 5 ms. The start of injection (SOI) was determined during post-processing the images on a qualitative basis. The SOI for different cases was found to be different and also it was different with both the injectors used in this thesis.

3.3. Image post-processing

A ready-made code was used to read the acquired images from the videos obtained by high speed camera. These images got converted into a processable format which included information such as number of frames and frame rate.

Convolution method for vectors was used to create sharp and blur images. Now, to obtain an average, mean was made out of these two images to obtain the optimum value. Since a sharp image has to be obtained to determine the boundary conditions so as to obtain the geometrical characteristics of the jet, these images were converted into binary format. To enhance the

background, individual frames were subtracted from previous frame. Subtraction of individual frames were done multiple times throughout the programme to acquire sharper images with reduced noise. Now, the gaps and holes were filled inside the main jet region assuming no holes were present inside the jet area and the area was filled up to acquire boundary conditions of the jet. In the next step, Gaussian filter was used to reduce noise and smooth out the image further more. In this code, appropriate thresholds were also used and they were determined by qualitative analysis. The injector positions were also determined at the beginning of the code by manual method so as to obtain the correct geometrical parameters. As described earlier, subtractions of individual frames were made multiple times to acquire more sharper images. Maximum boundary conditions were determined using the code. Maximum penetration and widths were determined considering boundary pixel data. The jet data for all the gases used along with both the injectors have been further analysed and all the relevant Matlab codes have been presented in Appendix.

3.3.1. Experimental matrix

The data points considered for experimental purposed of this thesis have been presented in the **Error! Reference source not found.**.1. below.

Table 3.1 Data points considered for experimental analysis of gas jets

Gases	Injector Types	Voltage	Injection pressure	Chamber pressure	Number of readings	Ratio
He, H2, CH4	SH, HC	100	40	5	10	8
He, H2, CH4	SH, HC	100	40	10	10	4
He, H2, CH4	SH, HC	100	40	20	10	2
He, H2, CH4	SH, HC	100	50	10	10	5
He, H2, CH4	SH, HC	100	60	5	10	12
He, H2, CH4	SH, HC	100	60	10	10	6
He, H2, CH4	SH, HC	100	60	15	10	4
He, H2, CH4	SH, HC	100	60	20	10	3
He, H2, CH4	SH, HC	100	60	30	10	2
He, H2, CH4	SH, HC	100	80	5	10	16
He, H2, CH4	SH, HC	100	80	10	10	8
He, H2, CH4	SH, HC	100	80	20	10	4
He, H2, CH4	SH, HC	100	100	5	10	20
He, H2, CH4	SH, HC	100	100	10	10	10
He, H2, CH4	SH, HC	100	100	20	10	5
He, H2, CH4	SH, HC	100	100	25	10	4
H2, CH4	HC	90	100	10	3	10
H2, CH4	HC	110	100	10	3	10
H2, CH4	HC	120	100	10	3	10
H2, CH4	HC	130	100	10	3	10

Mostly 10 trials (some cases have 3 trials) have been taken for each case considered as depicted in table 3.1. This means for each case, the average data of all these jets have been considered so as to get optimum results. As shown in Figure. 3.4., 10 trials of jet penetration have been averaged to 1 curve depicting average penetration for that particular case. The ratio obtained here is the pressure ratio or the value of IP:CP.

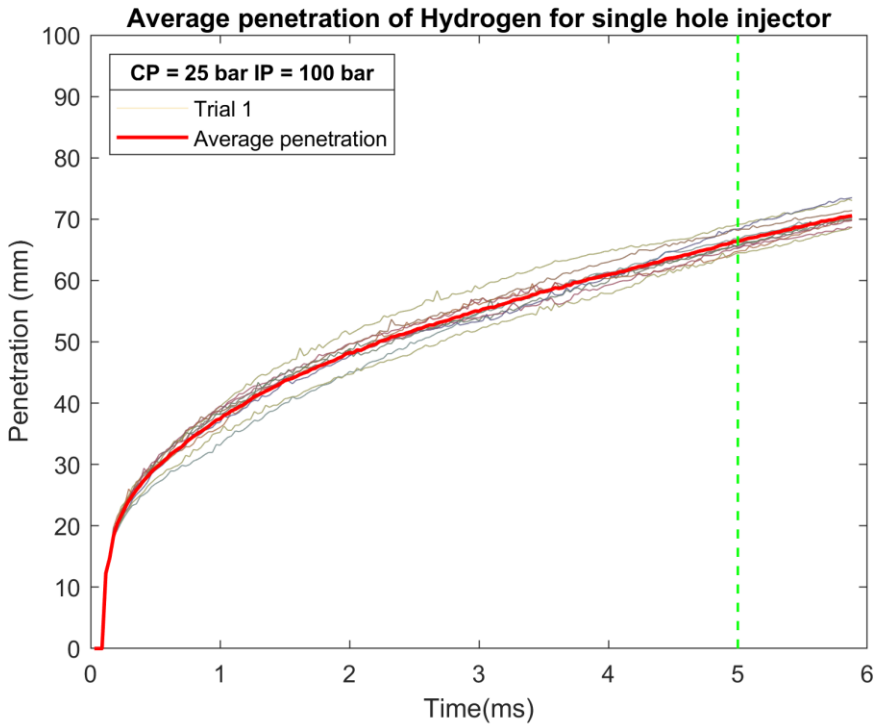

Figure 3.4. Averaged jet value for 10 trails for the case with IP:CP=100:25 bar.

3.4. Operating conditions

For convenience, the flow inside the hose, injector, and through the nozzle is considered to be entropic and unidirectional. An assumption is made that the injection pressure and ambient temperature are considered to be stagnation properties. The HC injector used is of convergent type and the flow is sonic for the considered values of PR. The jets are also underexpanded and hence Mach number (M) is assumed to be 1 at the nozzle exit. For comparison purposes, the equations described here are considered the same as the ones used in the Master's thesis by Tapio Laitinen [42].

Now, the stagnation temperature T_0 is assumed to be same as room temperature and ρ_0 is stagnation pressure. For convenience, we have assumed T_0 to be 22 °C. The ratio of specific heats γ is considered, 1.41 for Hydrogen, 1.667 for Helium, and 1.32 for Methane.

$$\frac{T_o}{T_n} = 1 + \frac{\gamma - 1}{2} M^2 \tag{6}$$

Nozzle exit density can be calculated by the following equation:

$$\frac{\rho_o}{\rho_n} = \left(\frac{T_o}{T_n}\right)^{\frac{\gamma}{\gamma-1}} \tag{7}$$

Formula for momentum flow rate is given as follows:

$$\dot{M} = \rho_n A_n U_n^2 \tag{8}$$

Here U_n is considered sonic as it is the flow velocity at the nozzle. A_n is the area of the nozzle. Density of the gas at nozzle is ρ_n. The real gas densities (density values) are derived from values of McCarty [44].

From thesis by Tapio Laitinen [42] we know that , Theoretical length for jet penetration can be calculated using the formula (9)

$$Z_t = \Gamma \left(\frac{\rho_n}{\rho_c}\, \pi d h\right)^{\frac{1}{4}} (U_n t)^{\frac{1}{2}} \tag{9}$$

This equation suggests that only density ratio $\frac{\rho_n}{\rho_c}$ (along with Un when jet isn't underexpanded) is not a constant. Rest all other values can be considered constants for all the cases considered in this thesis.

4. Results

Results of post-processed images and their analysis is depicted in this section. Jet penetration, right side and left side width of the jets from the centreline along with the jet area are analysed. A co-relation between Hydrogen and Methane jets considering single hole as well as hollow cone injector has been analysed. Different operating conditions such as changes in injection pressure or chamber pressure or changes in voltage have been studied for mentioned gases and injectors and analysed and the results of those have been presented in different sub-sections in the following section. Furthermore for a particular case, Helium gas is also considered to make comparison with Hydrogen as these gases have very similar properties.

Instantaneous jet evolution

A comparison of instantaneous images produced is depicted in Table 4.1. for all three gases using both injectors for PR 04 using high IP and high CP. Using qualitative analysis, a very small change in penetration is seen using HC injector upto 5 ms ASOI. Again, the penetration depth is considerably more for SH injector compared to HC injector using same conditions. General observations such as more tapered jets are obtained for SH injector whereas jets produced using HC injector have a comparatively equal width throughout the length of the jet.

There is a deviation of jet seen to the right side for He using HC injector at 5 ms. This was observed to be the manufacturing defect in HC injector holes causing jet to be non symmetric from where the jet was injected. But manually adjusting HC injector by rotating it to produce more symmetry along the axis of the jet made the results better for 2D analysis.

There are variations in images produced because the LED intensity and the schlieren setup was adjusted according to requirement during the experimental purpose.

Table 4.1. Jet evolution for He, H_2 and CH_4 for IP:CP = 100:25

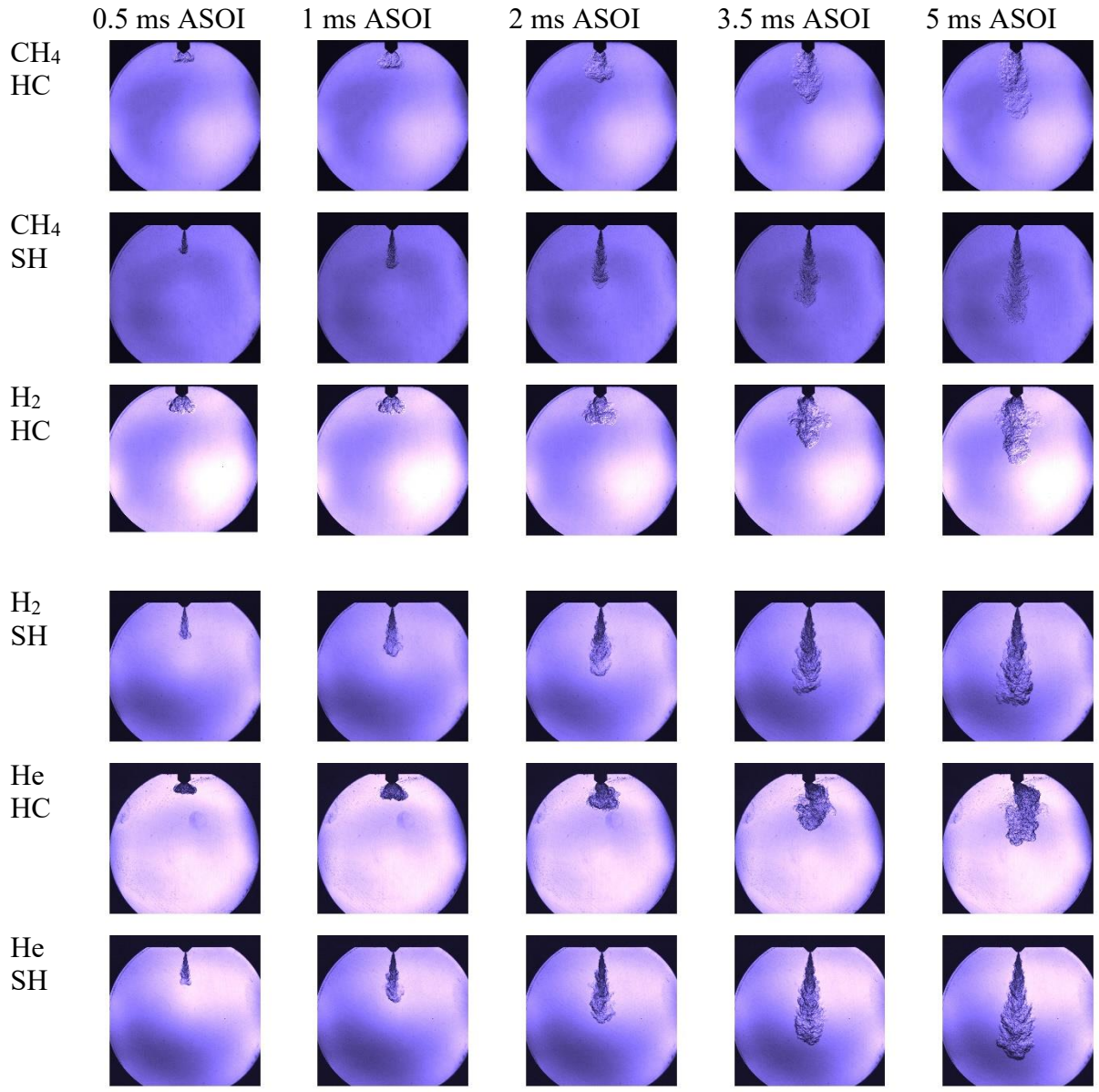

4.1. Jet penetration

4.1.1. Effect of ambient pressure on jet penetration

Figure 4.1 (a) and (b). depicts Methane jet penetration for hollow cone and single hole injectors with increasing chamber pressure as shown. Jet penetration has been observed to be increasing with decrease in chamber pressure. Also the data points of Jet with chamber pressure 5 bar become constant very quickly as the gas tends to occupy the volume of the cylinder for this case quickly. The low chamber pressure cases (i.e., roughly less than 5 bar) have been studied previously by Tapio Laitinen [42] where CP was 1.02 bar and IP was 61 bar. It created a curve of rather constant slope wherein the depth of penetration at the end of injection was somewhat

similar to what is obtained in experimental analysis of this thesis. This is possibly related to the ¼ - power of law dependency on ρr.

Jet penetration for hollow cone injectors can be divided into 2 phases because there is a step observed at around 20 mm penetration for both the gases after which the slope of penetration increases. But for single hole injector, using both the gases, this step is not observed. This step could probably occur in hollow cone injector because of the jet not being fully developed. Also, same injector was used in the thesis by Zaira Künsch [16] wherein it was explained the toroidal nature of the jet at the start of injection.

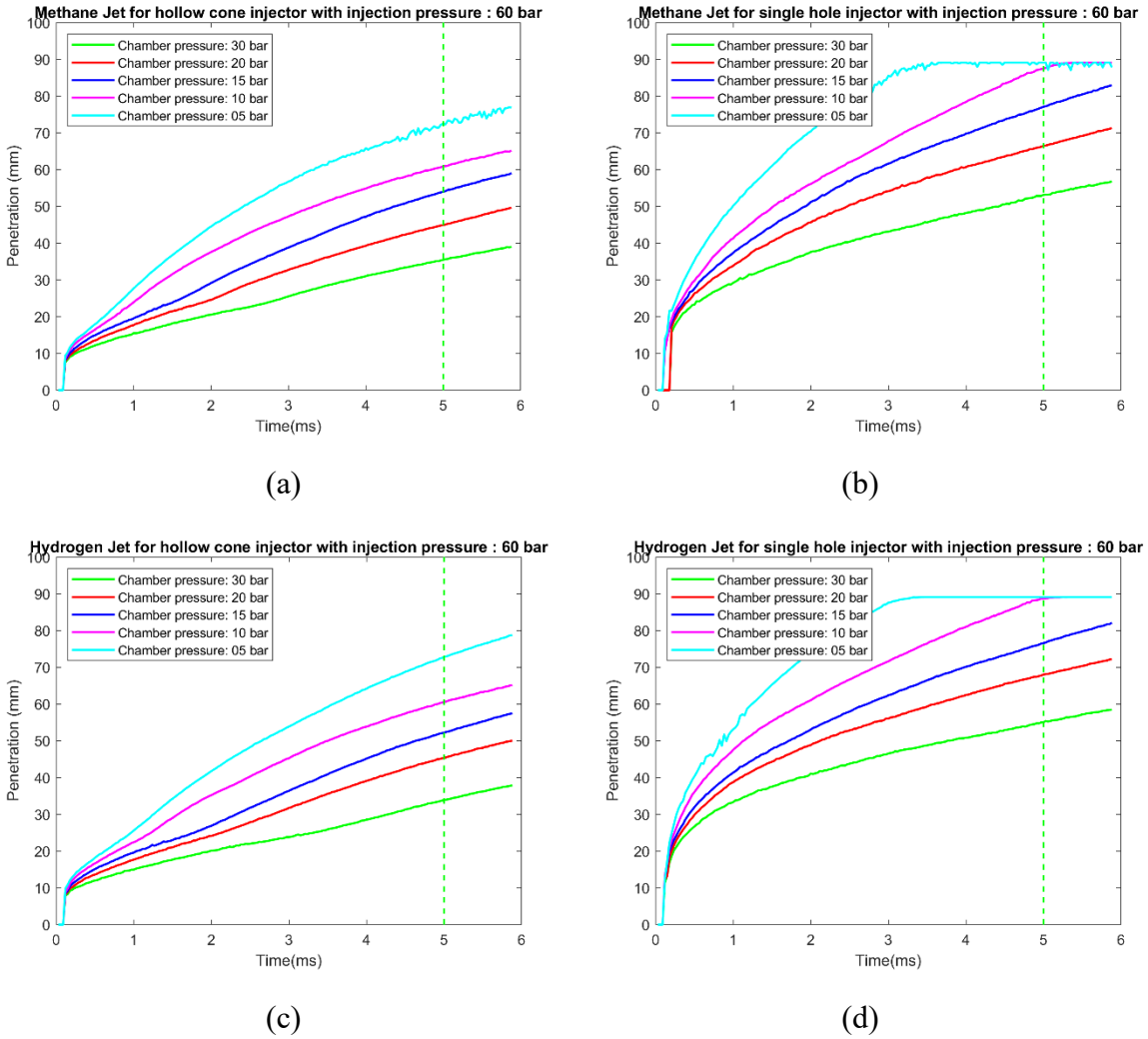

Figure 4.1. Methane and Hydrogen Jet penetration for hollow cone and single hole injectors with injection pressure 60 bar

Similar observation as mentioned above for Methane Jet Penetration has been observed by Hydrogen Jet as well i.e., jet penetration increases with decrease in chamber pressure. Moreover, the slopes of the obtained data for both gases using same injector have been found similar with almost identical penetration depths found when other conditions are kept constant.

The slopes of the curves obtained for both the gases are comparatively more constant for hollow cone injectors than for single hole injector. Jet curves obtained for single hole injector is seen to be gradually decreasing at the end of injection. The penetration is achieved highest for the case of least chamber pressure and the curve becomes constant indicating dispersion of gas in

the cylinder. Also the step observed for HC injectors is not present in the jets obtained by SH injector. The dispersion of the gas is more for lower chamber pressure values at the end of injection.

4.1.2. Effect of injection pressure on jet penetration

In general, we can see that as injection pressure increases, jet penetration increases for both the injectors. Similar observation can be made for Hydrogen jet as shown in Figure 4.2. (c) and (d) below. Also, one observation can be made from the graphs obtained is the rate of increase of penetration gets reduced as injection pressure is increased.

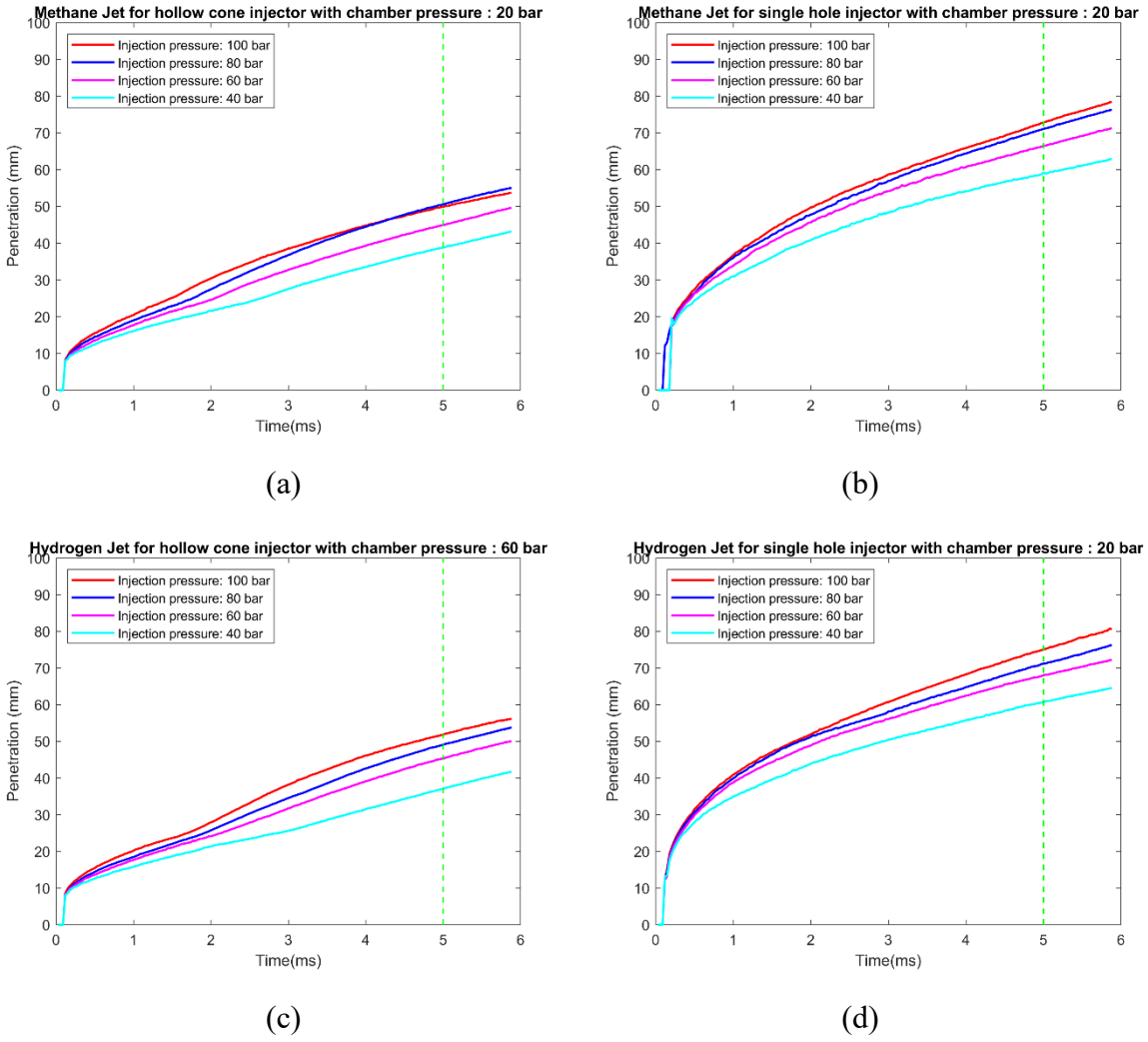

Figure 4.2. Methane and Hydrogen Jet penetration for hollow cone and single hole injectors with chamber pressure 20 bar

Again there is a step observed for jets of both gases emitted by HC injector. This step is occurring somewhere around when jet reaches 20-30 mm penetration. Although the timing at which the step occurs varies for different cases. Apparently the step occurs at around 3-4 ms ASOI for lower injection pressures such as at 40 bar compared to the higher injection pressure of 100 bar where the step occurs at around 2 ms. The rate of growth of curves obtained for both the gases using both the injectors decreases as the injection pressure goes on increasing. At very high pressures, there is a little overlap also seen in these curves obtained. The ¼

dependency on ρr could possibly explain this behaviour as also found out in thesis by Tapio Laitinen [42].

For HC injector the curves can be divided into 3 phases wherein the beginning of the curve has a rapidly increasing slope for under 0.5 ms. From around 0.5 ms to 3 ms depending on that particular case, the slope of the curve gradually increases and falls a little before a step occurs after which the slope increases slightly further and becomes roughly constant.

4.1.3. Effect of constant pressure ratio on jet penetration

Figure 4.3. depicts jet penetration for pressure ratio 04 with varying IP and CP as shown in the figure. It is seen that as the values of IP or CP increases, the jet penetration decreases or in other words, even if the pressure ratio is same, higher penetration can be achieved by lowering the values of IP or CP for both single hole as well as hollow cone injectors and also for Hydrogen as well as Methane gases.

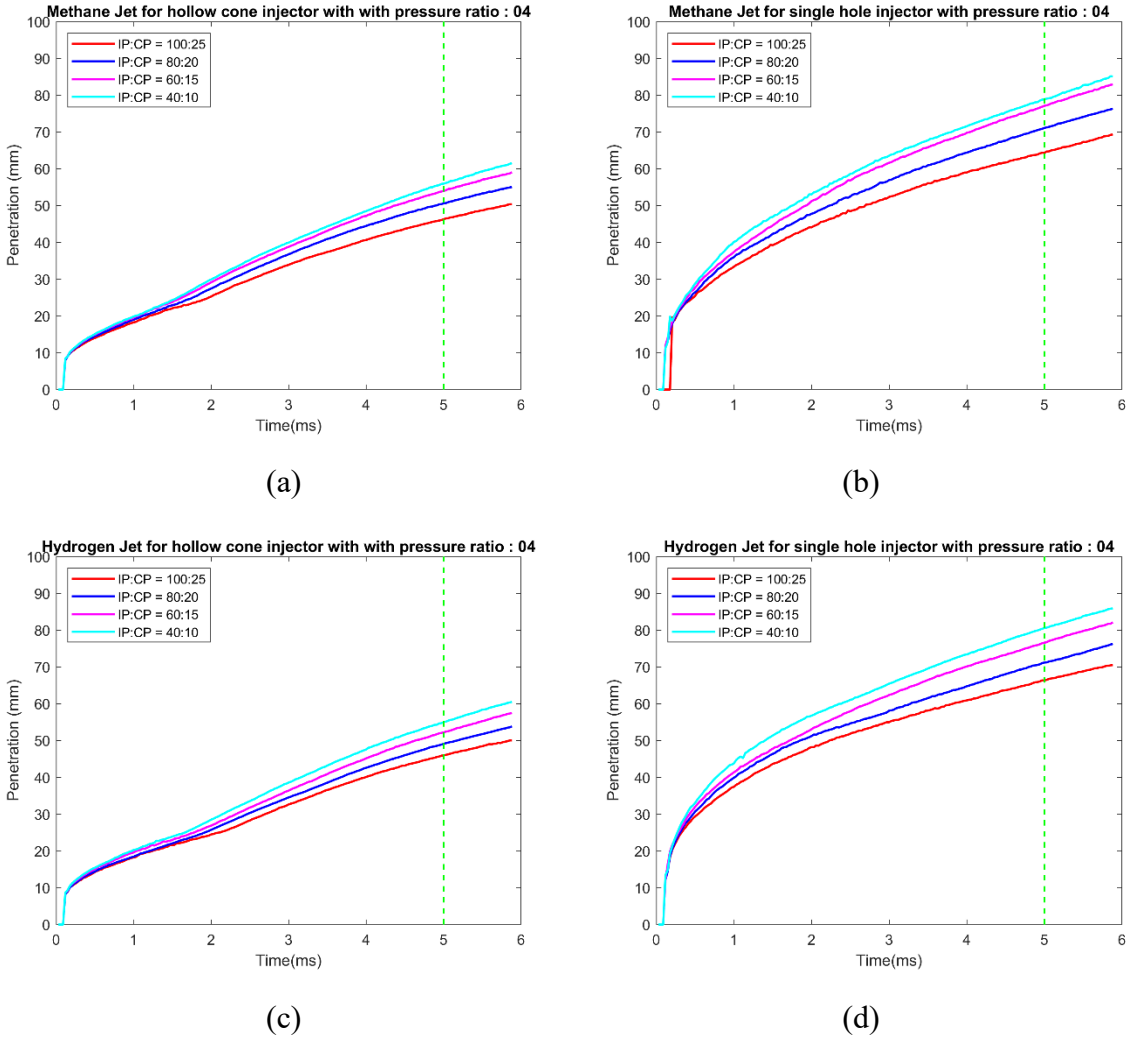

Figure 4.3. Methane and Hydrogen Jet penetration for hollow cone and single hole injectors with pressure ratio: 04

It should be noted that even with change in gas, penetration achieved for both the gases is identical if all other parameters are kept constant. The step formation is also identical for both the gases using HC injector. As the values of IP:CP go on increasing, the growth rate of curves

obtained for penetration go on decreasing. A comparatively smooth curve is obtained for SH injectors where the curve can be divided into 2 phases wherein the slope of the curve increases rapidly at the beginning (i.e., from the start of injection till around 0.5 ms). After which the slope of the curve starts to become constant and then decreases.

4.1.4. Effect of voltage on jet penetration

Figure 4.4. depicts the penetration of gases mentioned for hollow cone injector with CP 10 bar and IP 100 bar. It is evident that for both the gases, penetration increases with increase in voltage but the rate of increase in penetration decreases at higher values of voltage and it is seen to be near identical for both gases for 120 V and 130 V. This is likely to be an effect of needle lift wherein greater needle lift applies greater force which in turn increases the depth of penetration.

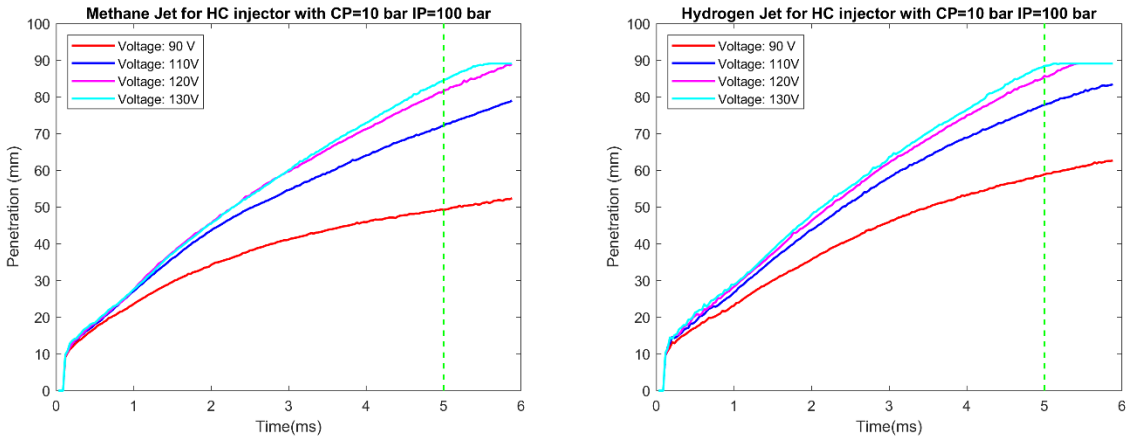

(a) (b)

Figure 4.4. Methane and Hydrogen Jet penetration for hollow cone injector with CP 10 bar and IP 100 bar with varying voltage

4.2. Jet width

4.2.1. Effect of ambient pressure on jet width

To measure the width, the distance between the centreline to left and right side of the jet have been separately considered here in this thesis. In general, considering both right and left sides for hollow cone as well as single hole injector, its evident that the width of the jet increases with decrease in ambient pressure while keeping injection pressure constant. Although the rate of increase in width with changes in ambient pressure is greater for single hole injector compared to hollow cone injector. This trend is evident in both the gases observed. The fluctuation in the curve is due to constant mapping of maximum width points for jet using a Matlab code.

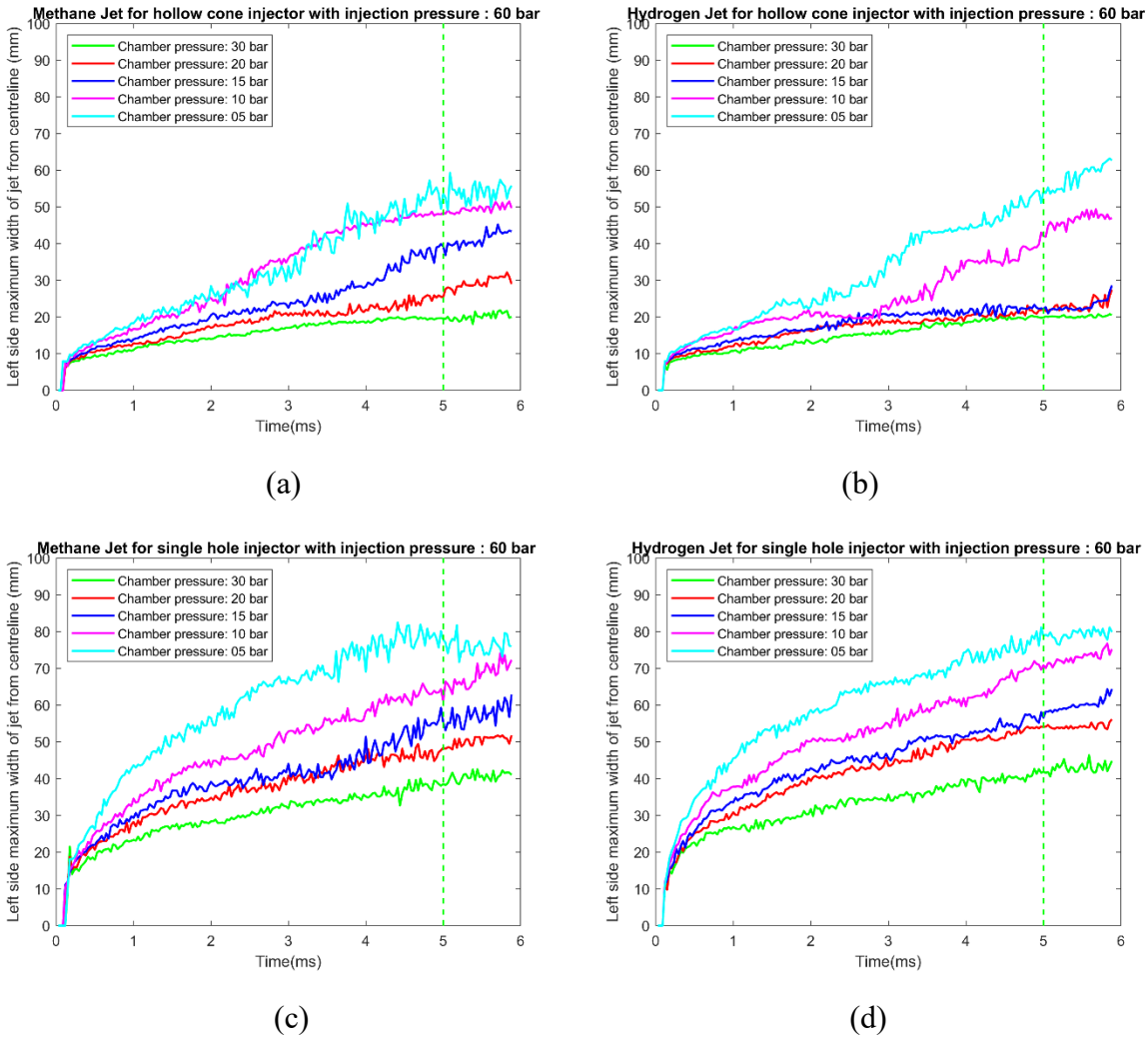

Figure 4.5. Methane and Hydrogen Jets left width for hollow cone and single hole injectors with injection pressure 60 bar

Considering same conditions along with using same HC injector, if we keep varying parameter as only gas used i.e., CH_4 or H_2, we can see in Figure 4.5. (a) and (b) that curves of higher ambient pressure (30 bar and 20 bar) are overlapping for left side width for Hydrogen. But the curve is comparatively distinct for left side width of Methane. But curves for lower CP i.e., 5 bar, 10 bar and even 15 bar are behaving differently for both the gases. For SH injector injecting both the gases, curves of widths obtained are more distinct although for CP 10 bar and 15 bar, the curves tend to be somewhat overlapping. For SH injector, in general, width is seen to be decreasing with increase in chamber pressure.

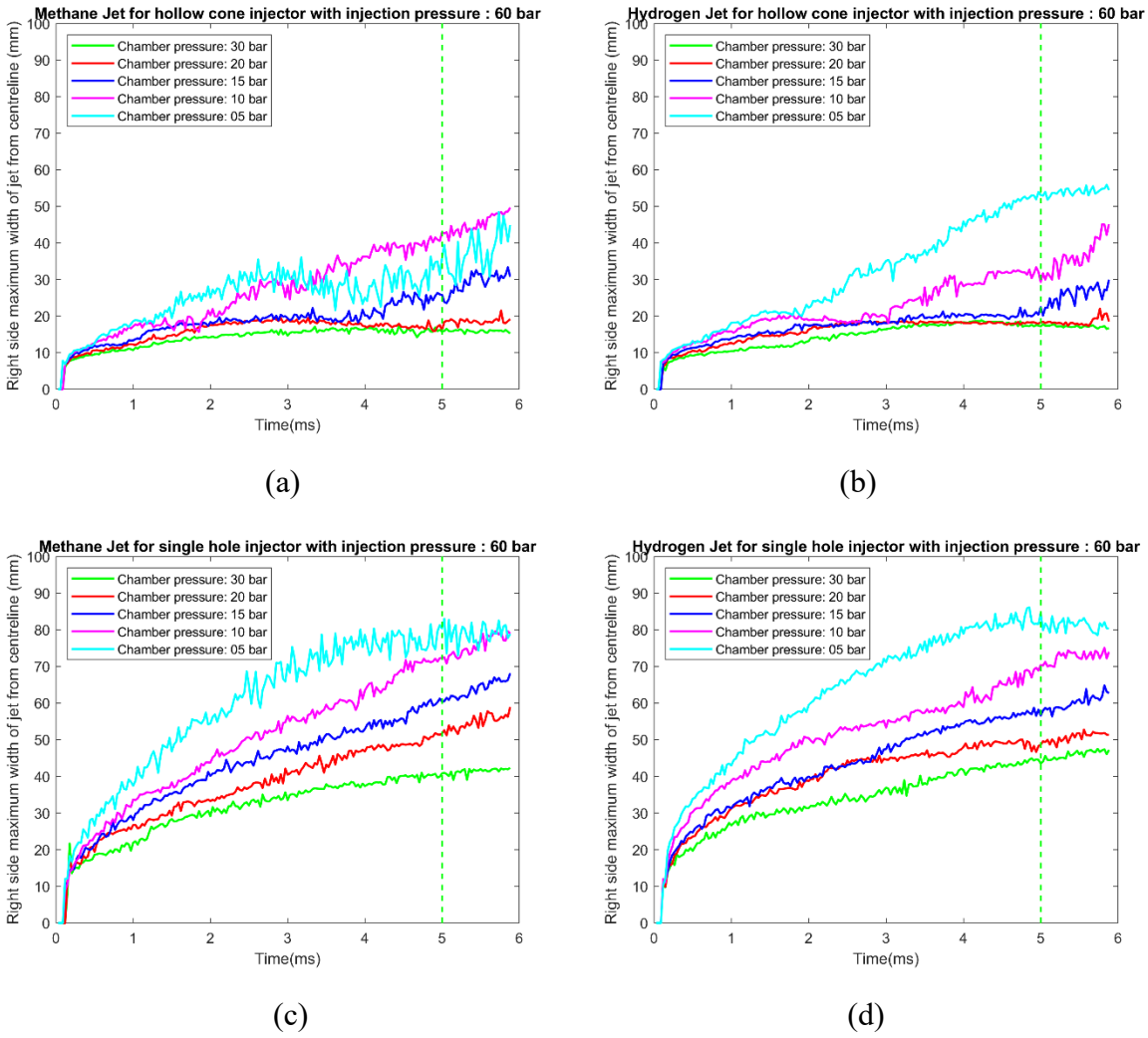

Figure 4.6. Methane and Hydrogen Jet right width for hollow cone and single hole injectors with injection pressure 60 bar

In general, the slope of the curve follows the trend of sudden increase followed by decreasing slope and ending with a constant curve for HC injectors for higher CP. The Curves formed by widths of HC injector with lower values of CP have a very different behaviour and need to be studied more. While considering width of the jets, with increase in ambient pressure, the slope of the curve decreases quickly and becomes constant and higher values of chamber pressure (i.e., from around 20 bar onwards) the curves are seen to be overlapping for hollow cone injector.

Now, the curves become more distinct (i.e., the curves overlap to a lesser extent for different values of chamber pressure) for single hole injector compared to hollow cone injectors. Increase in width with decrease in ambient pressure is observed here as well. Changes in gas used also tends to provide near similar values for single hole injector compared to hollow cone injector.

4.2.2. Effect of injection pressure on jet width

With increase in injection pressure, the slope of the curves tend to be low and decreasing making the widths constant. Also a lot of overlap is seen in slope even with increase in injection pressure to a higher value of 100 bar as seen in Figure 4.7.(a) and (b) for HC injectors using both the gases. The curve obtained by Methane jets using HC injector is rather more random compared to that obtained by Hydrogen. Although at the end of injection, the slope of the curve slightly increases and the curves of different jets become more distinct for Methane jets using HC injector compared to that of Hydrogen. This distinction is not found in SH injector using both the gases. The jet width curves obtained by HC injector can be divided into 3 phases. First there is a sudden increase in width seen at the start of injection from 0 ms to less than 0.5 ms. From 0.5ms to around 4 ms, the lope of the curve starts to decrease after which the slope of the curve increases until the width becomes constant indicating dispersion of gas.

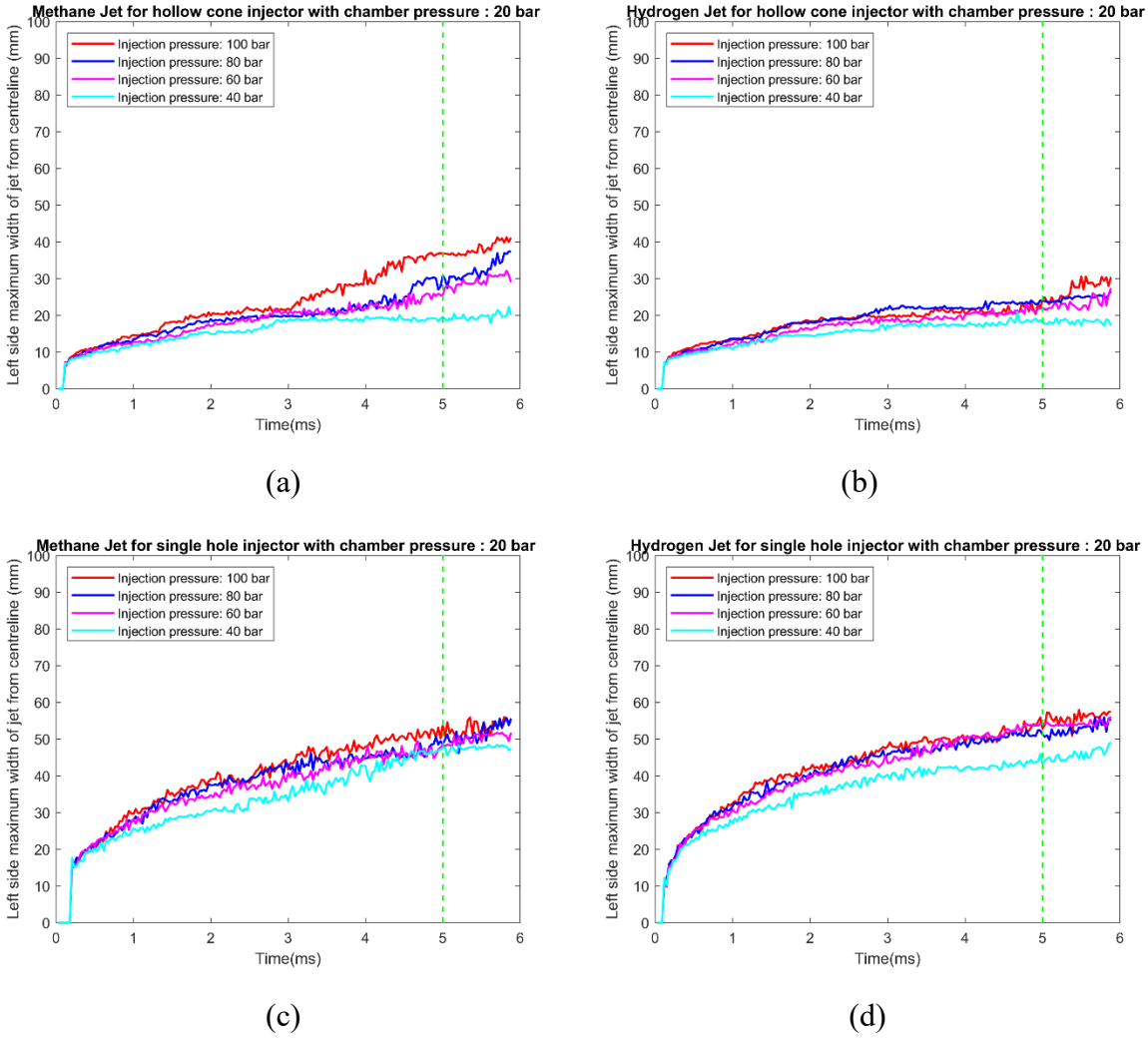

Figure 4.7. Methane and Hydrogen Jets left width for hollow cone and single hole injectors with chamber pressure 20 bar

The change in gas from Methane to Hydrogen does not affect much on values obtained for widths of hollow one injector except for values at the end of injection for higher injection

pressure. Also, not much difference is evident by increasing the injection pressure either to obtain higher widths for single hole injector. Also a very subtle (almost negligible) increase in width is still seen to occur with increase in injection pressure.

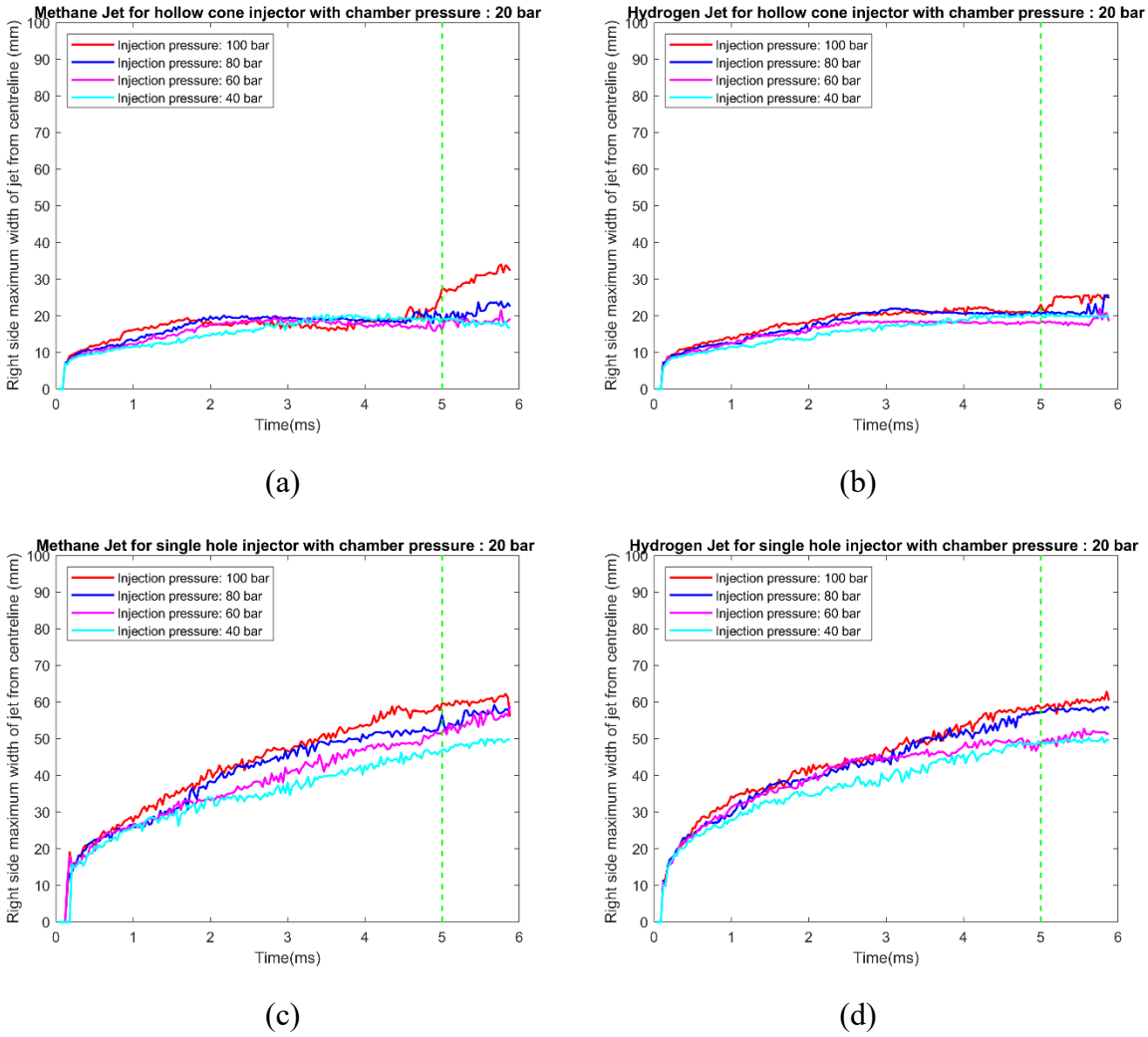

Figure 4.8. Methane and Hydrogen Jets right width for hollow cone and single hole injectors with chamber pressure 20 bar

Slope of curves for widths of SH injector tend to increase suddenly at the beginning of the injection after which it decreases gradually until the end of injection where the width becomes constant. Also the width of the jets for single hole injectors is comparatively higher than what is obtained by hollow cone injector being used. The overlap of curves for different values of injection pressure is less for single hole injector compared to hollow done injector. In general, with increase in injection pressure, the width of the jet is seen to be increasing albeit at a very slow rate for SH injector .

4.2.3. Effect of pressure ratio on jet width

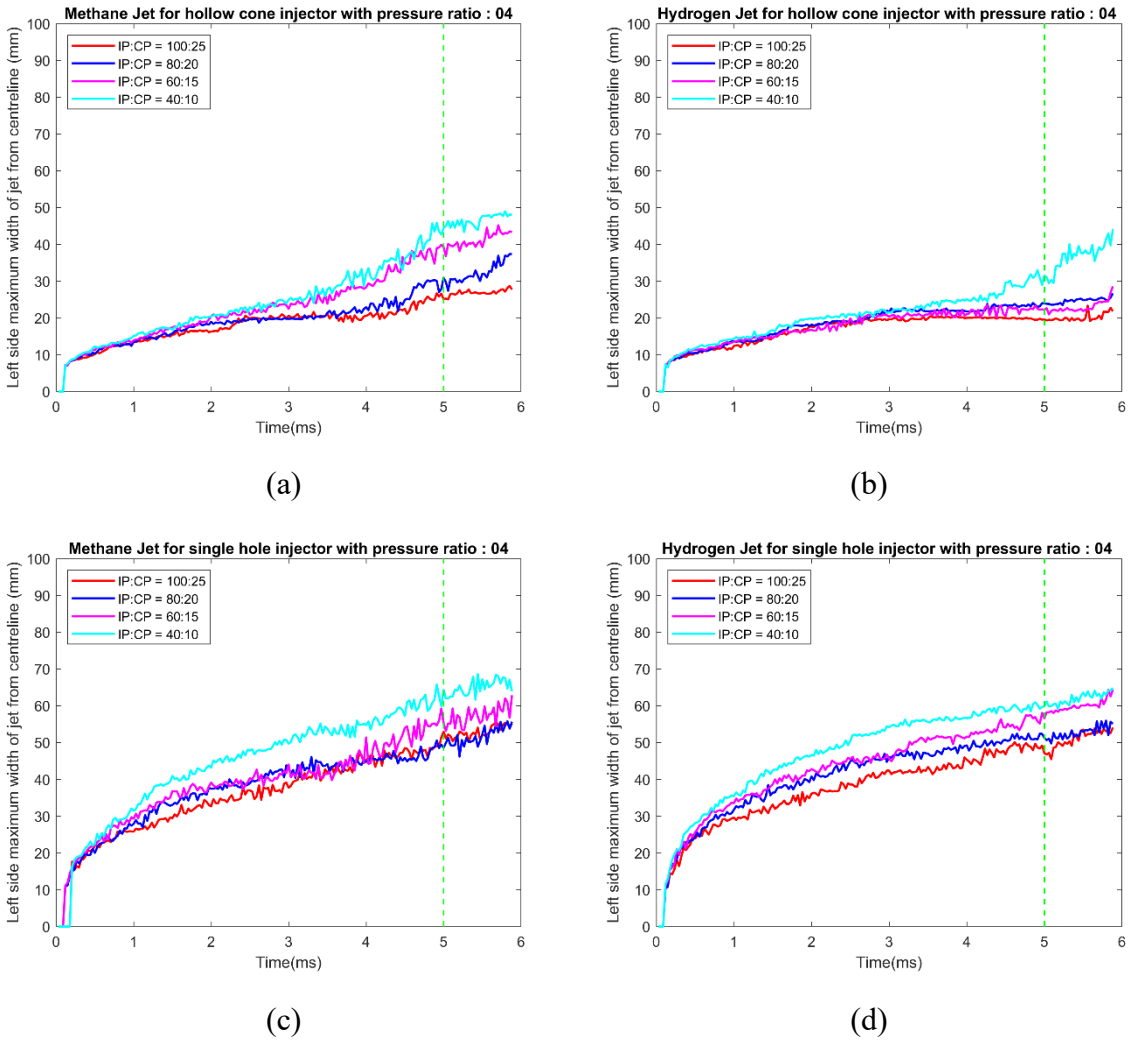

Figure 4.9. Methane and Hydrogen Jets left width for hollow cone and single hole injectors with pressure ratio: 4

With a constant pressure ratio (here 04) with varying values of IP and CP, it is seen that lower values of IP:CP have higher widths in general. Although with change in gas, there is better distinction and lesser overlap between curves of Methane compared to that of Hydrogen with same conditions using hollow cone injector. This can be seen for both side widths for both the gases.

The slope of the curves obtained for jets using single hole injector with constant pressure ratio is higher compared to that of hollow cone injector. Although in general, lower values of IP and CP have higher widths in general, there is a lot of overlap seen in these curves obtained.

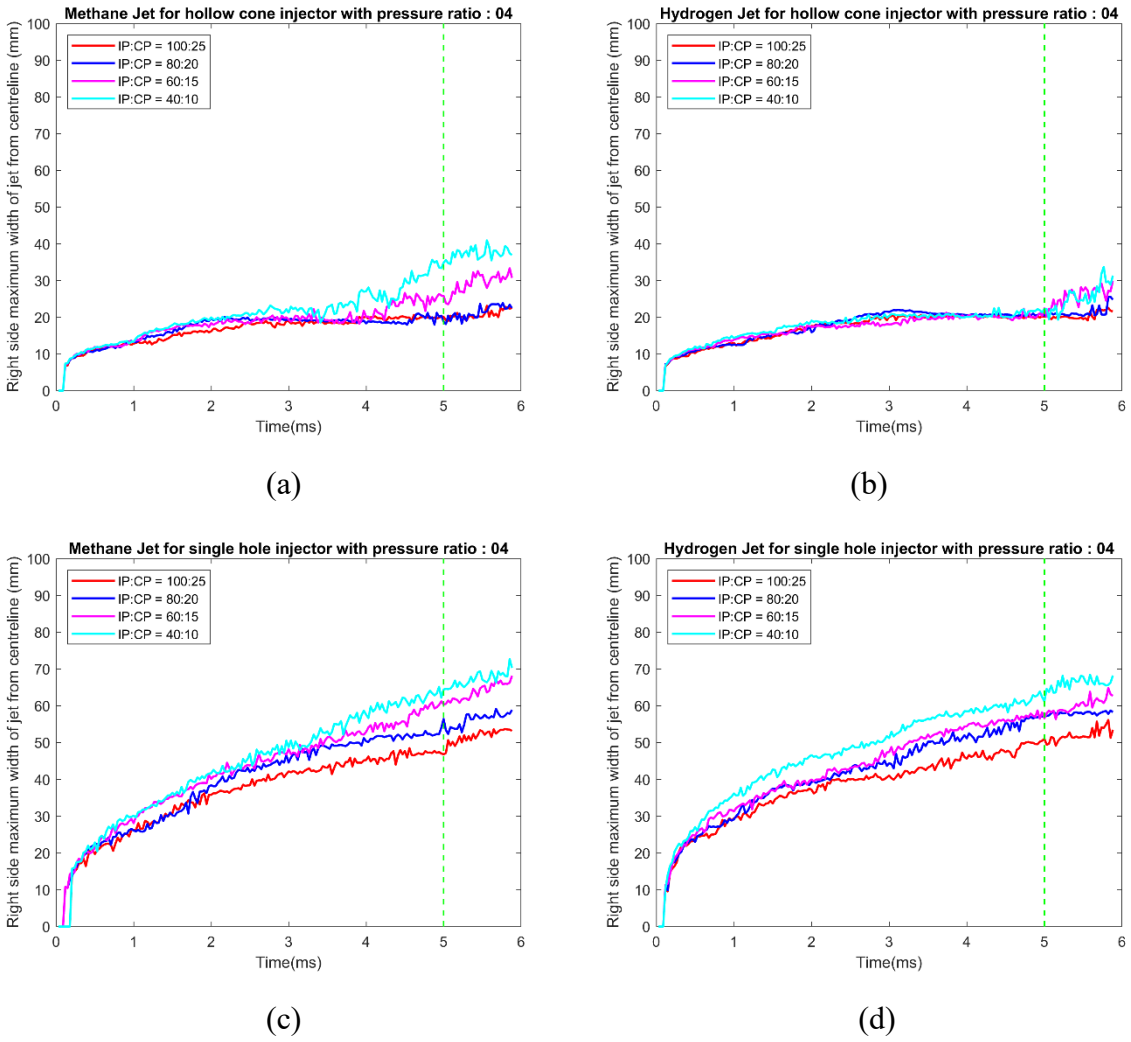

Figure 4.10. Methane and Hydrogen Jets right width for hollow cone and single hole injectors with pressure ratio: 4

Clear distinction cannot be made in right side or left side width obtained for same conditions using same trials. Similar trend is followed by right side widths obtained compared to those obtained on the left side.

4.2.4. Effect of voltage on jet width

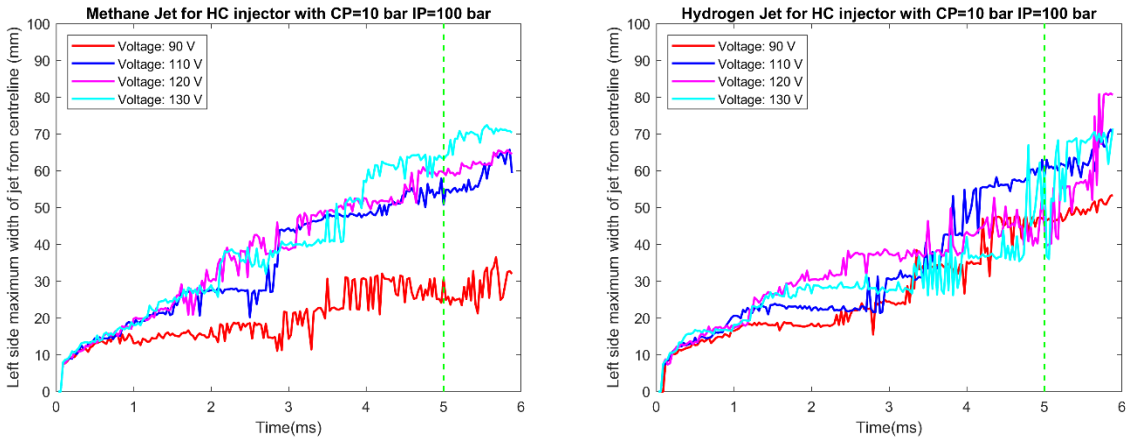

Figure 4.11. Methane and Hydrogen Jets left width for hollow cone injector with varying voltage with CP 10 bar and IP 100 bar

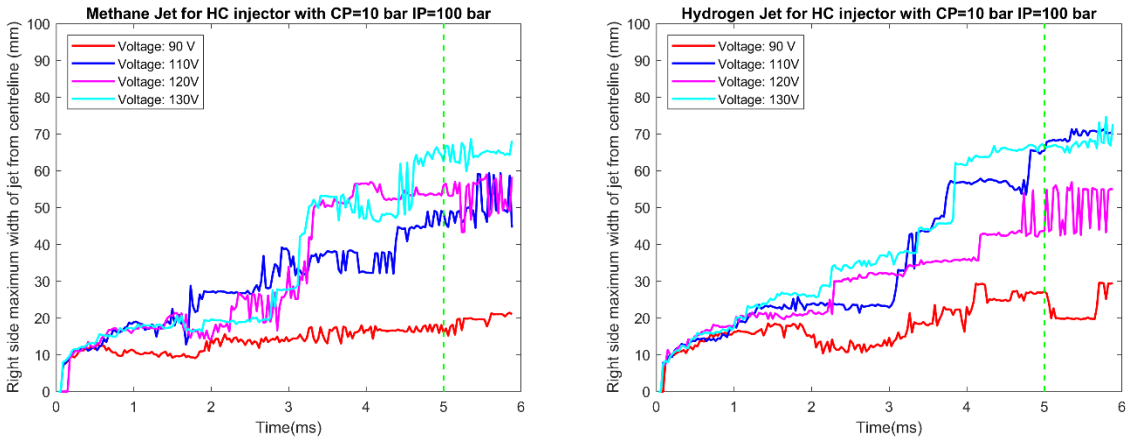

Figure 4.12. Methane and Hydrogen Jets right width for hollow cone injector with varying voltage with CP 10 bar and IP 100 bar

Lower values of voltage in general have lower widths for both the gases. But the curves for higher voltage values tend to overlap. Width curve obtained for 90V has been relatively low for both the gases using both the injectors. And it is a pretty much distinct curve obtained except for the left side of jet using HC injector with Hydrogen gas. A possible explanation to this could be the one sided biased ejection of the jet due to a manufacturing defect (asymmetry) found in HC injector.

4.3. Jet area

4.3.1. Effect of ambient pressure on jet area

With constant injection pressure of 60 bar and varying chamber pressure, in general, area increases with decrease in chamber pressure for both the injectors and gases used. But for single hole injector specifically for chamber pressure 5 bar, the slope of the curve tends to follow a weird trend for both the gases used. For all other cases (other than CP 5 bar) for single hole injector, the curve gradually increases with time till the curve attains a constant value. But for 5 bar CP, the slope of the curve reaches a higher value very quickly and then decreases. Also, for HC injector, the area appears to be directly proportional to time indicating the ρr relation to be square root.

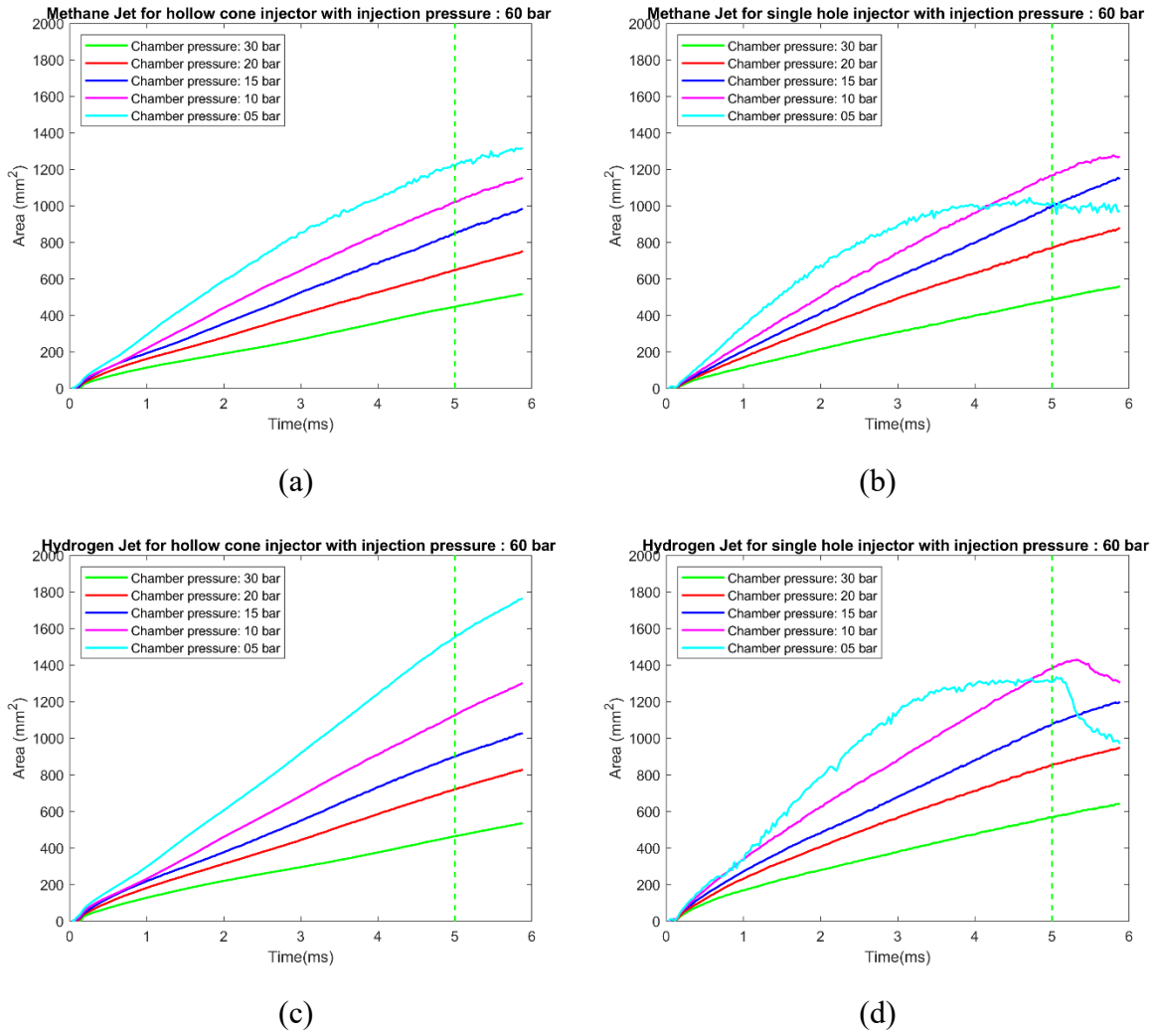

Figure 4.13. Methane and Hydrogen Jet Area for hollow cone and single hole injectors with injection pressure 60 bar

Now, the area for SH and HC injectors for similar operating conditions do not appear to vary much as converse to what was observed for penetration. We can see time dependency of area occurring for both the gases using both the injectors for most of the cases. Decrease in CP i.e., lower values of CP such as 5 bar and 10 bar tend to have slightly different curves for SH injector. There is a gradual increase in area obtained for these curves after which the slope of these curves start decreasing rapidly until the area finally becomes constant after the end of injection. The decline in area for CP 5 bar is seen to be occurring after 3 ms ASOI for both the gases using SH injector.

4.3.2. Effect of injection pressure on jet area

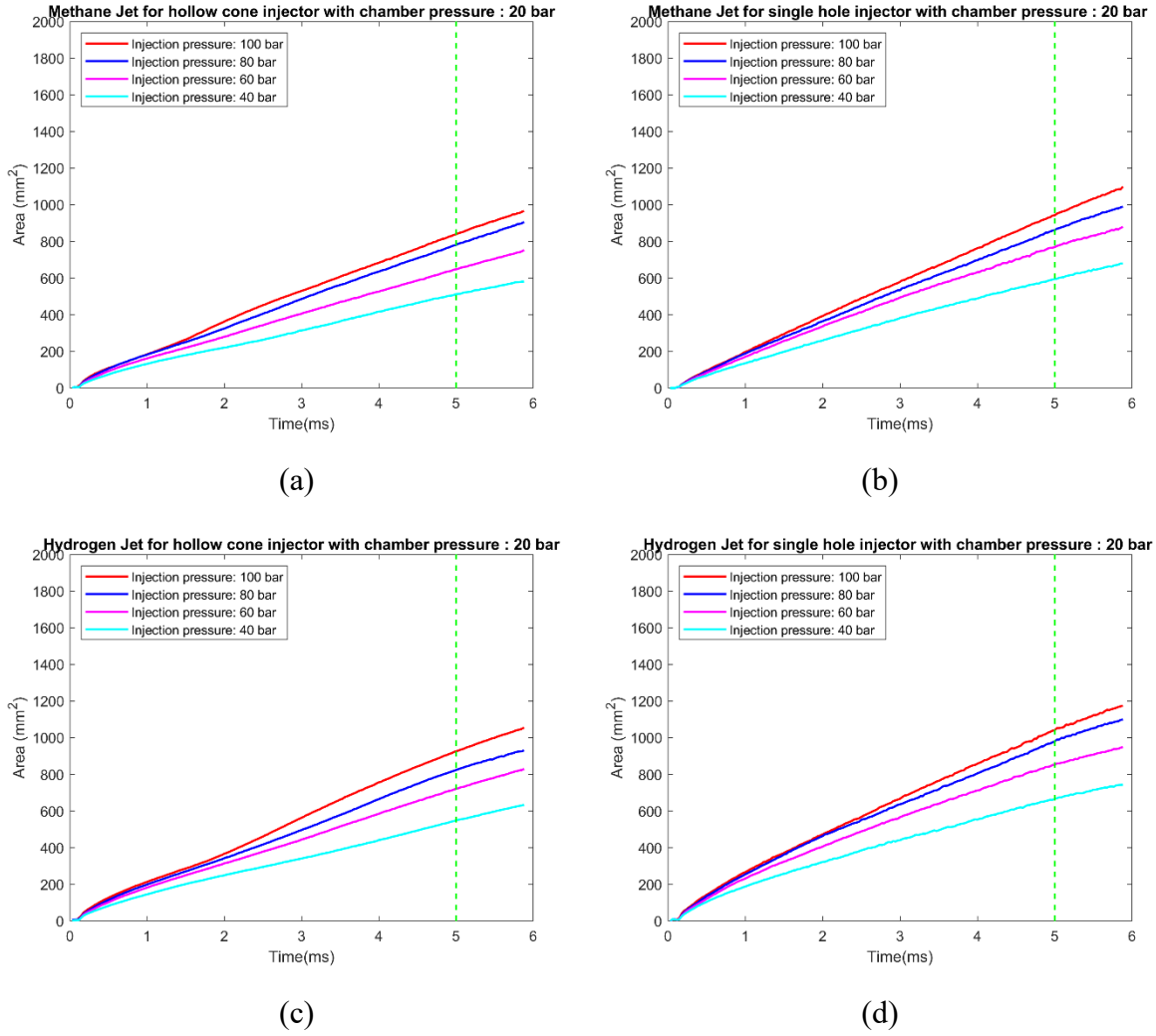

Figure 4.14. Methane and Hydrogen Jet Area for hollow cone and single hole injectors with chamber pressure 20 bar

Keeping chamber pressure constant at 20 bar, and varying the injection pressure we get curves of jets with gradually increasing area. For both the gases and injectors used, area of the jet is seen to be increasing with increase in injection pressure as expected. Although the rate of increase of the area gets reduced as injection pressure increases.

No irregularities are found in this case. And there is also a step occurring just around 2 ms for both the gases using HC injector. Whereas for SH injector the curve obtained is pretty smooth and shows area is directly proportional to time.

4.3.3. Effect of pressure ratio on jet area

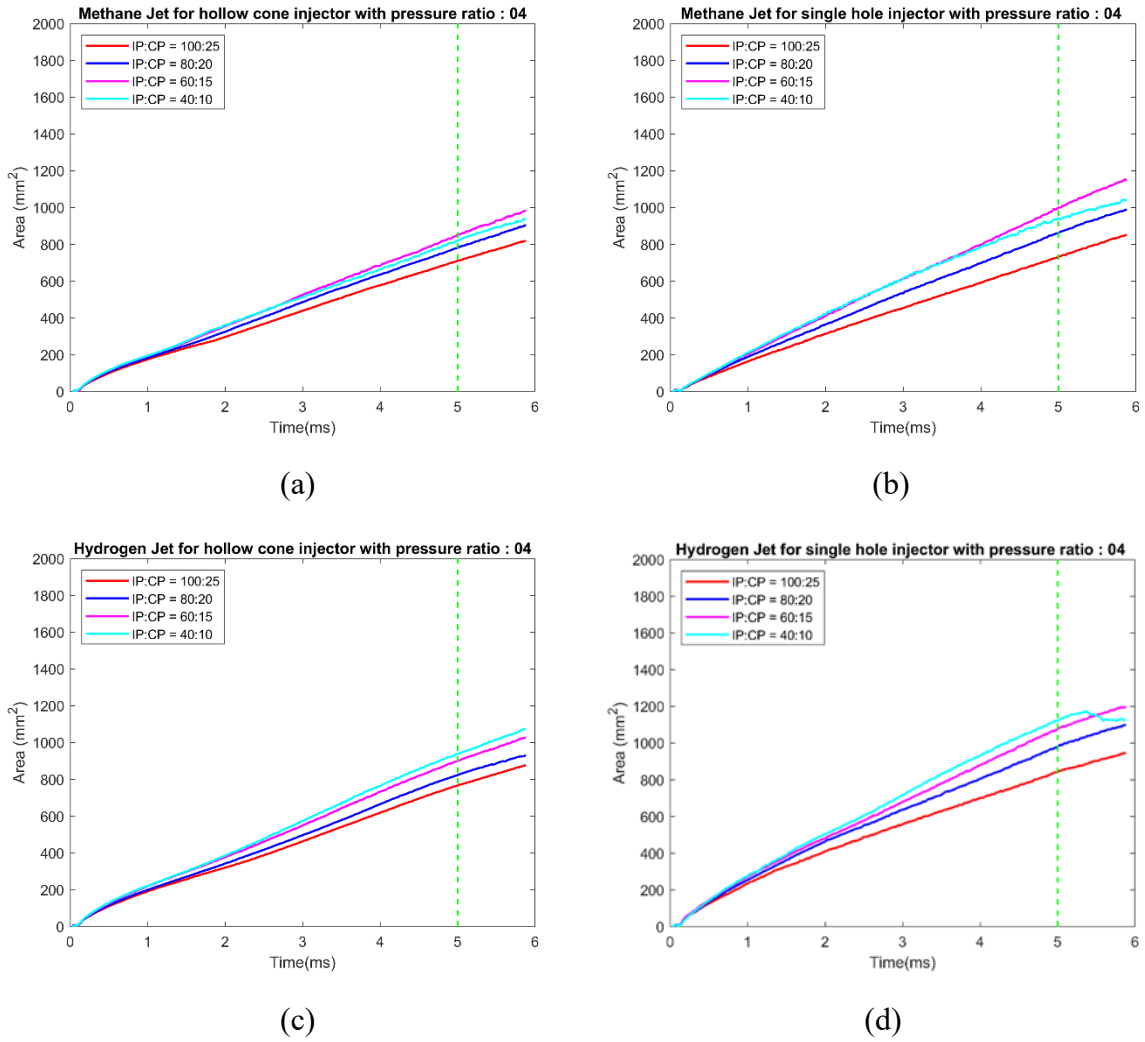

Figure 4.15. Methane and Hydrogen Jet Area for hollow cone and single hole injectors with pressure ratio : 04

For both injectors with constant pressure ratio of 4 bar and varying values of IP and CP, area of Methane gas gradually increases with time till it becomes constant. Although higher values of IP and CP in general tend to have lower area, specifically for case IP:CP=40:10 we can notice some deviation from the general trend. It tends to achieve the peak quicky and the slope of the curve decreases even before the injection stops. Similar trend is being observed for single hole injector using Hydrogen for this particular case.

A slight variation is being seen for the case IP:CP=40:10 for Methane jets using both the injectors. The area for this particular case is even lesser than that for the case of IP:CP=60:15. Although this unusual trend is not observed for Hydrogen gas especially before end of injection. Although while using SH injector, area for the case of IP:CP=40:10 tends to reduce immediately after end of injection for both the gases. Again a step is observed around 2 ms for HC injector using both the gases.

4.3.4. Effect of voltage on jet area

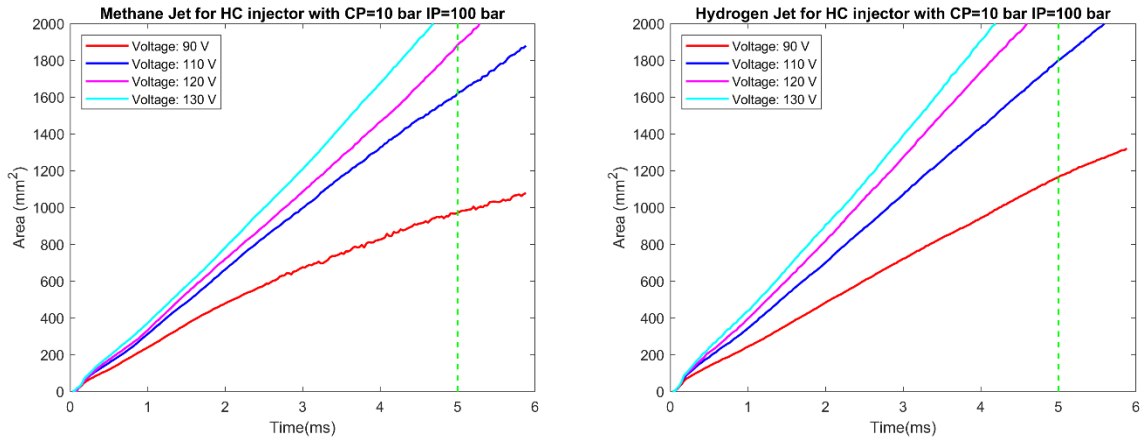

Figure 4.16. Methane and Hydrogen Jet Area for hollow cone injector with varying voltage

For hollow cone injector, using both gases with varying voltage and constant CP and IP, we can see that the slope of curves increases with increase in voltage. Although the rate of increase is greater for lower voltages and the rate of increase decreases as voltage gets higher. Also, with increase it voltage, we can see that area of jets increase very sharply. Again similar values of area are obtained for same conditions with different mentioned gases used.

4.4. Increasing Pressure ratios for He, H2 and CH4

4.4.1. Effect on penetration

With increasing pressure ratios along with varying values of IP and CP, we can clearly see that penetration increases. Although with same pressure ratios, we can see that penetration is higher for lower values of IP:CP. This trend is observed in both the gases used using both the injectors. Single hole injector has higher values of penetration here as expected. The step at around 2 ms is also observed for HC injector using all three mentioned gases.

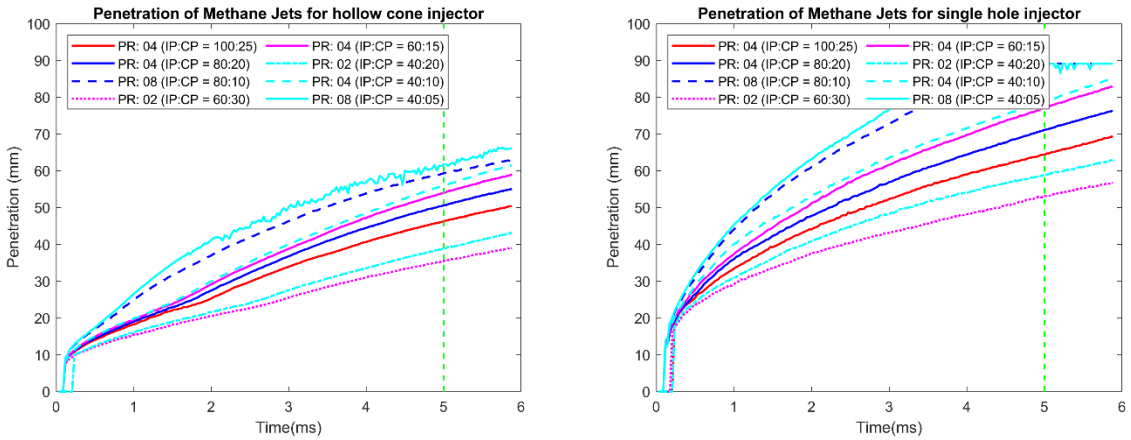

(a) (b)

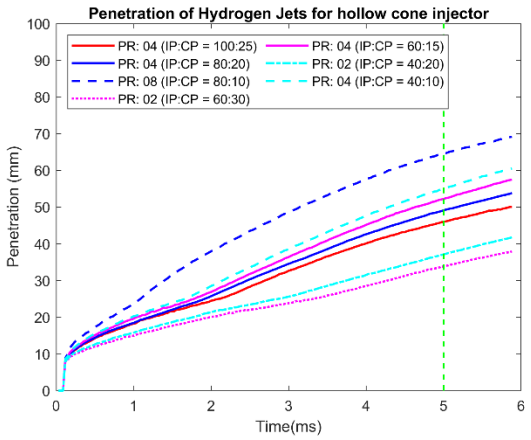

(c)

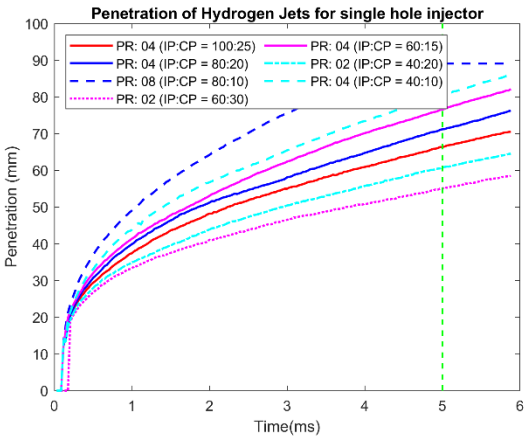

(d)

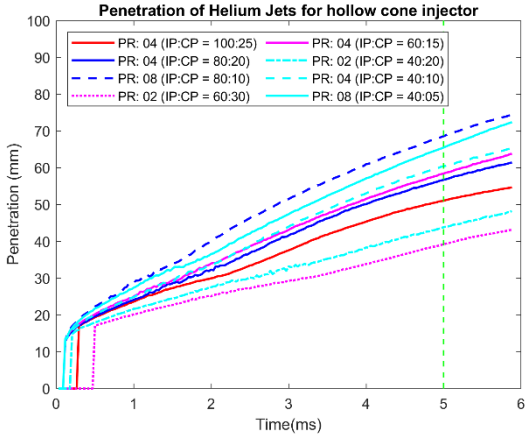

(e)

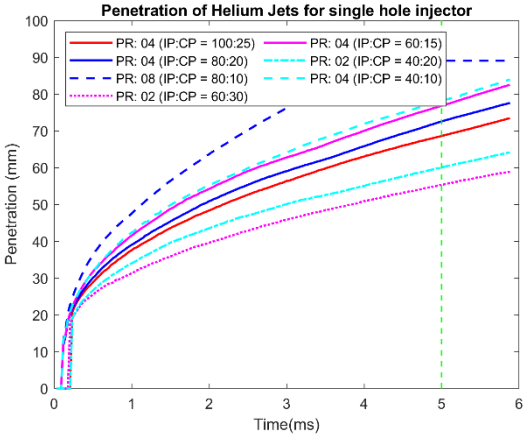

(f)

Figure 4.17. Methane, Hydrogen and Helium Jet Penetration for hollow cone and single hole injectors with increasing PR

4.4.2. Effect on Width

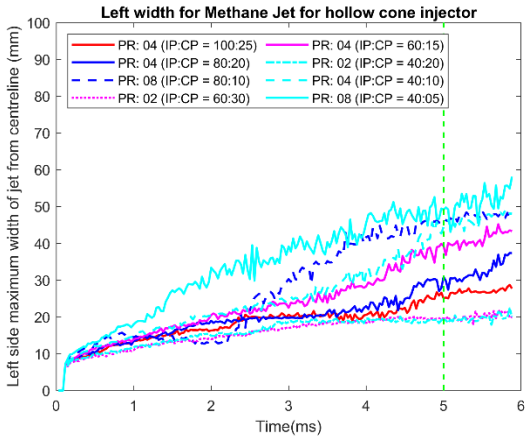

(a)

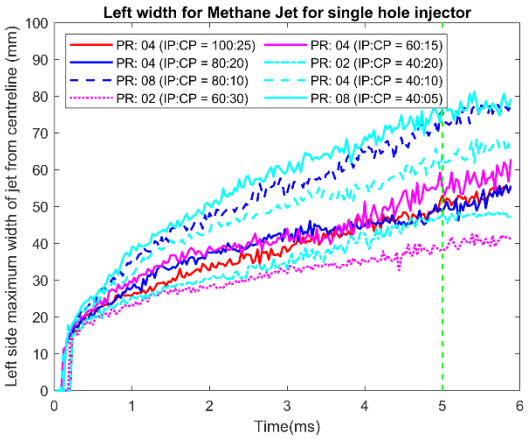

(b)

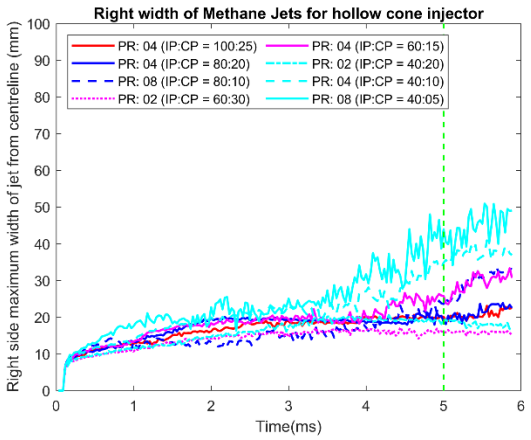

(c)

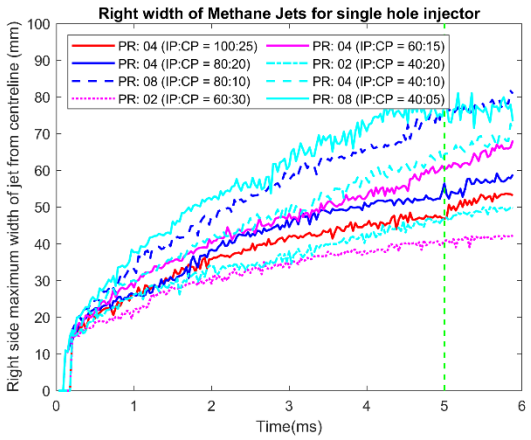

(d)

Figure 4.18. Methane Jet widths for hollow cone and single hole injectors with increasing PR

Increasing pressure ratio with varying values of IP and CP results in greater widths of the jets in general. Although there is a lot of overlap seen for curves of jets obtained using hollow cone injector. Whereas curves for single hole injectors are comparatively more distinct with lesser overlap. Within the same pressure ratio category, highest width of jets is obtained by lowering the values of IP:CP.

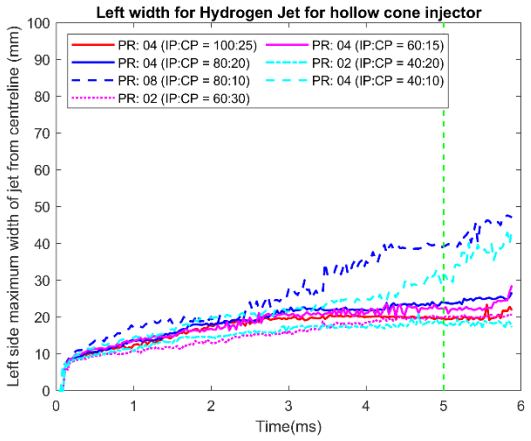

(a)

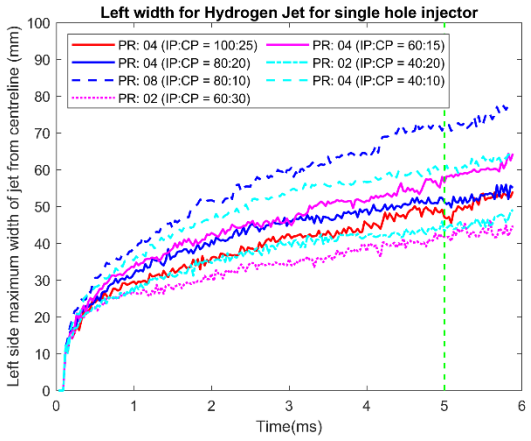

(b)

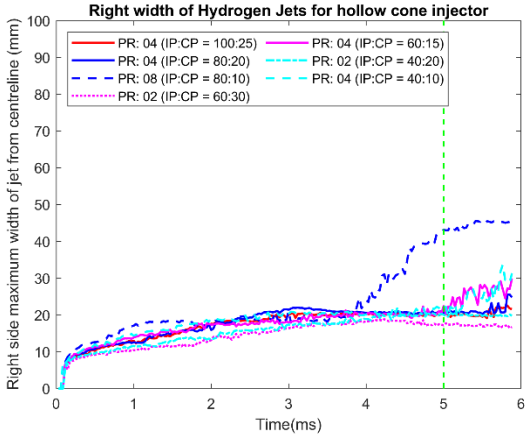

(c)

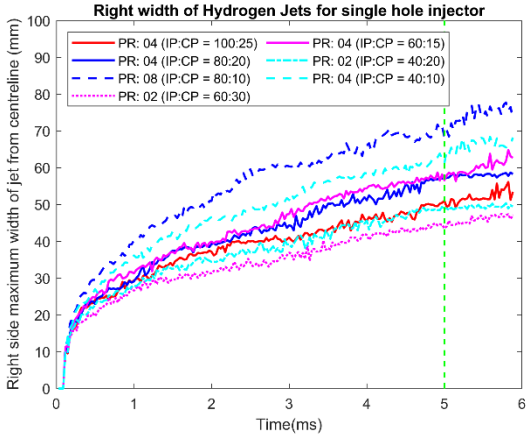

(d)

Figure 4.19. Hydrogen Jet widths for hollow cone and single hole injectors with increasing PR

Again for Hydrogen jets using hollow cone injectors, according to conditions mentioned in Figure. 4.19 above depict the curves for widths of jets. These curves tend to be overlapping more for hollow cone injectors. Single hole injector show more distinct curves. Also with increasing in pressure ratio, widths of the jets goes on increasing. Widths of the curves increases gradually for single hole injector compared to that of hollow cone injector which has a more constant curve indicating constant width.

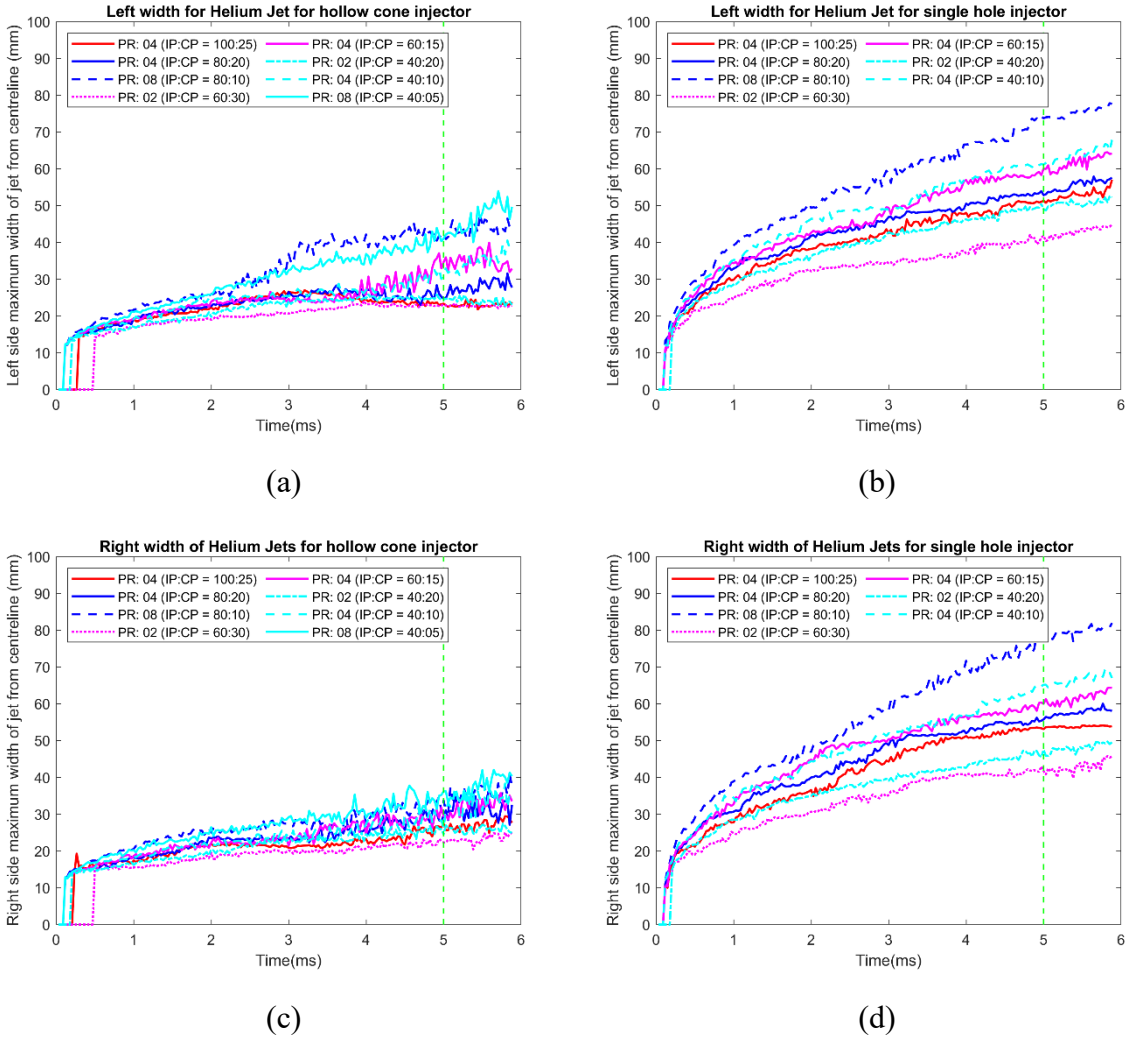

Figure 4.20. Helium Jet widths for hollow cone and single hole injectors with increasing PR

Width curve pattens for Helium also do not differ much from those obtained for Methane and Hydrogen. There is excessive overlap found in curves for Helium width especially on right side for increasing pressure ratios. As expected, the width curves obtained for SH injector are more distinct than those for HC injector.

4.4.3. Effect on Area

As expected, lower pressure ratios have lower area for Methane jets using both the injectors. For same pressure ratios, higher values of IP:CP have lower values of area. Although. In general, values of area goes on increasing with increase in pressure ratios. The area obtained indicated by the curves is gradually increasing till the end of injection after which the slope starts to decrease and the area becomes constant. But there is one unique curve obtained for the case with PR 08 with IP:CP=40:05 where the slope of the curve increases gradually in the beginning but starts to decrease rapidly even before the injection time ends.

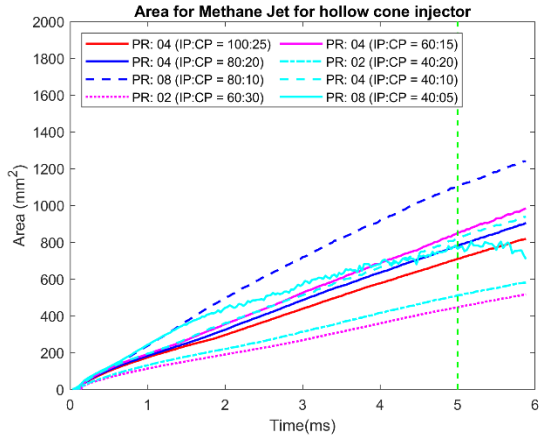

(a)

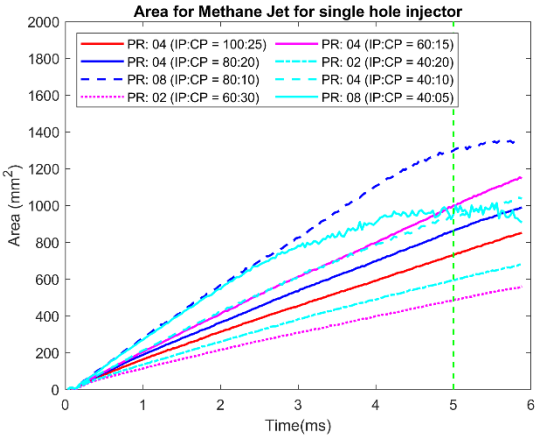

(b)

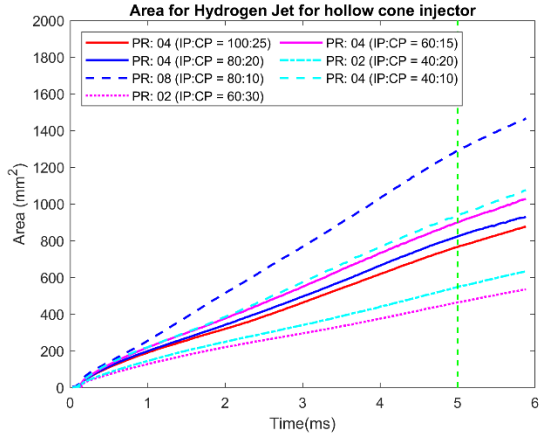

(c)

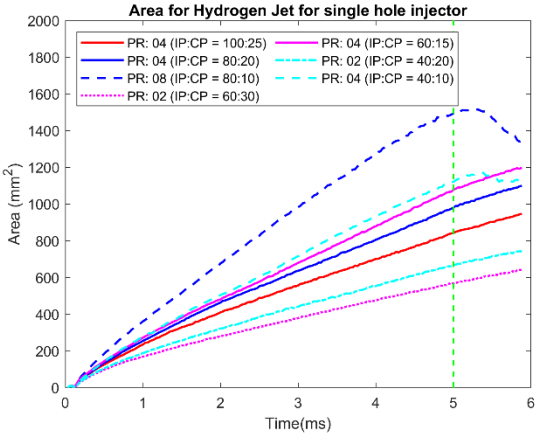

(d)

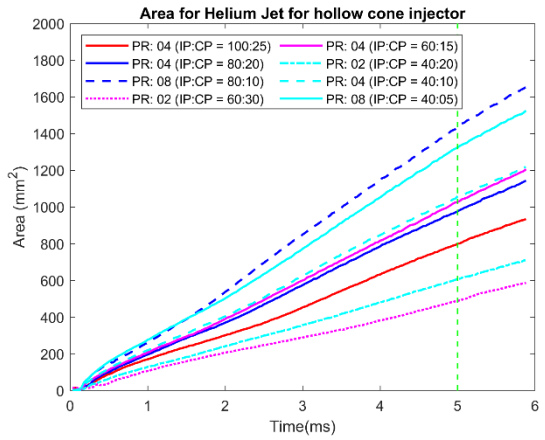

(e)

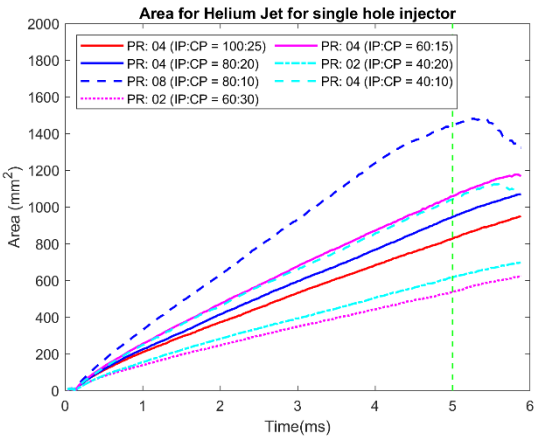

(f)

Figure 4.21. Methane, Hydrogen and Helium Jet Area for hollow cone and single hole injectors with increasing PR

Now again for Hydrogen jets using both the injectors, the area for increasing pressure ratios goes on increasing. As seen for the Methane case of PR 08 with IP:CP=40:05, for Hydrogen jets, schlieren effect is seen to be quite weak hence it cannot be plotted easily for the same case. For hollow cone injector using Hydrogen, the area gradually increase till the end of injection. Here, area is seen to be directly proportional to time. For single hole injector, this is the same case for most cases although for 2 particular cases as shown in the fig. 4.21., the curves start to decrease immediately after end of injection. The step is still obtained for all the gases using HC injector at around 2 ms. For SH injectors using all three mentioned gases, cases IP:CP = 40:10, IP:CP = 80:10, and IP:CP = 40:05 (only for Methane), the curves behave differently than expected roughly at the end of injection.

5. Discussions

Time evolution of the gas jet

As depicted in Table 4.1., using He, H_2 or CH_4 gases would have similar profiles for similar conditions if injector being used is same (i.e., here either HC or SH injector) which cannot be differentiated with naked eye and qualitative analysis. However, Jet studies do depict the subtle patterns noticed in jet properties as discussed in the previous section. A subtle distinction was noticed for the jet studies compared to that of what was indicated in Master's thesis of Tapio Laitinen. That thesis studied jet characteristics in horizontal direction where in which it used hollow cone injector. It was thought that the upward tendency of the jet is probably due to buoyance effect whereas while studying the same gas with same injector, it was found in this thesis that the irregularity effect was due to manufacturing defect. This defect was manually adjusted by adjusting the position of the injector by rotating it in a way to produce and generate more symmetrical output in 2D jet studies. Also S-shaped conical profiles formed in the case of HC injector have also been observed in this thesis as it was discussed in the thesis by Zaira Künsch. As Schlieren imagining was primarily used to detect the boundary conditions of the jet parameters, it is out of the scope of the thesis to determine the velocity measurements and flow patterns of these shapes formed by toroidal vortices. Jets formed by single hole injectors does not seem to experience this phenomenon and inspite of similar conditions used, Jets resulting from using SH injectors tend to have a tapered profile with higher penetration depths.

Jet penetration

The curve profiles obtained for jets produced by SH and HC injectors are different. Although the use of gas (i.e., He, H_2 or CH_4) did not seem to have any significant effect of the profile of the jet curves obtained. The penetration increased with increase in PR. But for values for IP:CP having same PR, the penetration was less for higher values of IP:CP and vice versa. This could be because of the losses inside the injector resulting in deceased density during nozzle exit. Also, the rate of growth rate has been found to have a very subtle decrease as there is increase in PR. This was found for all gases using both the injectors. The 3 phases of the curve obtained were very steep slope (0-0.5ms), slow growth of slope (0.5-1 ms) and constant slope were observed by not only in this thesis but also by Tapio for HC injector. The occurrence of step at roughly around 20 mm was observed to be subtle compared to what was mentioned in the thesis by Tapio. For higher PR, this step occurs before 20 mm. Jets caused by SH injectors had a rather smoother curve without the observance of the step. But for jets caused by SH injector, the three phases as discussed earlier occurred at different times are, the initial phase of steep increase is again found to be at 0-0.5 ms. Slow growth phase again occurred at around 0.5-1 ms. A step which was observed for HC injector is seen absent for SH injector jets. Also, constant PR cases did not have same curves. The properties of these cases were similar to those found in HC injector i.e., higher injector pressure had lower curves for jets. The growth rate of the curves with increasing PR was found to be comparatively more with H_2 and He. Whereas, growth rate got deceased with increasing PR for CH_4.

Jet widths

There was a clear distinction with the curves formed by jets using HC injector and SH injector. An overlap in curves was observed more for HC injector even with increase in PR. Although in general, higher values of PR tended to have higher curves. There was a steady decline in the slope of the curves observed for HC injectors. Whereas jets observed by SH injector had comparatively stable curves in their third phase. Many cases for curves obtained for widths had overlapping curves with a distinction of cases with very high injection pressure values with high PR. Furthermore, the irregularity in manufacturing found in HC injector had a tendency for jets to be biased on 1 side. Although this error was minimized by manually adjusting the injector position by rotating it to obtain more symmetrical jets.

Jet area

Curve properties found for jet areas are similar to those which were determined for jet penetration. This holds true for all 3 gases using both the injectors. Except for a few irregularities as discussed in the result section, with increase in PR, the curves have higher values. A particular variation was found for the case with IP:CP=40:05 especially for CH4. There was a decrease in the slope observed. Same case for other 2 gases had lower schlieren effect which could not produce good results and hence could not be further analysed. Schlieren effect for lower values of IP:CP were a bit challenging to produce and analyse. These cases should be further analysed by different methods.

Increasing Voltage

It was found that there was a increase in penetration and area with increase in voltage for HC injector using CH_4 or H_2. Although the rate of increase was not much for higher voltages. Same was applicable for widths but the curves for widths obtained at higher voltages had a tendency to overlap. Hence not much distinction can be made for widths with high voltage. This was also verified by Zaira Künsch as an effect of needle lift.

6. Conclusion and future work

Considering the global need of moving towards a sustainable economy, Hydrogen is known to have a potential of being an excellent fuel for SI engines. The technology albeit new, has a great potential as it can be easily incorporated in existing infrastructure. DI strategy of Hydrogen fuel injection is becoming more popular in research area as it has many advantages over PFI strategies.

To convert existing diesel engines into Hydrogen operated fuel engines, it is necessary to study not just the DI, engines, but also the injector properties as it is considered to be one of the major factors which could determine if this concept can be put in practical usage or not. [45]

Experimental investigation of Hydrogen, Helium and Methane gas jets were carried out with an objective of providing preliminary information about the behaviour of unignited gas jets using hollow cone piezoelectric injector and single hole injector. Schlieren imaging technique was used for this purpose so as to analyse the 2D gas jet properties. The study aimed to analyse parameters such as gas jet penetration, area , width and effect of voltage using varying control parameters such as injection pressure and chamber pressure. This study involve using different combinations of gases and injectors along with varying control parameters. Furthermore, using Schlieren technique, images were captured using a high speed camera and these images were analysed using a Matlab routine.

Multiple readings were taken for each case considered for experimental analysis. All the readings obtained were further averaged to acquire more consistent and accurate results. The investigated chamber pressure was varied between 5 bar and 30 bar, whereas injection pressure ranged from 40 bar to 100 bar.

A comparison was made with previous studies wherein horizontal jet were studied. As thought in the previous studies about the buoyance effect of the jet, it was found out in this thesis that it is not the case. A scope of future studies include investigating of timing for mixture formation in homogeneous gas fuel mixture. Also, PIV (Particle image velocimetry) can be used to analyse the velocity of jets.

A detail analysis can also be made further using the same data obtained in this thesis. Jet opening angle and the abnormal curves obtained for various cases of jets as discussed in the result section can be further analysed.

7. References

[1] UN Environment Programme, "Emissions Gap Report 2019," 26 November 2019. [Online]. Available: https://www.unep.org/resources/emissions-gap-report-2019.

[2] "Facts about the Climate Emergency," [Online]. Available: https://www.unenvironment.org/explore-topics/climate-change/facts-about-climate-emergency.

[3] A. Schüers, F. Gerbig, A. Wimmer and K. Kovac, "Thermodynamic analysis of the working process of hydrogen internal combustion engines with direct injection," in *9th Symposium 'The Working Process of the Internal Combustion Engine' Institute for Internal Combustion Engines and Thermodynamics*, 2003.

[4] European Commission, "A European Strategy for low-emission mobility," 16 02 2017. [Online]. Available: https://ec.europa.eu/clima/policies/transport_en. [Accessed 15 04 2021].

[5] "Explaining road transport emissions (A non-technical guide)," *European Environment Agency,* 2016.

[6] C. White, R. Steeper and A. Lutz, "The hydrogen-fueled internal combustion engine: a technical review," *Int. J. of Hydrogen Energy,* vol. 31, no. 10, pp. 1292-1305, 2006.

[7] L. Das, "Exhaust emission characterization of hydrogen-operated engine system: Nature of pollutants and their control techniques," *Int. J. of Hydrogen Energy,* vol. 16, no. 11, pp. 765-775, 1991.

[8] R. Hefner III, "The age of energy gases," *International Journal of Hydrogen Energy,* vol. 27, no. 1, pp. 1-9, 2002.

[9] C. Acar and I. Dincer, "The potential role of hydrogen as a sustainable transportation fuel to combat global warming," *Int. J. of Hydrogen Energy,* vol. 45, no. 5, pp. 3396-3406, 29 January 2020.

[10] United States Environmental Protection Agency, "Sources of Greenhouse Gas Emissions," 14 04 2021. [Online]. Available: https://www.epa.gov/ghgemissions/sources-greenhouse-gas-emissions. [Accessed 01 05 2021].

[11] European Parliament, "CO2 emissions from cars: facts and figures (Infographics)," 18 04 2019. [Online]. Available: https://www.europarl.europa.eu/news/en/headlines/society/20190313STO31218/co2-emissions-from-cars-facts-and-figures-infographics. [Accessed 02 05 2021].

[12] D. J. Adolf, D. C. H. Balzer, D. J. Louis, D.-I. U. Schabla, P. D. M. Fischedick, D. K. Arnold, D.-S. A. Pastowski and D.-I. D. Schüwer, "Shell Hydrogen Study Energy of the Future? Sustainable Mobility through Fuel Cells and H2," *Researchgate,* 2017.

[13] M. Malesky, "Minimum Oxygen Concentration for Human Breathing," 10 03 2018. [Online]. Available: https://sciencing.com/minimum-oxygen-concentration-human-breathing-15546.html. [Accessed 01 05 2021].

[14] "Facts about Hydrogen and Helium," Inficon, [Online]. Available: http://sensistor.com/wp-content/uploads/2015/05/Facts-about-hydrogen-and-helium.pdf. [Accessed 15 03 2021].

[15] "Hydrogen embrittlement," 3 May 2021. [Online]. Available: https://en.wikipedia.org/wiki/Hydrogen_embrittlement.

[16] Z. Künsch, "Experimental Investigation on the Gas Jet Behaviour for a Hollow Cone Piezo Injector," Aalto University, Espoo, 2013.

[17] "Use of biodiesel and hydrogen as fuel in C I engine," 2016. [Online]. Available: http://hdl.handle.net/10603/143451.

[18] S. Szwaja and K. Grab-Rogalinski , "Hydrogen combustion in a compression ignition diesel engine Pages," *International Journal of Hydrogen Energy,* vol. Volume 34, pp. 4413-4421, 2009.

[19] T. Korakianitis, A. Namasivayam and R. Crookes, "Hydrogen dual-fuelling of compression ignition engines with emulsified biodiesel as pilot fuel," *Int. Journal of Hydrogen Energy,* vol. 35, no. 24, pp. 13329-13344, 2010.

[20] L. Das, "Hydrogen Engine: Research and Development (R&D) programmes in Indian Institute of Technology (IIT)," *International Journal of Hydrogen Energy,* vol. 27, no. 9, pp. 953-965, 2002.

[21] L. Das, "Near-term introduction of hydrogen engines for automotive and agricultural application," *International Journal of Hydrogen Energy,* vol. 27, no. 5, pp. 479-487, 2002.

[22] F. Liu, CFD Study on Hydrogen Engine Mixture Formation and Combustion, 2004.

[23] G. Antunes , R. Mikalsen and A. Roskilly , "An experimental study of a direct injection compression ignition hydrogen engine," *International Journal of Hydrogen Energy,* vol. 34, no. 15, pp. 2539-2547, 2009.

[24] M. Masood, M. Ishrat and A. Reddy, "Computational combustion and emission analysis of hydrogen–diesel blends with experimental verification," *Int. J. of Hydrogen Energy,* vol. 32, no. 13, pp. 2539-2547, 2007.

[25] S. Verhelst and T. Wallner, "Hydrogen-Fueled Internal Combustion Engines," *Progress in Energy and Combustion Science,* vol. 35, no. 6, pp. 490-527, Dec 2009.

[26] S. Verhelst and T. Wallner , "Hydrogen-fueled internal combustion engines," *Department of Flow, Heat and Combustion Mechanics, Ghent University,* pp. 1-80, 2009.

[27] G. K. M. B. C. a. F. H. Kiesgen, "The New 12-Cylinder Hydrogen Engine in the 7 Series: The H2 ICE Age Has Begun," *SAE Transactions,* vol. 115, pp. 275-283, 2006.

[28] A. Klugescheid, "BMW introduces world's first hydrogen-drive luxury performance car - the BMW HYDROGEN 7 [Press Release]," 12 09 2006. [Online]. Available:

https://www.press.bmwgroup.com/usa/article/detail/T0017694EN_US/bmw-introduces-world-s-first-hydrogen-drive-luxury-performance-car-the-bmw-hydrogen-7?language=en_US.

[29] H. L.-B. S. G. M. D. W. T. D. M. T. K. T. Wallner, "Fuel economy and emissions evaluation of BMW Hydrogen 7 Mono-Fuel demonstration vehicles," *International Journal of Hydrogen Energy,* vol. 33, no. 24, pp. 7607-7618, 2008.

[30] S. Szwabowski , S. Hashemi, W. Stockhausen, R. Natkin, L. Reams, D. Kabat and C. Potts, "Ford hydrogen engine powered P2000 vehicle," *SAE Paper No. 2002-01-0243,* 2002.

[31] R. Natkin, A. Denlinger, M. Younkins, A. Weimer, S. Hashemi and A. Vaught, "Ford 6.8L Hydrogen IC Engine for the E-450 Shuttle Van," SAE Technical Paper 2007-01-4096, United States, 2007.

[32] A. Richardson, R. Gopalakrishnan, T. Chhaya, S. Deasy and J. Kohn, "Design Considerations for Hydrogen Management System on Ford Hydrogen Fueled E-450 Shuttle Bus," *SAE Int. J. Commer. Veh.,* vol. 2, no. 1, pp. 101-109, 2009.

[33] R. Gopalakrishnan, M. Throop, A. Richardson and J. Lapetz, "Engineering the Ford H2 IC Engine Powered E-450 Shuttle Bus," *SAE Technical Paper 2007-01-4095,* p. 11, 2007.

[34] J. Lapetz, R. Natkin and V. Zanardelli, "The design, development, validation and delivery of the Ford H2ICE E-450 shuttle bus," in *1st Int. Symp on Hydrogen Internal Combustion Engines*, Graz, Austria, 2006.

[35] N. L. Johnson, A. A. Amsden, J. D. Naber and D. L. Siebers, "Three-dimensional computer modeling of hydrogen injection and combustion," in *95 SMC Simulation Multiconference: simulation as a critical technology*, Phoenix, United States, 1995.

[36] E. Overend, "Hydrogen Combustion Engines," 1999.

[37] R. Owston, V. Magi and J. Abraham, "Fuel-Air Mixing Characteristics of DI Hydrogen Jets," *SAE Paper No. 2008-01-1041,* pp. 693-712, 2009.

[38] K. Bülent Yüceil and M. Volkan Ötügen, "Scaling parameters for underexpanded supersonic jets," *Physics of Fluids,* vol. 14, no. 12, pp. 4206-4215, 2002.

[39] K. Takeyuki, K. Takayoshi, S. Hidemi, Y. Yoshitaka and M. Yasuo, "A study on behavior of a transient hydrogen jet in a high swirl flow," in *THIESEL 2002 Conference on Thermo- and Fluid Dynamic Processes in Diesel Engines*, Valencia, 2002.

[40] W. Kirchweger, R. Haslacher, M. Hallmannsegger and U. Gerke, "Applications of the LIF method for the diagnostics of the combustion process of gas-IC-engines," *Experiments in Fluids,* vol. 43, no. 2-3, pp. 329-340, 2007.

[41] W. Kirchweger, H. Eichlseder, F. Gerbig and U. Gerke, "Optical measurement methods for the optimization of the hydrogen DI combustion," in *7th International Symposium on Internal Combustion Engines Diagnostics*, Baden-Baden, Germany, 2006.

[42] T. Laitinen, "An Experimental Investigation of a Hydrogen Jet Behavior," Aalto University, Espoo, 2020.

[43] . G. Settles, Schlieren and Shadowgraph Techniques, 1. ed., Ed., Berlin Heidelberg: Springer-Verlag, 2001.

[44] R. D. Mc Carty, "Thermodynamic Properties of Helium 4 from 2 to 1500 K at Pressures to 10^8 Pa," *Journal of Physical and Chemical Reference Data 2, 923 (1973),* 29 October 2009.

[45] P. Westberg, "Development of hydrogen compression ignition engine," Aalto University, Espoo, 2020.

[46] A. Ainsalo, "Optical characterization of high-pressure methanol sprays," Aalto University, Espoo, 2018.

[47] R. Sallinen, "Optical spray measurements of alternative fuels," Aalto University, Espoo, 2017.

[48] M. Raffel, C. J. Kähler, C. E. Willert, S. T. Wereley, J. Kompenhans and F. Scarano, Particle Image Velocimetry, Göttingen: Springer International, 2017.

[49] T. Uemura, Y. Ueda and M. Iguchi, Flow Visualization in Materials Processing, vol. 27, Japan: Springer International, 2018.

[50] R. D. Shekar and H. R. Purushothama, "Hydrogen Induction to Diesel Engine Working on Bio Diesel: A Review," *Procedia Earth and Planetary Science,* vol. 11, pp. 385-392, 2015.

[51] A. M. Abo El Ela, Y. A. Eldrainy, M. M. Elkasaby and A. M. Nour, "Effect of replacing nitrogen with helium on a closed cycle diesel engine performance," *Alexandria Engineering Journal,* vol. 55, pp. 2251-2256, 2016.

[52] Y. Karagöz, T. Sandalcı, L. Yüksek, A. S. Dalkılıc and S. Wongwises, "Effect of hydrogen–diesel dual-fuel usage on performance, emissions and diesel combustion in diesel engines," *Advances in Mechanical Engineering,* vol. 8, no. 8, pp. 1-13, 2016.

[53] A. Dhole, R. Yarasu, D. Lata and A. Priyam, "Effect on performance and emissions of a dual fuel diesel engine using hydrogen and producer gas as secondary fuels," *International Journal of Hydrogen Energy,* vol. 39, pp. 8087-8097, 2014.

[54] G. Tüccar and E. Uludamar, "Emission and engine performance analysis of a diesel engine using hydrogen enriched pomegranate seed oil biodiesel," *International Journal of Hydrogen Energy,* vol. 43, no. 38, pp. 18014-18019, 2018.

[55] A. Ehrs, "Development of a premixed charge hydrogen engine," Aalto University, Espoo, 2020.

[56] Y. Karagöz, T. Sandalcı, L. Yüksek and A. Dalkılıç, "Engine performance and emission effects of diesel burns enriched by hydrogen on differnt engine loads," *International Journal of Hydrogen Energy,* vol. 40, pp. 6702-6713, 2015.

[57] N. Saravanan and G. Nagarajan, "Experimental investigation on a DI dual fuel engine with hydrogen injection," *International Journal of Energy Research,* vol. 33, pp. 295-308, 2009.

[58] S. Nag, P. Sharma, A. Gupta and A. Dhar, "Experimental study of engine performance and emissions for hydrogen diesel dual fuel engine with exhaust gas recirculation," *International Journal of Hydrogen Energy,* vol. 44, no. 23, pp. 12163-12175, 2019.

[59] Hydrogen and Fuel Cell Technologies office, "Hydrogen Fuel Cell Engines and Related Technologies," College of the Desert, Palm Desert , 2001.

[60] K.-S. C. Wang, "In-Flight Imaging of Transverse Gas Jets Injected Into Transonic and Supersonic Crossflows: Design and Development," National Aeronautics and Space Administration, Los Angeles, 1994.

[61] R. Andoga, L. Főző, M. Schrötter, M. Češkovič, S. Szabo, R. Bréda and M. Schreiner, "Intelligent Thermal Imaging-Based Diagnostics of Turbojet Engines," *Applied Sciences,* vol. 9, no. 11, p. 2253, May 2019.

[62] A. Davidhazy, "Introduction to shadowgraph and schlieren imaging," RIT Scholar Works, Rochester, 2006.

[63] J. V. Pastor, P. Olmeda, J. Martín and F. Lewiski, "Methodology for Optical Engine Characterization by Means of the Combination of Experimental and Modeling Techniques," *Applied Sciences,* vol. 8, no. 12, p. 2571, 2018.

[64] P. Prechtl, F. Dorer, B. Ofner, S. Eisen and F. Mayinger, "Modern optical measurement techniques applied in a rapid compression machine for the investigation of internal combustion engine concepts," Technische Universität München, Garching, 1998.

[65] P. Boillat, E. Lehmann, P. Trtik and M. Cochet, "Neutron imaging of fuel cells - Recent trends and future prospects," *Current Opinion in Electrochemistry,* vol. 5, no. 1, pp. 3-10, 2017.

[66] O. H. Ghazal, "Performance and combustion characteristic of CI engine fueled with hydrogen enriched diesel," *International Journal of Hydrogen Energy,* vol. 38, no. 35, pp. 15469-15476, 2013.

[67] S. Biswas, Physics of Turbulent Jet Ignition, West Lafayette: Springer Theses, 2018, pp. 1-230.

[68] Shashank. M, "Piezoelectric Diesel Injectors & Emission Control," *International Journal of Science and Research (IJSR),* vol. 4, no. 1, pp. 1-3, 2015.

[69] A. W. Gena, C. Voelker and G. S. Settles, "Qualitative and quantitative schlieren optical measurement of the human thermal plume," *Indoor Air,* vol. 30, no. 4, pp. 757-766, 2020.

[70] R. Juknelevičius, A. Rimkus, S. Pukalskas and J. Matijošius, "Research of performance and emission indicators of the compression-ignition engine powered by hydrogen - Diesel mixtures," *International Journal of Hydrogen Energy,* vol. 44, no. 20, pp. 10129-10138, 2019.

[71] B. Schmidt, "Schlieren Visualization," California Institute of Technology, Pasadena, 2015.

[72] S. A. Skeen, J. Manin and L. M. Pickett, "Simultaneous formaldehyde PLIF and high-speed schlieren imaging for ignition visualization in high-pressure spray flames," *Proceedings of the Combustion Institute,* vol. 35, no. 3, pp. 3167-3174, 2015.

[73] D. Geng, Q. Zhang, Y. Dong and D. Li, "Study on the characteristics of gas jet for engine using high speed photography," in *International Conference on New Technology of Agricultural*, Zibo, 2011.

[74] K. M. A. K. T. S. N. Wakayama, "Development of Hydrogen Rotary Engine Vehicle," in *World Hydrogen Energy Conference 2016*, Lyon, France, 2006.

[75] W. N. R. K. D. R. L. e. a. Stockhausen, "Ford P2000 Hydrogen Engine Design and Vehicle Development Program," SAE Technical Paper 2002-01-0240, United States, 2002.

[76] Inficon AB, "Some facts about Hydrogen and Helium gas," Sensistor, Linköping, 2015.

[77] S. Szwaja and K. Grab-Rogalinski, "Hydrogen combustion in a compression ignition diesel engine," *International Journal of Hydrogen Energy,* vol. 34, no. 10, pp. 4413-4421, 2009.

[78] J. Gomes Antunes, R. Mikalsen and A. Roskilly, "An experimental study of a direct injection compression ignition hydrogen engine," *Int. Journal of Hydrogen Energy,* vol. 34, no. 15, pp. 6516-6522, 2009.

[79] A. Jörg, C. Balzer, J. Louis, A. Schabla, U. Schabla, M. Fischedick, K. Arnold, A. Pastowski and D. Schüwer, "Shell Hydrogen Study Energy of the Future? Sustainable Mobility through Fuel Cells and H2," Shell Deutschland Oil GmbH, Germany, 2017.

[80] Climate Central, "Emissions Sources," 19 February 2020. [Online]. Available: https://www.climatecentral.org/gallery/graphics/emissions-sources-2020. [Accessed 30 03 2021].

[81] UN environment programme, "Facts about the Climate Emergency," 25 01 2021. [Online]. Available: https://www.unep.org/explore-topics/climate-change/facts-about-climate-emergency. [Accessed 15 04 2021].

[82] ebmpapst, "The energy of the future," 2021. [Online]. Available: https://mag.ebmpapst.com/en/industries/heating/the-energy-of-the-future_14311/. [Accessed 02 04 2021].

[83] UN Environment Programme, "Emissions Gap Report 2019," 26 11 2019. [Online]. Available: https://www.unep.org/resources/emissions-gap-report-2019. [Accessed 10 04 2021].

[84] European Commission, "Causes of climate change," 28 06 2017. [Online]. Available: https://ec.europa.eu/clima/change/. [Accessed 10 04 2021].

[85] I. Singh, "Use of biodiesel and hydrogen as fuel in C I engine," Shodhganga, Longowal, 2016.

[86] K. L. Minh, S. Kook and E. R. Hawkes, "The planar imaging of laser induced fluorescence of fuel and hydroxyl for a wall-interacting jet in a single-cylinder, automotive-size, optically accessible diesel engine," *Fuel,* vol. 140, pp. 143-155, 15 January 2015.

[87] Z. Wu, W. Zhao, Z. Li, J. Deng, Z. Hu and L. Li, "A Review of Engine Fuel Injection Studies Using Synchrotron Radiation X-ray Imaging," *Automotive Innovation,* vol. 2, pp. 79-92, 21 May 2019.

[88] J. Yu, H. Hillamo, V. Vuorinen, T. Sarjovaara, O. Kaario and M. Larmi, "Experimental investigation of characteristics of transient low pressure wall-impinging gas jet," in *J. of Physics: Conf. Ser.*, Warsaw, Poland, 2011.

[89] A. Safitri, "Infrared Optical Imaging Techniques for Gas Visualization and Measurement," A&M University, Texas, 2011.

[90] "Causes of climate change," 05 01 2021. [Online]. Available: https://ec.europa.eu/clima/change/causes_en#:~:text=Humans%20are%20increasingly%20influencing%20the,greenhouse%20effect%20and%20global%20warming..

[91] S. Verhelst, S. Verstraeten and R. Sierens, "A comprehensive overview of hydrogen engine design features," *Journal of Automobile,* vol. 221, pp. 911-920, 2005.

APPENDIX 1

1.1 Code for instantaneous jets

Make

```
clear;

 addpath 'Z:\Desktop\Dharamsi_Aishwarya-Hydrogen_Jet_Experiment\Matlab_Jonny\CineReader-
master\matlab'
 %addpath 'Y:\Research\Active_projects\Master-thesis-projects\Dharamsi_Aishwarya-
Hydrogen_Jet_Experiment\Matlab_Jonny\CineReader-master\matlab'
% addpath 'Y:\Research\Active_projects\Master-thesis-projects\Dharamsi_Aishwarya-
Hydrogen_Jet_Experiment\Matlab_Jonny\CineReader-master\matlab'
%compile
```

Test

```
clear;
pause(0.2);
rootDir = 'X:\Optical_research\2020_Aishwarya_Hydrogen-Schlieren\Methane\Single hole
injector\20201012-Testing_VC_IP_100_CP_25';
%cines = {'testCineC.cine', 'testCine_flipHC.cine', 'testCine_flipVC.cine',
'testCine_flipHVC.cine'};
cines = {'T1_IP_100_CP_25_01.cine'};

for r = 1:1
%cines = {strcat('1_4mm-12bar-20bar',sprintf('%g',r),'.cine')};
    for k = 1:numel(cines)
        spice = CineReader(fullfile(rootDir, cines{k}));
%     spice
%     profile on


       Im(r).I(1).imgray=rgb2gray(spice.read(1));

        for j = 2:250%2:spice.NumberOfFrames
            Im(r).I(j).im = spice.read(j);
            Im(r).I(j).imgray = rgb2gray(Im(r).I(j).im);

            Im(r).I(j).img1= Im(r).I(j).imgray-Im(r).I(j-1).imgray ;
            if j>10
            Im(r).I(j).img2= Im(r).I(j).imgray-Im(r).I(j-2).imgray ;
            Im(r).I(j).img3= Im(r).I(j).imgray-Im(r).I(j-3).imgray ;
            Im(r).I(j).img4= Im(r).I(j).imgray-Im(r).I(j-4).imgray ;

                else
            Im(r).I(j).img2= Im(r).I(j).imgray-Im(r).I(1).imgray ;
            Im(r).I(j).img3= Im(r).I(j).imgray-Im(r).I(1).imgray ;
Im(r).I(j).img4= Im(r).I(j).imgray-Im(r).I(1).imgray ;

                end
```

```
            Im(r).I(j).img = Im(r).I(j).img1+Im(r).I(j).img2+Im(r).I(j).img3+Im(r).I(j).img4;
        %profile viewer
            figure(1);
            imshow(Im(r).I(j).im*3) % replace j with frame no for images
    %truesize([800 800])
%             mask = Im(r).I(j).img>threshold*max(Im(r).I(j).img(:));
%             Pixels=round(0.2*sum(mask(:)));
%             Id=bwareaopen(mask,Pixels,8);
%             Id2=imfill(Id,'holes');
%             Id3 = bsxfun(@times, Im(r).I(j).im, cast(Id2, class(Im(r).I(j).im)));
%
%             Im(r).I(j).Id = Id3;
%             %figure(2);
%             %imagesc(Id3)
%             %colormap(parula(1000))
    end


%     figure(3)
%     imshow(Im(r).I(j).im)
%     title('Raw image')
%     axis tight
%     hold on
    end
end
% for t = 1:10
%     Im(11).I(j).Id = Im(11).I(j).Id + Im(t).I(j).Id;
% end
% Im(11).I(j).Id = Im(11).I(j).Id/r
%figure(2);
%imagesc()
%colormap(parula(1000))
```

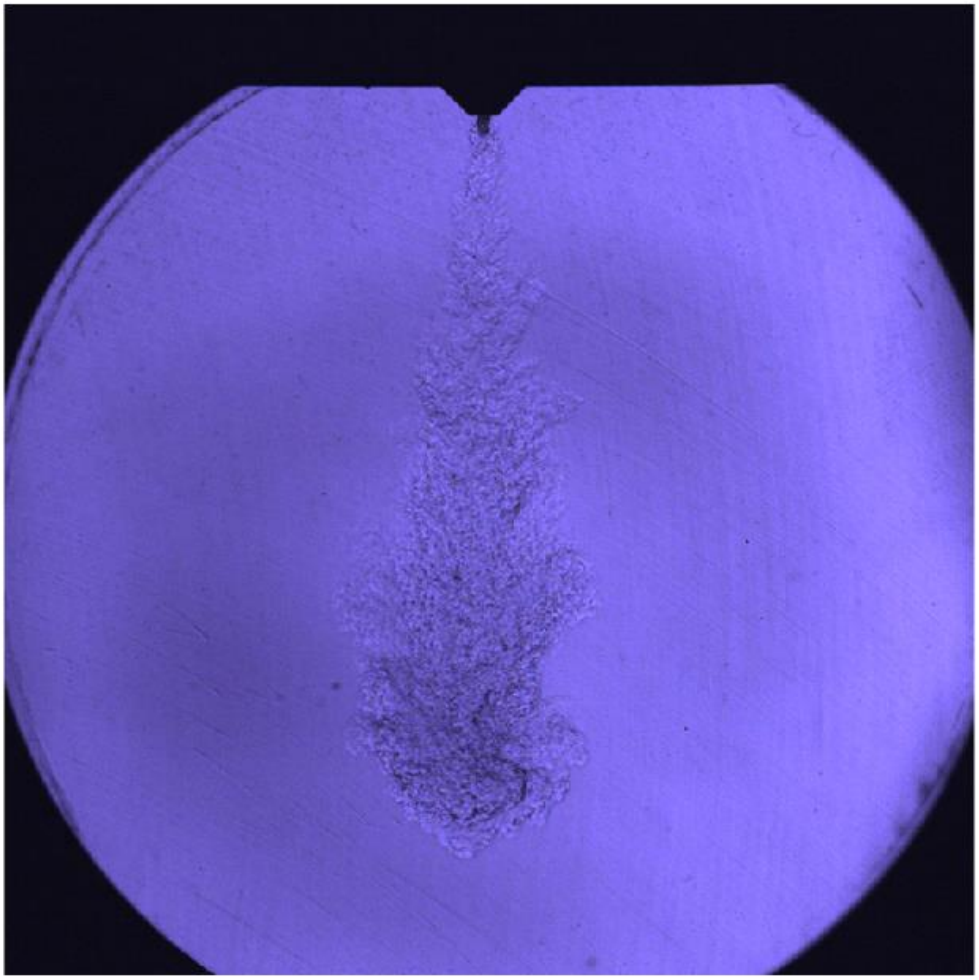

reverse order

Published with MATLAB® R2020b

1.2 Code for acquiring boundary conditions and geometrical parameters

```
% CODE FOR ACQUIRING BOUNDARY CONDITIONS, GEOMETRICAL PARAMETERS

addpath 'Z:\MatlabCode2020\Photron_MRAW_read_function_cih'
addpath 'Z:\MatlabCode2020\LEOII_Imaging'
addpath 'Z:\MatlabCode2020\LEOII_Imaging\natsortfiles'
addpath 'Z:\MatlabCode2020\CineReader-master\matlab'
addpath 'Z:\MatlabCode2020\GasInjection\CannyEdgeDetector'
addpath 'Y:\Research\Active_projects\Master-thesis-projects\Dharamsi_Aishwarya-
Hydrogen_Jet_Experiment\Matlab_Jonny\CineReader-master\matlab'
addpath 'Y:\Research\Active_projects\Master-thesis-projects\Dharamsi_Aishwarya-
Hydrogen_Jet_Experiment\Matlab_Jonny\natsortfiles'

addpath 'Z:\Desktop\Dharamsi_Aishwarya-Hydrogen_Jet_Experiment\Matlab_Jonny'
addpath 'Z:\Desktop\Dharamsi_Aishwarya-Hydrogen_Jet_Experiment\Matlab_Jonny\natsortfiles'
addpath 'Z:\Desktop\Dharamsi_Aishwarya-Hydrogen_Jet_Experiment\Matlab_Jonny\CineReader-
master\matlab'

% Start with a folder and get a list of all subfolders.
% Finds and prints names of all files in
% that folder and all of its subfolders.
% Similar to imageSet() function in the Computer Vision System Toolbox:
http://www.mathworks.com/help/vision/ref/imageset-class.html
clc;    % Clear the command window.
workspace;  % Make sure the workspace panel is showing.
format long g;
format compact;
Dinj=7.7;
pix2mm=(408-342)/Dinj;

% X=[350 376 396 420];
% Y=[60 84 84 60];

X=[343 343 373 381 409 409];
Y=[10 42 68 68 42 10];

% Define a starting folder.
start_path = fullfile(matlabroot, '\toolbox');
if ~exist(start_path, 'dir')
    start_path = matlabroot;
end
% Ask user to confirm or change.
uiwait(msgbox('Pick a starting folder on the next window that will come up.'));
topLevelFolder = uigetdir(start_path);
if topLevelFolder == 0
    return;
end
% Get list of all subfolders.
allSubFolders = genpath(topLevelFolder);
% Parse into a cell array.
remain = allSubFolders;
listOfFolderNames = {};
while true
    [singleSubFolder, remain] = strtok(remain, ';');
```

```
    if isempty(singleSubFolder)
        break;
    end
    listOfFolderNames = [listOfFolderNames singleSubFolder];

    LOfFNs=natsortfiles(listOfFolderNames);
end
numberOfFolders = length(LOfFNs);
% Process all image files in those folders.


for kk = 1 : numberOfFolders
    % Get this folder and print it out.
    thisFolder = LOfFNs{kk};
    fprintf('Processing folder %s\n', thisFolder);

    % Get ALL files.
    filePattern = sprintf('%s/*.cine', thisFolder);
    baseFileNames = dir(filePattern);

    numberOfImageFiles = length(baseFileNames);
    if numberOfImageFiles >= 1
        % Go through all those files.
        for f = 1 : numberOfImageFiles
            fullFileName = fullfile(thisFolder, baseFileNames(f).name);
            [pathstr,name,ext] = fileparts(fullFileName);
            newFilename = fullfile( pathstr,strcat(name,ext));
            I(f).spice = CineReader(newFilename);
        end
    end
end
figure('position',[50 50 900 600])


time=1000/I(f).spice.FrameRate:1000/I(f).spice.FrameRate:200*1000/I(f).spice.FrameRate; %run
individually for time

threshold1=0.4; %change this for different cases C1=0.45;C2=;C3=0.5;C4=0.25
threshold2=0.55;



for f=1:numberOfImageFiles
    for n=1:200%1:spice.NumberOfFrames
        I(f).I(n).imgray=rgb2gray(I(f).spice.read(n));

        maskX = [-1 0 1 ; -2 0 2; -1 0 1];
        maskY = [-1 -4 -1 ; 0 0 0 ; 1 4 1] ;

        resX1 = conv2(I(f).I(n).imgray, maskX,'same'); % convolution method for sharp and
blur images
        resY1 = conv2(I(f).I(n).imgray, maskY,'same');
        magnitude1 = sqrt(resX1.^2 + resY1.^2); % averaged value for above two images


        magnitude1 = magnitude1 > threshold1*mean(I(f).I(n).imgray,'All'); % convert images
to binary
```

```
        magnitude2 = bwareaopen(magnitude1,20); % fill up the open areas


        imsub= imgaussfilt(I(f).I(n).imgray,4)-imbilatfilt(I(f).I(n).imgray,4,2); % Gausian
filter used,  Sharper - blured image to get the boundary
        magnitude3=imbinarize(imsub); % Convert the image  to binary in this step

        magnitude4=imbinarize(magnitude2-magnitude3); % ¨Substraction twice to get rid of
noise

        magnitude5=imbinarize(magnitude3+magnitude4);
        magnitude5 = bwareaopen(magnitude5,1500);

        magnitude6=imbinarize(magnitude5-magnitude3);
        magnitude7 = bwareaopen(magnitude6,8);
        se = strel('disk',20);

        magnitude7 = imdilate(magnitude7 ,se);

        resX0 = conv2(I(f).I(1).imgray, maskX,'same'); % post processing of the 1st image,
only 1st window visible
        resY0 = conv2(I(f).I(1).imgray, maskY,'same');
        magnitude0 = sqrt(resX0.^2 + resY0.^2);

        magnitude8= magnitude0>threshold2*mean(I(f).I(1).imgray,'All');

        magnitude9=imbinarize(magnitude6-magnitude8); % Subtraction to get only the jet
(without window)
        magnitude9 = bwareaopen(magnitude9,20);
        se0 = strel('disk',4);
        magnitude9 = imdilate( magnitude9  ,se0);

        CC1 = bwconncomp(magnitude9,8);
        S1 = regionprops(CC1, 'Area');

        allAreas1 = sort([S1.Area]); % reorder the area from max to min area
        if ~isempty( allAreas1)
            magnitude9 = bwareaopen(magnitude9, (max(allAreas1)-1));
        else
            magnitude9=zeros(size(magnitude9));
        end
        magnitude9=imfill(magnitude9,'holes');

        [I(f).I(n).B1,I(f).I(n).L1]= bwboundaries(magnitude9,'noholes'); % index  of the
boundary (B1)

        if ~isempty(I(f).I(n).B1) % check if there is a contour

            [max_size, max_index] = max(cellfun('size', I(f).I(n).B1, 1)); % find maximum
boundary size
            I(f).I(n).Px=max(I(f).I(n).B1{max_index}(:,1))-4;

            I(f).I(n).TOPWidth= max(min(X)+(max(X)-min(X))*0.5-I(f).I(n).B1{max_index}(:,2));

            I(f).I(n).BotWidth=max(I(f).I(n).B1{max_index}(:,2)-(min(X)+(max(X)-
min(X))*0.5));

            I(f).I(n).TIndPx= find(I(f).I(n).B1{max_index}(:,2)==min(X)+(max(X)-min(X))*0.5-
```

```
I(f).I(n).TOPWidth);
            I(f).I(n).TOPPy= mean(I(f).I(n).B1{max_index}(I(f).I(n).TIndPx,1));

            I(f).I(n).BIndPx= find(I(f).I(n).B1{max_index}(:,2)==min(X)+(max(X)-
min(X))*0.5+I(f).I(n).BotWidth);
            I(f).I(n).BOTPy= mean(I(f).I(n).B1{max_index}(I(f).I(n).BIndPx,1));

            RES(f).P(n,:)=I(f).I(n).Px/pix2mm;
            RES(f).A(n,:)=max(allAreas1)/pix2mm^2;
            RES(f).RW(n,:)=I(f).I(n).TOPPy/pix2mm;
            RES(f).LW(n,:)=I(f).I(n).BOTPy/pix2mm;


            figure(2)
            imshowpair(magnitude2,magnitude8,'montage')

            hold on


            hold on
            line([min(X)+(max(X)-min(X))*0.5 min(X)+(max(X)-min(X))*0.5],[1 800],...
                'Color','r', 'LineWidth', 0.5,'LineStyle','--');

            hold on
            for q = 1:length(I(f).I(n).B1)
                boundary = I(f).I(n).B1{q};

            end


            % Get the x and y coordinates.
            x = boundary(:, 2);
            y = boundary(:, 1);

            % Now smooth with a Savitzky-Golay sliding polynomial filter
            % (for smoothing the boundry of jet)
            windowWidth = 25;
            polynomialOrder = 7;
            smoothX = sgolayfilt(x, polynomialOrder, windowWidth);
            smoothY = sgolayfilt(y, polynomialOrder, windowWidth);
            plot(smoothX, smoothY, 'b', 'LineWidth', 1)


            hold on
            line([min(X)+(max(X)-min(X))*0.5-200 min(X)+(max(X)-
min(X))*0.5+200],[I(f).I(n).Px I(f).I(n).Px],...
                'Color','r', 'LineWidth', 0.5,'LineStyle','--');

            line([min(X)+(max(X)-min(X))*0.5-I(f).I(n).TOPWidth min(X)+(max(X)-min(X))*0.5-
I(f).I(n).TOPWidth],[I(f).I(n).TOPPy-50 I(f).I(n).TOPPy+50],...
                'Color','r', 'LineWidth', 0.5,'LineStyle','--');
            line([min(X)+(max(X)-min(X))*0.5+I(f).I(n).BotWidth min(X)+(max(X)-
min(X))*0.5+I(f).I(n).BotWidth],[I(f).I(n).BOTPy-50 I(f).I(n).BOTPy+50],...
                'Color','r', 'LineWidth', 0.5,'LineStyle','--');


        end
```

```
    end
    RES(f).P(1:3,:)=0;


end

MatName= 'H2HC100_10V120'
MatExtention='.mat';
MatFile = fullfile(topLevelFolder, [MatName MatExtention]);
% save(MatFile, 'I','RES','X','Y','-v7.3')
save(MatFile,'RES','X','Y')
```

Published with MATLAB® R2020b

1.3 Code for generating graphs

```
% Methane
% pressure ratio : 04

% Single Hole

clear all


addpath 'X:\Optical_research\2020_Aishwarya_Hydrogen-Schlieren\Methane\Single hole
injector\20201012-Testing_VC_IP_100_CP_25'
CH4SH100_25=load('CH4SH100_25.mat')

addpath 'X:\Optical_research\2020_Aishwarya_Hydrogen-Schlieren\Methane\Single hole
injector\20201012-Testing_VC_IP_80_CP_20'
CH4SH80_20=load('CH4SH80_20.mat')

addpath 'X:\Optical_research\2020_Aishwarya_Hydrogen-Schlieren\Methane\Single hole
injector\20201012-Testing_VC_IP_60_CP_15'
CH4SH60_15=load('CH4SH60_15.mat')

addpath 'X:\Optical_research\2020_Aishwarya_Hydrogen-Schlieren\Methane\Single hole
injector\20201012-Testing_VC_IP_40_CP_10'
CH4SH40_10=load('CH4SH40_10.mat')


time=1000/34000:1000/34000:200*1000/34000;


%Average penetration

for n=1:size(CH4SH100_25.RES,2)
    PeneCH4SH100_25(:,n)=CH4SH100_25.RES(n).P;
end
PeneCH4SH100_25(4,:)=min(PeneCH4SH100_25(4,:));
 PeneCH4SH100_25(1:4,:)=0;
  PeneCH4SH100_25(5,:)=min(PeneCH4SH100_25(5,:));
AvgPeneCH4SH100_25=mean(PeneCH4SH100_25,2);
AvgPeneCH4SH100_25(1:6,:)=0;

for n=1:size(CH4SH80_20.RES,2)
    PeneCH4SH80_20(:,n)=CH4SH80_20.RES(n).P;
end
PeneCH4SH80_20(4,:)=min(PeneCH4SH80_20(4,:));
  PeneCH4SH80_20(5,:)=min(PeneCH4SH80_20(5,:));
AvgPeneCH4SH80_20=mean(PeneCH4SH80_20,2);

for n=1:size(CH4SH60_15.RES,2)
    PeneCH4SH60_15(:,n)=CH4SH60_15.RES(n).P;
end
PeneCH4SH60_15(4,:)=min(PeneCH4SH60_15(4,:));
  PeneCH4SH60_15(5,:)=min(PeneCH4SH60_15(5,:));
AvgPeneCH4SH60_15=mean(PeneCH4SH60_15,2);

for n=1:size(CH4SH40_10.RES,2)
```

```
    PeneCH4SH40_10(:,n)=CH4SH40_10.RES(n).P;
end
PeneCH4SH40_10(4,:)=min(PeneCH4SH40_10(4,:));
  PeneCH4SH40_10(5,:)=min(PeneCH4SH40_10(5,:));
AvgPeneCH4SH40_10=mean(PeneCH4SH40_10,2);


%Average area

for n=1:size(CH4SH100_25.RES,2)
    AreaCH4SH100_25(:,n)=CH4SH100_25.RES(n).A;
end
AreaCH4SH100_25(4,:)=min(AreaCH4SH100_25(4,:));
  AreaCH4SH100_25(5,:)=min(AreaCH4SH100_25(5,:));
AvgAreaCH4SH100_25=mean(AreaCH4SH100_25,2);

for n=1:size(CH4SH80_20.RES,2)
    AreaCH4SH80_20(:,n)=CH4SH80_20.RES(n).A;
end
AreaCH4SH80_20(4,:)=min(AreaCH4SH80_20(4,:));
  AreaCH4SH80_20(5,:)=min(AreaCH4SH80_20(5,:));
AvgAreaCH4SH80_20=mean(AreaCH4SH80_20,2);

for n=1:size(CH4SH60_15.RES,2)
    AreaCH4SH60_15(:,n)=CH4SH60_15.RES(n).A;
end
AreaCH4SH60_15(4,:)=min(AreaCH4SH60_15(4,:));
  AreaCH4SH60_15(5,:)=min(AreaCH4SH60_15(5,:));
AvgAreaCH4SH60_15=mean(AreaCH4SH60_15,2);

for n=1:size(CH4SH40_10.RES,2)
    AreaCH4SH40_10(:,n)=CH4SH40_10.RES(n).A;
end
AreaCH4SH40_10(4,:)=min(AreaCH4SH40_10(4,:));
  AreaCH4SH40_10(5,:)=min(AreaCH4SH40_10(5,:));
AvgAreaCH4SH40_10=mean(AreaCH4SH40_10,2);



figure(1)
p1=plot(time,AvgPeneCH4SH100_25,'r','LineWidth',1.5)
hold on
p2=plot(time,AvgPeneCH4SH80_20,'b','LineWidth',1.5)
hold on
p3=plot(time,AvgPeneCH4SH60_15,'m','LineWidth',1.5)
hold on
p4=plot(time,AvgPeneCH4SH40_10,'c','LineWidth',1.5)
xlabel('Time(ms)')
ylabel('Penetration (mm)')
hold on
xlim([0 6])
ylim([0 100])

title('Methane Jet for single hole injector with pressure ratio : 04');
line([time(:,170) time(:,170)],[0 2000],'color','g','LineStyle','--','LineWidth',1)

hold on
lgd=legend([p1 p2 p3 p4],{'IP:CP = 100:25','IP:CP = 80:20','IP:CP = 60:15','IP:CP = 40:10'},
```

```
'Location','northwest');

path='\\home.org.aalto.fi\dharama1\data\Desktop\Dharamsi_Aishwarya-
Hydrogen_Jet_Experiment\Thesis graphs\Pressure ratio 04';
filename = sprintf('CH4_SH_PR04_Pene.png');
print(gcf, fullfile(path, filename), '-dpng','-r300')

figure(2)
p1=plot(time,AvgAreaCH4SH100_25,'r','LineWidth',1.5)
hold on
p2=plot(time,AvgAreaCH4SH80_20,'b','LineWidth',1.5)
hold on
p3=plot(time,AvgAreaCH4SH60_15,'m','LineWidth',1.5)
hold on
p4=plot(time,AvgAreaCH4SH40_10,'c','LineWidth',1.5)
xlabel('Time(ms)')
ylabel('Area (mm^2)')
hold on
xlim([0 6])
ylim([0 2000])

title('Methane Jet for single hole injector with pressure ratio : 04 ');
line([time(:,170) time(:,170)],[0 2000],'color','g','LineStyle','--','LineWidth',1)

hold on
lgd=legend([p1 p2 p3 p4],{'IP:CP = 100:25','IP:CP = 80:20','IP:CP = 60:15','IP:CP = 40:10'},
'Location','northwest');

path='\\home.org.aalto.fi\dharama1\data\Desktop\Dharamsi_Aishwarya-
Hydrogen_Jet_Experiment\Thesis graphs\Pressure ratio 04';
filename = sprintf('CH4_SH_PR04_Area.png');
print(gcf, fullfile(path, filename), '-dpng','-r300')

% Right Width

for n=1:size(CH4SH100_25.RES,2)
    RWCH4SH100_25(:,n)=CH4SH100_25.RES(n).RW;
end
RWCH4SH100_25(4,:)=min(RWCH4SH100_25(4,:));
RWCH4SH100_25(1:3,:)=0;
  RWCH4SH100_25(5,:)=min(RWCH4SH100_25(5,:));
AvgRWCH4SH100_25=mean(RWCH4SH100_25,2);
AvgRWCH4SH100_25(1:6,:)=0;

for n=1:size(CH4SH80_20.RES,2)
    RWCH4SH80_20(:,n)=CH4SH80_20.RES(n).RW;
end
RWCH4SH80_20(4,:)=min(RWCH4SH80_20(4,:));
RWCH4SH80_20(1:3,:)=0;
  RWCH4SH80_20(5,:)=min(RWCH4SH80_20(5,:));
AvgRWCH4SH80_20=mean(RWCH4SH80_20,2);

for n=1:size(CH4SH60_15.RES,2)
    RWCH4SH60_15(:,n)=CH4SH60_15.RES(n).RW;
end
RWCH4SH60_15(4,:)=min(RWCH4SH60_15(4,:));
RWCH4SH60_15(1:3,:)=0;
  RWCH4SH60_15(5,:)=min(RWCH4SH60_15(5,:));
```

```
AvgRWCH4SH60_15=mean(RWCH4SH60_15,2);

for n=1:size(CH4SH40_10.RES,2)
    RWCH4SH40_10(:,n)=CH4SH40_10.RES(n).RW;
end
RWCH4SH40_10(4,:)=min(RWCH4SH40_10(4,:));
RWCH4SH40_10(1:3,:)=0;
  RWCH4SH40_10(5,:)=min(RWCH4SH40_10(5,:));
AvgRWCH4SH40_10=mean(RWCH4SH40_10,2);
AvgRWCH4SH40_10(1:6,:)=0;

figure(3)
p1=plot(time,AvgRWCH4SH100_25,'r','LineWidth',1.5)
hold on
p2=plot(time,AvgRWCH4SH80_20,'b','LineWidth',1.5)
hold on
p3=plot(time,AvgRWCH4SH60_15,'m','LineWidth',1.5)
hold on
p4=plot(time,AvgRWCH4SH40_10,'c','LineWidth',1.5)
xlabel('Time(ms)')
ylabel('Right side maximum width of jet from centreline (mm)')
hold on
xlim([0 6])
ylim([0 100])

title('Methane Jet for single hole injector with pressure ratio : 04');
line([time(:,170) time(:,170)],[0 2000],'color','g','LineStyle','--','LineWidth',1)

hold on
lgd=legend([p1 p2 p3 p4],{'IP:CP = 100:25','IP:CP = 80:20','IP:CP = 60:15','IP:CP = 40:10'},
'Location','northwest');

path='\\home.org.aalto.fi\dharama1\data\Desktop\Dharamsi_Aishwarya-
Hydrogen_Jet_Experiment\Thesis graphs\Pressure ratio 04';
filename = sprintf('CH4_SH_PR04_RightWidth.png');
print(gcf, fullfile(path, filename), '-dpng','-r300')


% Left width

for n=1:size(CH4SH100_25.RES,2)
    LWCH4SH100_25(:,n)=CH4SH100_25.RES(n).LW;
end
LWCH4SH100_25(4,:)=min(LWCH4SH100_25(4,:));
LWCH4SH100_25(1:3,:)=0;
  LWCH4SH100_25(5,:)=min(LWCH4SH100_25(5,:));
AvgLWCH4SH100_25=mean(LWCH4SH100_25,2);
AvgLWCH4SH100_25(1:6,:)=0;

for n=1:size(CH4SH80_20.RES,2)
    LWCH4SH80_20(:,n)=CH4SH80_20.RES(n).LW;
end
LWCH4SH80_20(4,:)=min(LWCH4SH80_20(4,:));
LWCH4SH80_20(1:3,:)=0;
  LWCH4SH80_20(5,:)=min(LWCH4SH80_20(5,:));
AvgLWCH4SH80_20=mean(LWCH4SH80_20,2);

for n=1:size(CH4SH60_15.RES,2)
```

```
    LWCH4SH60_15(:,n)=CH4SH60_15.RES(n).LW;
end
LWCH4SH60_15(4,:)=min(LWCH4SH60_15(4,:));
LWCH4SH60_15(1:3,:)=0;
  LWCH4SH60_15(5,:)=min(LWCH4SH60_15(5,:));
AvgLWCH4SH60_15=mean(LWCH4SH60_15,2);

for n=1:size(CH4SH40_10.RES,2)
    LWCH4SH40_10(:,n)=CH4SH40_10.RES(n).LW;
end
LWCH4SH40_10(4,:)=min(LWCH4SH40_10(4,:));
LWCH4SH40_10(1:3,:)=0;
  LWCH4SH40_10(5,:)=min(LWCH4SH40_10(5,:));
AvgLWCH4SH40_10=mean(LWCH4SH40_10,2);
AvgLWCH4SH40_10(1:6,:)=0;

figure(4)
p1=plot(time,AvgLWCH4SH100_25,'r','LineWidth',1.5)
hold on
p2=plot(time,AvgLWCH4SH80_20,'b','LineWidth',1.5)
hold on
p3=plot(time,AvgLWCH4SH60_15,'m','LineWidth',1.5)
hold on
p4=plot(time,AvgLWCH4SH40_10,'c','LineWidth',1.5)
xlabel('Time(ms)')
ylabel('Left side maximum width of jet from centreline (mm)')
hold on
xlim([0 6])
ylim([0 100])

title('Methane Jet for single hole injector with pressure ratio : 04');
line([time(:,170) time(:,170)],[0 2000],'color','g','LineStyle','--','LineWidth',1)

hold on
lgd=legend([p1 p2 p3 p4],{'IP:CP = 100:25','IP:CP = 80:20','IP:CP = 60:15','IP:CP = 40:10'},
'Location','northwest');

path='\\home.org.aalto.fi\dharama1\data\Desktop\Dharamsi_Aishwarya-
Hydrogen_Jet_Experiment\Thesis graphs\Pressure ratio 04';
filename = sprintf('CH4_SH_PR04_LeftWidth.png');
print(gcf, fullfile(path, filename), '-dpng','-r300')

% ------------------------------------------------------------------------

% Hollow cone

addpath 'X:\Optical_research\2020_Aishwarya_Hydrogen-Schlieren\Methane\Hollow cone
injector\Injector new position (more symmetric)\20201022-Testing_VC_IP_100_CP_25'
CH4HC100_25=load('CH4HC100_25.mat')

addpath 'X:\Optical_research\2020_Aishwarya_Hydrogen-Schlieren\Methane\Hollow cone
injector\Injector new position (more symmetric)\20201022-Testing_VC_IP_80_CP_20'
CH4HC80_20=load('CH4HC80_20.mat')

addpath 'X:\Optical_research\2020_Aishwarya_Hydrogen-Schlieren\Methane\Hollow cone
injector\Injector new position (more symmetric)\20201022-Testing_VC_IP_60_CP_15'
CH4HC60_15=load('CH4HC60_15.mat')
```

```
addpath 'X:\Optical_research\2020_Aishwarya_Hydrogen-Schlieren\Methane\Hollow cone
injector\Injector new position (more symmetric)\20201022-Testing_VC_IP_40_CP_10'
CH4HC40_10=load('CH4HC40_10.mat')


time=1000/34000:1000/34000:200*1000/34000;


%Average penetration

for n=1:size(CH4HC100_25.RES,2)
    PeneCH4HC100_25(:,n)=CH4HC100_25.RES(n).P;
end
PeneCH4HC100_25(4,:)=min(PeneCH4HC100_25(4,:));
  PeneCH4HC100_25(5,:)=min(PeneCH4HC100_25(5,:));
AvgPeneCH4HC100_25=mean(PeneCH4HC100_25,2);

for n=1:size(CH4HC80_20.RES,2)
    PeneCH4HC80_20(:,n)=CH4HC80_20.RES(n).P;
end
PeneCH4HC80_20(4,:)=min(PeneCH4HC80_20(4,:));
  PeneCH4HC80_20(5,:)=min(PeneCH4HC80_20(5,:));
AvgPeneCH4HC80_20=mean(PeneCH4HC80_20,2);

for n=1:size(CH4HC60_15.RES,2)
    PeneCH4HC60_15(:,n)=CH4HC60_15.RES(n).P;
end
PeneCH4HC60_15(4,:)=min(PeneCH4HC60_15(4,:));
  PeneCH4HC60_15(5,:)=min(PeneCH4HC60_15(5,:));
AvgPeneCH4HC60_15=mean(PeneCH4HC60_15,2);

for n=1:size(CH4HC40_10.RES,2)
    PeneCH4HC40_10(:,n)=CH4HC40_10.RES(n).P;
end
PeneCH4HC40_10(4,:)=min(PeneCH4HC40_10(4,:));
  PeneCH4HC40_10(5,:)=min(PeneCH4HC40_10(5,:));
AvgPeneCH4HC40_10=mean(PeneCH4HC40_10,2);


%Average area

for n=1:size(CH4HC100_25.RES,2)
    AreaCH4HC100_25(:,n)=CH4HC100_25.RES(n).A;
end
AreaCH4HC100_25(4,:)=min(AreaCH4HC100_25(4,:));
  AreaCH4HC100_25(5,:)=min(AreaCH4HC100_25(5,:));
AvgAreaCH4HC100_25=mean(AreaCH4HC100_25,2);

for n=1:size(CH4HC80_20.RES,2)
    AreaCH4HC80_20(:,n)=CH4HC80_20.RES(n).A;
end
AreaCH4HC80_20(4,:)=min(AreaCH4HC80_20(4,:));
  AreaCH4HC80_20(5,:)=min(AreaCH4HC80_20(5,:));
AvgAreaCH4HC80_20=mean(AreaCH4HC80_20,2);

for n=1:size(CH4HC60_15.RES,2)
    AreaCH4HC60_15(:,n)=CH4HC60_15.RES(n).A;
end
```

```
AreaCH4HC60_15(4,:)=min(AreaCH4HC60_15(4,:));
  AreaCH4HC60_15(5,:)=min(AreaCH4HC60_15(5,:));
AvgAreaCH4HC60_15=mean(AreaCH4HC60_15,2);

for n=1:size(CH4HC40_10.RES,2)
    AreaCH4HC40_10(:,n)=CH4HC40_10.RES(n).A;
end
AreaCH4HC40_10(4,:)=min(AreaCH4HC40_10(4,:));
  AreaCH4HC40_10(5,:)=min(AreaCH4HC40_10(5,:));
AvgAreaCH4HC40_10=mean(AreaCH4HC40_10,2);



figure(5)
p1=plot(time,AvgPeneCH4HC100_25,'r','LineWidth',1.5)
hold on
p2=plot(time,AvgPeneCH4HC80_20,'b','LineWidth',1.5)
hold on
p3=plot(time,AvgPeneCH4HC60_15,'m','LineWidth',1.5)
hold on
p4=plot(time,AvgPeneCH4HC40_10,'c','LineWidth',1.5)
xlabel('Time(ms)')
ylabel('Penetration (mm)')
hold on
xlim([0 6])
ylim([0 100])

title('Methane Jet for hollow cone injector with with pressure ratio : 04');
line([time(:,170) time(:,170)],[0 2000],'color','g','LineStyle','--','LineWidth',1)

hold on
lgd=legend([p1 p2 p3 p4],{'IP:CP = 100:25','IP:CP = 80:20','IP:CP = 60:15','IP:CP = 40:10'},
'Location','northwest');

path='\\home.org.aalto.fi\dharama1\data\Desktop\Dharamsi_Aishwarya-
Hydrogen_Jet_Experiment\Thesis graphs\Pressure ratio 04';
filename = sprintf('CH4_HC_PR04_Pene.png');
print(gcf, fullfile(path, filename), '-dpng','-r300')

figure(6)
p1=plot(time,AvgAreaCH4HC100_25,'r','LineWidth',1.5)
hold on
p2=plot(time,AvgAreaCH4HC80_20,'b','LineWidth',1.5)
hold on
p3=plot(time,AvgAreaCH4HC60_15,'m','LineWidth',1.5)
hold on
p4=plot(time,AvgAreaCH4HC40_10,'c','LineWidth',1.5)
xlabel('Time(ms)')
ylabel('Area (mm^2)')
hold on
xlim([0 6])
ylim([0 2000])

title('Methane Jet for hollow cone injector with pressure ratio : 04');
line([time(:,170) time(:,170)],[0 2000],'color','g','LineStyle','--','LineWidth',1)

hold on
lgd=legend([p1 p2 p3 p4],{'IP:CP = 100:25','IP:CP = 80:20','IP:CP = 60:15','IP:CP = 40:10'},
```

```
'Location','northwest');

path='\\home.org.aalto.fi\dharama1\data\Desktop\Dharamsi_Aishwarya-
Hydrogen_Jet_Experiment\Thesis graphs\Pressure ratio 04';
filename = sprintf('CH4_HC_PR04_Area.png');
print(gcf, fullfile(path, filename), '-dpng','-r300')

% Right Width

for n=1:size(CH4HC100_25.RES,2)
    RWCH4HC100_25(:,n)=CH4HC100_25.RES(n).RW;
end
RWCH4HC100_25(4,:)=min(RWCH4HC100_25(4,:));
RWCH4HC100_25(1:3,:)=0;
  RWCH4HC100_25(5,:)=min(RWCH4HC100_25(5,:));
AvgRWCH4HC100_25=mean(RWCH4HC100_25,2);

for n=1:size(CH4HC80_20.RES,2)
    RWCH4HC80_20(:,n)=CH4HC80_20.RES(n).RW;
end
RWCH4HC80_20(4,:)=min(RWCH4HC80_20(4,:));
RWCH4HC80_20(1:3,:)=0;
  RWCH4HC80_20(5,:)=min(RWCH4HC80_20(5,:));
AvgRWCH4HC80_20=mean(RWCH4HC80_20,2);

for n=1:size(CH4HC60_15.RES,2)
    RWCH4HC60_15(:,n)=CH4HC60_15.RES(n).RW;
end
RWCH4HC60_15(4,:)=min(RWCH4HC60_15(4,:));
RWCH4HC60_15(1:3,:)=0;
  RWCH4HC60_15(5,:)=min(RWCH4HC60_15(5,:));
AvgRWCH4HC60_15=mean(RWCH4HC60_15,2);

for n=1:size(CH4HC40_10.RES,2)
    RWCH4HC40_10(:,n)=CH4HC40_10.RES(n).RW;
end
RWCH4HC40_10(4,:)=min(RWCH4HC40_10(4,:));
RWCH4HC40_10(1:3,:)=0;
  RWCH4HC40_10(5,:)=min(RWCH4HC40_10(5,:));
AvgRWCH4HC40_10=mean(RWCH4HC40_10,2);


figure(7)
p1=plot(time,AvgRWCH4HC100_25,'r','LineWidth',1.5)
hold on
p2=plot(time,AvgRWCH4HC80_20,'b','LineWidth',1.5)
hold on
p3=plot(time,AvgRWCH4HC60_15,'m','LineWidth',1.5)
hold on
p4=plot(time,AvgRWCH4HC40_10,'c','LineWidth',1.5)
xlabel('Time(ms)')
ylabel('Right side maximum width of jet from centreline (mm)')
hold on
xlim([0 6])
ylim([0 100])

title('Methane Jet for hollow cone injector with pressure ratio : 04');
line([time(:,170) time(:,170)],[0 2000],'color','g','LineStyle','--','LineWidth',1)
```

```
hold on
lgd=legend([p1 p2 p3 p4],{'IP:CP = 100:25','IP:CP = 80:20','IP:CP = 60:15','IP:CP = 40:10'},
'Location','northwest');

path='\\home.org.aalto.fi\dharama1\data\Desktop\Dharamsi_Aishwarya-
Hydrogen_Jet_Experiment\Thesis graphs\Pressure ratio 04';
filename = sprintf('CH4_HC_PR04_RightWidth.png');
print(gcf, fullfile(path, filename), '-dpng','-r300')


% Left width

for n=1:size(CH4HC100_25.RES,2)
    LWCH4HC100_25(:,n)=CH4HC100_25.RES(n).LW;
end
LWCH4HC100_25(4,:)=min(LWCH4HC100_25(4,:));
LWCH4HC100_25(1:3,:)=0;
  LWCH4HC100_25(5,:)=min(LWCH4HC100_25(5,:));
AvgLWCH4HC100_25=mean(LWCH4HC100_25,2);


for n=1:size(CH4HC80_20.RES,2)
    LWCH4HC80_20(:,n)=CH4HC80_20.RES(n).LW;
end
LWCH4HC80_20(4,:)=min(LWCH4HC80_20(4,:));
LWCH4HC80_20(1:3,:)=0;
  LWCH4HC80_20(5,:)=min(LWCH4HC80_20(5,:));
AvgLWCH4HC80_20=mean(LWCH4HC80_20,2);

for n=1:size(CH4HC60_15.RES,2)
    LWCH4HC60_15(:,n)=CH4HC60_15.RES(n).LW;
end
LWCH4HC60_15(4,:)=min(LWCH4HC60_15(4,:));
LWCH4HC60_15(1:3,:)=0;
  LWCH4HC60_15(5,:)=min(LWCH4HC60_15(5,:));
AvgLWCH4HC60_15=mean(LWCH4HC60_15,2);

for n=1:size(CH4HC40_10.RES,2)
    LWCH4HC40_10(:,n)=CH4HC40_10.RES(n).LW;
end
LWCH4HC40_10(4,:)=min(LWCH4HC40_10(4,:));
LWCH4HC40_10(1:3,:)=0;
  LWCH4HC40_10(5,:)=min(LWCH4HC40_10(5,:));
AvgLWCH4HC40_10=mean(LWCH4HC40_10,2);

figure(8)
p1=plot(time,AvgLWCH4HC100_25,'r','LineWidth',1.5)
hold on
p2=plot(time,AvgLWCH4HC80_20,'b','LineWidth',1.5)
hold on
p3=plot(time,AvgLWCH4HC60_15,'m','LineWidth',1.5)
hold on
p4=plot(time,AvgLWCH4HC40_10,'c','LineWidth',1.5)
xlabel('Time(ms)')
ylabel('Left side maximum width of jet from centreline (mm)')
hold on
xlim([0 6])
```

```
ylim([0 100])

title('Methane Jet for hollow cone injector with pressure ratio : 04');
line([time(:,170) time(:,170)],[0 2000],'color','g','LineStyle','--','LineWidth',1)

hold on
lgd=legend([p1 p2 p3 p4],{'IP:CP = 100:25','IP:CP = 80:20','IP:CP = 60:15','IP:CP = 40:10'},
'Location','northwest');

path='\\home.org.aalto.fi\dharama1\data\Desktop\Dharamsi_Aishwarya-
Hydrogen_Jet_Experiment\Thesis graphs\Pressure ratio 04';
filename = sprintf('CH4_HC_PR04_LeftWidth.png');
print(gcf, fullfile(path, filename), '-dpng','-r300')
```

```
CH4SH100_25 =
  struct with fields:

    RES: [1×10 struct]
      X: [343 343 373 381 409 409]
      Y: [10 42 68 68 42 10]
CH4SH80_20 =
  struct with fields:

    RES: [1×10 struct]
      X: [343 343 373 381 409 409]
      Y: [10 42 68 68 42 10]
CH4SH60_15 =
  struct with fields:

    RES: [1×10 struct]
      X: [343 343 373 381 409 409]
      Y: [10 42 68 68 42 10]
CH4SH40_10 =
  struct with fields:

    RES: [1×10 struct]
      X: [343 343 373 381 409 409]
      Y: [10 42 68 68 42 10]
p1 =
  Line with properties:

              Color: [1 0 0]
          LineStyle: '-'
          LineWidth: 1.5
             Marker: 'none'
         MarkerSize: 6
    MarkerFaceColor: 'none'
              XData: [1×200 double]
              YData: [1×200 double]
              ZData: [1×0 double]

  Use GET to show all properties
p2 =
  Line with properties:

              Color: [0 0 1]
          LineStyle: '-'
```

```
          LineWidth: 1.5
             Marker: 'none'
         MarkerSize: 6
    MarkerFaceColor: 'none'
              XData: [1×200 double]
              YData: [1×200 double]
              ZData: [1×0 double]

  Use GET to show all properties
p3 =
  Line with properties:

              Color: [1 0 1]
          LineStyle: '-'
          LineWidth: 1.5
             Marker: 'none'
         MarkerSize: 6
    MarkerFaceColor: 'none'
              XData: [1×200 double]
              YData: [1×200 double]
              ZData: [1×0 double]

  Use GET to show all properties
p4 =
  Line with properties:

              Color: [0 1 1]
          LineStyle: '-'
          LineWidth: 1.5
             Marker: 'none'
         MarkerSize: 6
    MarkerFaceColor: 'none'
              XData: [1×200 double]
              YData: [1×200 double]
              ZData: [1×0 double]

  Use GET to show all properties
p1 =
  Line with properties:

              Color: [1 0 0]
          LineStyle: '-'
          LineWidth: 1.5
             Marker: 'none'
         MarkerSize: 6
    MarkerFaceColor: 'none'
              XData: [1×200 double]
              YData: [1×200 double]
              ZData: [1×0 double]

  Use GET to show all properties
p2 =
  Line with properties:

              Color: [0 0 1]
          LineStyle: '-'
          LineWidth: 1.5
             Marker: 'none'
```

```
          MarkerSize: 6
    MarkerFaceColor: 'none'
              XData: [1×200 double]
              YData: [1×200 double]
              ZData: [1×0 double]

  Use GET to show all properties
p3 =
  Line with properties:

              Color: [1 0 1]
          LineStyle: '-'
          LineWidth: 1.5
             Marker: 'none'
          MarkerSize: 6
    MarkerFaceColor: 'none'
              XData: [1×200 double]
              YData: [1×200 double]
              ZData: [1×0 double]

  Use GET to show all properties
p4 =
  Line with properties:

              Color: [0 1 1]
          LineStyle: '-'
          LineWidth: 1.5
             Marker: 'none'
          MarkerSize: 6
    MarkerFaceColor: 'none'
              XData: [1×200 double]
              YData: [1×200 double]
              ZData: [1×0 double]

  Use GET to show all properties
p1 =
  Line with properties:

              Color: [1 0 0]
          LineStyle: '-'
          LineWidth: 1.5
             Marker: 'none'
          MarkerSize: 6
    MarkerFaceColor: 'none'
              XData: [1×200 double]
              YData: [1×200 double]
              ZData: [1×0 double]

  Use GET to show all properties
p2 =
  Line with properties:

              Color: [0 0 1]
          LineStyle: '-'
          LineWidth: 1.5
             Marker: 'none'
          MarkerSize: 6
    MarkerFaceColor: 'none'
```

```
              XData: [1×200 double]
              YData: [1×200 double]
              ZData: [1×0 double]

  Use GET to show all properties
p3 =
  Line with properties:

              Color: [1 0 1]
          LineStyle: '-'
          LineWidth: 1.5
             Marker: 'none'
         MarkerSize: 6
    MarkerFaceColor: 'none'
              XData: [1×200 double]
              YData: [1×200 double]
              ZData: [1×0 double]

  Use GET to show all properties
p4 =
  Line with properties:

              Color: [0 1 1]
          LineStyle: '-'
          LineWidth: 1.5
             Marker: 'none'
         MarkerSize: 6
    MarkerFaceColor: 'none'
              XData: [1×200 double]
              YData: [1×200 double]
              ZData: [1×0 double]

  Use GET to show all properties
p1 =
  Line with properties:

              Color: [1 0 0]
          LineStyle: '-'
          LineWidth: 1.5
             Marker: 'none'
         MarkerSize: 6
    MarkerFaceColor: 'none'
              XData: [1×200 double]
              YData: [1×200 double]
              ZData: [1×0 double]

  Use GET to show all properties
p2 =
  Line with properties:

              Color: [0 0 1]
          LineStyle: '-'
          LineWidth: 1.5
             Marker: 'none'
         MarkerSize: 6
    MarkerFaceColor: 'none'
              XData: [1×200 double]
              YData: [1×200 double]
```

```
              ZData: [1×0 double]

  Use GET to show all properties
p3 =
  Line with properties:

              Color: [1 0 1]
          LineStyle: '-'
          LineWidth: 1.5
             Marker: 'none'
         MarkerSize: 6
    MarkerFaceColor: 'none'
              XData: [1×200 double]
              YData: [1×200 double]
              ZData: [1×0 double]

  Use GET to show all properties
p4 =
  Line with properties:

              Color: [0 1 1]
          LineStyle: '-'
          LineWidth: 1.5
             Marker: 'none'
         MarkerSize: 6
    MarkerFaceColor: 'none'
              XData: [1×200 double]
              YData: [1×200 double]
              ZData: [1×0 double]

  Use GET to show all properties
CH4HC100_25 =
  struct with fields:

    RES: [1×10 struct]
      X: [343 343 373 381 409 409]
      Y: [10 42 68 68 42 10]
CH4HC80_20 =
  struct with fields:

    RES: [1×10 struct]
      X: [343 343 373 381 409 409]
      Y: [10 42 68 68 42 10]
CH4HC60_15 =
  struct with fields:

    RES: [1×10 struct]
      X: [343 343 373 381 409 409]
      Y: [10 42 68 68 42 10]
CH4HC40_10 =
  struct with fields:

    RES: [1×10 struct]
      X: [343 343 373 381 409 409]
      Y: [10 42 68 68 42 10]
p1 =
  Line with properties:
```

```
              Color: [1 0 0]
          LineStyle: '-'
          LineWidth: 1.5
             Marker: 'none'
         MarkerSize: 6
    MarkerFaceColor: 'none'
              XData: [1×200 double]
              YData: [1×200 double]
              ZData: [1×0 double]

  Use GET to show all properties
p2 =
  Line with properties:

              Color: [0 0 1]
          LineStyle: '-'
          LineWidth: 1.5
             Marker: 'none'
         MarkerSize: 6
    MarkerFaceColor: 'none'
              XData: [1×200 double]
              YData: [1×200 double]
              ZData: [1×0 double]

  Use GET to show all properties
p3 =
  Line with properties:

              Color: [1 0 1]
          LineStyle: '-'
          LineWidth: 1.5
             Marker: 'none'
         MarkerSize: 6
    MarkerFaceColor: 'none'
              XData: [1×200 double]
              YData: [1×200 double]
              ZData: [1×0 double]

  Use GET to show all properties
p4 =
  Line with properties:

              Color: [0 1 1]
          LineStyle: '-'
          LineWidth: 1.5
             Marker: 'none'
         MarkerSize: 6
    MarkerFaceColor: 'none'
              XData: [1×200 double]
              YData: [1×200 double]
              ZData: [1×0 double]

  Use GET to show all properties
p1 =
  Line with properties:

              Color: [1 0 0]
          LineStyle: '-'
```

```
          LineWidth: 1.5
             Marker: 'none'
         MarkerSize: 6
    MarkerFaceColor: 'none'
              XData: [1×200 double]
              YData: [1×200 double]
              ZData: [1×0 double]

  Use GET to show all properties
p2 =
  Line with properties:

              Color: [0 0 1]
          LineStyle: '-'
          LineWidth: 1.5
             Marker: 'none'
         MarkerSize: 6
    MarkerFaceColor: 'none'
              XData: [1×200 double]
              YData: [1×200 double]
              ZData: [1×0 double]

  Use GET to show all properties
p3 =
  Line with properties:

              Color: [1 0 1]
          LineStyle: '-'
          LineWidth: 1.5
             Marker: 'none'
         MarkerSize: 6
    MarkerFaceColor: 'none'
              XData: [1×200 double]
              YData: [1×200 double]
              ZData: [1×0 double]

  Use GET to show all properties
p4 =
  Line with properties:

              Color: [0 1 1]
          LineStyle: '-'
          LineWidth: 1.5
             Marker: 'none'
         MarkerSize: 6
    MarkerFaceColor: 'none'
              XData: [1×200 double]
              YData: [1×200 double]
              ZData: [1×0 double]

  Use GET to show all properties
p1 =
  Line with properties:

              Color: [1 0 0]
          LineStyle: '-'
          LineWidth: 1.5
             Marker: 'none'
```

```
          MarkerSize: 6
      MarkerFaceColor: 'none'
                XData: [1×200 double]
                YData: [1×200 double]
                ZData: [1×0 double]

  Use GET to show all properties
p2 =
  Line with properties:

                Color: [0 0 1]
            LineStyle: '-'
            LineWidth: 1.5
               Marker: 'none'
          MarkerSize: 6
      MarkerFaceColor: 'none'
                XData: [1×200 double]
                YData: [1×200 double]
                ZData: [1×0 double]

  Use GET to show all properties
p3 =
  Line with properties:

                Color: [1 0 1]
            LineStyle: '-'
            LineWidth: 1.5
               Marker: 'none'
          MarkerSize: 6
      MarkerFaceColor: 'none'
                XData: [1×200 double]
                YData: [1×200 double]
                ZData: [1×0 double]

  Use GET to show all properties
p4 =
  Line with properties:

                Color: [0 1 1]
            LineStyle: '-'
            LineWidth: 1.5
               Marker: 'none'
          MarkerSize: 6
      MarkerFaceColor: 'none'
                XData: [1×200 double]
                YData: [1×200 double]
                ZData: [1×0 double]

  Use GET to show all properties
p1 =
  Line with properties:

                Color: [1 0 0]
            LineStyle: '-'
            LineWidth: 1.5
               Marker: 'none'
          MarkerSize: 6
      MarkerFaceColor: 'none'
```

```
              XData: [1×200 double]
              YData: [1×200 double]
              ZData: [1×0 double]

  Use GET to show all properties
p2 =
  Line with properties:

              Color: [0 0 1]
          LineStyle: '-'
          LineWidth: 1.5
             Marker: 'none'
         MarkerSize: 6
    MarkerFaceColor: 'none'
              XData: [1×200 double]
              YData: [1×200 double]
              ZData: [1×0 double]

  Use GET to show all properties
p3 =
  Line with properties:

              Color: [1 0 1]
          LineStyle: '-'
          LineWidth: 1.5
             Marker: 'none'
         MarkerSize: 6
    MarkerFaceColor: 'none'
              XData: [1×200 double]
              YData: [1×200 double]
              ZData: [1×0 double]

  Use GET to show all properties
p4 =
  Line with properties:

              Color: [0 1 1]
          LineStyle: '-'
          LineWidth: 1.5
             Marker: 'none'
         MarkerSize: 6
    MarkerFaceColor: 'none'
              XData: [1×200 double]
              YData: [1×200 double]
              ZData: [1×0 double]

  Use GET to show all properties
```

Published with MATLAB® R2020b